LBL-33766
UC-413

Lawrence Berkeley Laboratory
UNIVERSITY OF CALIFORNIA

Studies of Berkelium and Neptunium Isotopes

S.A. Kreek
(Ph.D. Thesis)

March 1993

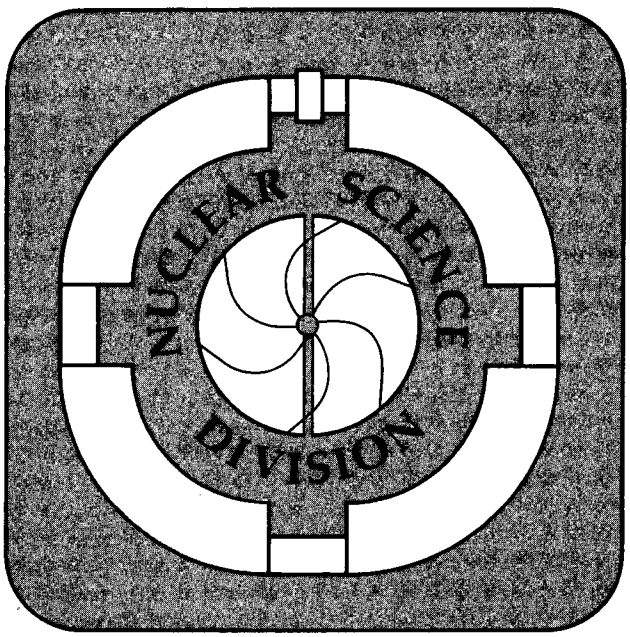

Prepared for the U.S. Department of Energy under Contract Number DE-AC03-76SF00098

DISCLAIMER

LBL-33766

Studies of Berkelium and Neptunium Isotopes

S.A. Kreek

Ph.D. Thesis

Nuclear Science Division
Lawrence Berkeley Laboratory
Mail Stop 70A-3307
University of California
Berkeley, CA 94720

March 5, 1993

This work was supported in part by the U.S. Department of Energy through the Division of Nuclear Physics of the Office of High Energy and Nuclear Physics under Contracts DE-AC03-76SF00098 (LBL) and W-7405ENG48 (LLNL).


PRINTED ON
RECYCLED PAPER

Abstract

Studies of Berkelium and Neptunium Isotopes

by

Steven Andrew Kreek

Doctor of Philosophy in Chemistry

University of California at Berkeley

Professor Darleane C. Hoffman, Chair

Electron-capture delayed fission (ECDF) was studied in the new isotope ^{238}Bk produced via the ^{241}Am(75-MeV α, 7n)^{238}Bk reaction. The half-life is 144 ± 5 seconds. The mass-yield distribution is predominantly asymmetric and the most probable pre-neutron emission total kinetic energy (TKE) of fission is 174 ± 5 MeV. The ECDF mode in ^{238}Bk was verified by an x-ray–fission coincidence experiment which indicated that the fission lifetime is between about 10^{-15} and 10^{-9} seconds. The isotope was assigned as ^{238}Bk through chemical separation and observation of the known 2.4-hour ^{238}Cm daughter. The production cross section (σ) is 150 ± 10 nb and the delayed fission probability (P_{DF}) is $(4.8 \pm 2) \times 10^{-4}$.

ECDF was positively identified in ^{228}Np produced via the ^{233}U(50-MeV p, 6n)^{228}Np reaction. The half-life of the fission activity is 61.4 ± 1.4 seconds. The mass-yield distribution is predominantly asymmetric with a symmetric component of about 2%. The TKE is 165 ± 5 MeV for the asymmetric component and approximately 150 ± 5 MeV for the symmetric component. The ECDF mode was verified by an x-ray–fission coincidence experiment which indicated that ^{228}U does not have a fission isomer populated in the ECDF. The isotope was assigned as ^{228}Np based on chemical

separation and observation of known progeny activities. The ratio of electron-capture (EC) to alpha decay is 1.5 ± 0.4. The σ is 35 ± 3 μb and the P_{DF} is $(2.0 \pm 0.9) \times 10^{-4}$.

The isotope ^{252}Bk was produced via a ^{4}H transfer reaction between 107-MeV ^{18}O and a ^{248}Cm target. Observation of ^{252}Cf, the EC daughter of ^{252}Bk, in chemically separated Bk fractions yields a half-life 1.8 ± 0.5 minutes and a σ of 47 ± 10 μb.

Dedication

This thesis is dedicated to those people who have made a significant contribution to my development as a scientist:

- My Parents and Step-Parents, Peter Kreek, Helen I. Workley, Patricia G. Kreek and Frederick J. Workley. Their continuous support and encouragement made completion of this work possible.
- Frederick W. Terman (United States Naval Post-Graduate School, Monterey, CA) and Frederick E. Terman (Stanford University, Palo Alto, CA, deceased). From a very early age, they were role models for my life. The experience I gained and the encouragement I received, through exposure to these scientific professionals is immeasurable. I will always be grateful.
- Dr. Peter A. J. Englert (San Jose State University, San Jose, CA). His research guidance and enthusiasm for nuclear and radiochemistry sparked my interest in the field.
- Dr. Darleane C. Hoffman and Dr. Kenneth E. Gregorich (University of California at Berkeley and Lawrence Berkeley Laboratory, Berkeley, CA). Under their guidance, my research skills were tuned. Their wisdom and encouragement made completion of this work possible, as well as fun.
- My Wife, Tamee Lynn Kreek. Her patience through the writing and editing phase of this dissertation made my life much easier. Her continuous encouragement helped me get past the aggravation associated with completing a manuscript of this size.

Contents

List of Figures

List of Tables

Acknowledgments

The author is grateful to the other members, past and present, of the Lawrence Berkeley Laboratory Heavy Element Nuclear and Radiochemistry Group (D.C. Hoffman, K.E. Gregorich, D.M. Lee, M.J. Nurmia, K.R. Czerwinski, C.M. Gannett, H.L. Hall, T.M. Hamilton, N.J. Hannink, R.A. Henderson, C.D. Kacher, B. Kadkhodayan, M.R. Lane, J.D. Leyba, M.F. Mohar, M.P. Neu, E.R. Sylwester, and A. Türler) for their assistance. The author will not emphasize (I just did) the extremely large contributions of K.E. Gregorich and B. Kadkhodayan to the completion of this dissertation. Anyway, they have probably gone *running* somewhere (we can only hope they'll get lost).

The author is grateful to his unborn child. He (She) played a large role in motivating the completion of this work. I heard "Hurry-up, you need a job, *FAST*" from many people (including my wife).

The author is grateful to the engineers responsible for the alpiners hut out-house (alp horns) at the top of the Jungfraujoch, Switzerland. Their design led to many thought provoking discussions.

The author wishes to thank the staff and crew of the Lawrence Berkeley Laboratory 88-Inch Cyclotron for their patience and assistance.

The author wishes to thank the U.S. Department of Energy, transplutonium element production facility at the Oak Ridge National Laboratory for use of the ^{248}Cm.

This work was supported in part by the Director, Office of Energy Research, Division of Nuclear Physics of the Office of High Energy and Nuclear Physics of the U.S. Department of Energy under Contracts DE-AC03-76SF00098 (LBL) and W-7405-ENG-48 (LLNL).

1 Introduction

1.1 Discovery of Bk and Np

The first successful attempt to produce elements beyond uranium was in 1940. McMillan et al., synthesized Np by irradiating ^{nat}U with slow neutrons [McMillan, 1940]. An excellent overview of the discovery process is given in [Seaborg, 1990]. The produced activities, which were thought by McMillan et al. to be new elements, were determined to be products formed by the fission of uranium into two smaller fragments [Hahn, 1939]. The discovery of the first transuranium element, neptunium, came as part of an attempt by McMillan et al. [McMillan, 1940] to study the fission process. McMillan et al. showed that ^{239}Np was formed from the beta decay of ^{239}U which was produced by the $^{238}U(n,\gamma)^{239}U$ reaction. The formation reaction is:

$$^{238}U + {}^{1}n \longrightarrow {}^{239}U^{*} \longrightarrow {}^{239}Np + \beta^{-} + \nu'$$

Separations were performed on the unknown beta activity ($t_{1/2}$ = 2.355 days). It was found that the element was chemically similar to uranium. They identified the new activity as an isotope of Np (^{239}Np) via chemical separations. The postulate about a new series in the periodic table, the actinide series, was reinforced by these data. An overview of the origin of the actinide series is given in [Seaborg, 1991]. This was the first definitive evidence that an inner electron shell, the 5f shell, is filled in the transuranium region of the elements [McMillan, 1940].

Weighable quantities of Np, as ^{237}Np ($t_{1/2} = 2.14 \times 10^{6}$ years), were first obtained in 1944 by Magnusson et al. [Magnusson, 1948]. Figure 1-1 shows a periodic table in its currently accepted form with a separate series for the

lanthanides and actinides which denotes the filling of the 4f and 5f electronic shells, respectively.

The most important prerequisite to the process of making transcurium elements was the manufacture of sufficiently large quantities of americium and curium to serve as target material [Seaborg, 1990]. Berkelium was discovered in 1949 by Thompson et al. [Thompson, 1950] by bombarding ^{241}Am with alpha particles. The production reaction is ^{241}Am(α, 2n)^{243}Bk. Thompson and his coworkers separated berkelium by cation exchange chromatography with ammonium citrate as the eluant [Thompson, 1950]. Berkelium eluted from the cation exchange column before Cm and Am and was identified by alpha-pulse-height analysis and conversion-electron x-ray spectroscopy. Berkelium-243 ($t_{1/2}$ = 4.5 hours) has a small alpha branch, 0.15%, which was characterized by Chetham-Strode in 1956 [Chetham-Strode, 1956]. It was found that Bk has a 3+/4+ oxidation state couple [Thompson, 1950] [Thompson, 1950A] which is unique among the transplutonium elements and makes separation from the other trivalent actinides, after oxidation to the 4+ state, relatively easy. This is accomplished with such methods as extraction into di-2-ethylhexylorthophosphoric acid (HDEHP) [Knauer, 1968] [Higgins, 1960] [Peppard, 1957] [Peppard, 1957A].

1.2 Objectives of this Study

1.2.1 Study Nuclear Properties of New Isotopes

Synthesis and study of the nuclear properties of new isotopes is required to refine existing nuclear decay models. One objective of this dissertation is to provide experimental data for the previously unknown isotopes, ^{228}Np, ^{238}Bk, and ^{252}Bk. Currently, the discovery of new isotopes is rather rare because of the difficulties involved in production and detection.

Throughout the 1940's, 50's, and 60's many new elements and isotopes were discovered. In the 1970's and 80's, the rate decreased for several reasons. First, the few groups studying the heavy elements had exhausted many of the target projectile combinations useful for synthesizing new elements and isotopes. It is extremely difficult to find target projectile combinations which yield large cross sections and produce activities which have sufficiently long half-lives to allow detailed study. Second, isotopes far from stability have short half-lives which requires rapid separation and detection techniques. Rapid chemical separation techniques, such as the Automated Chromatographic Chemical Element Separation System [Kreek, 1992A], were not readily available. On the other hand, interest in fission promoted searches for new isotopes in this region.

In studies of fission, it was thought that all spontaneous fission, as well as low energy neuton-induced fission, resulted in asymmetric mass division (the nucleus divides in two fragments of significantly different mass). It was not until Balagna et al. [Balagna, 1971] discovered a symmetric fission component in the spontaneous fission of ^{257}Fm, that new life was given to the study of spontaneous fission in the heavy elements.

Currently, the availability of heavy element target material such as ^{241}Am, ^{233}U, ^{248}Cm, and ^{249}Bk and the ability of accelerators to provide high intensity beams have enabled researchers to continue to probe the limits of nuclear stability in the heavy elements by opening the doorway to extremely neutron-deficient and relatively neutron-rich nuclei. Reaching very neutron-rich nuclei is limited by target projectile combinations and reaction cross sections. However, this is being approached in a new fashion with the possibility of accelerating radioactive nuclear beams [Casten, 1991]. The advances in target technology, such as multiple target arrays [Hall, 1989A],

have also enabled researchers to study nuclei which otherwise would be produced at too small a rate to make determination of nuclear properties practical. With light ion bombardments, multiple target arrays increase the effective target thickness, which would ordinarily be limited by the small recoil momentum of the compound nucleus.

1.2.2 Extend Studies of Delayed Fission to New Isotopes

Because a comprehensive model that predicts all aspects of the fission process has yet to be developed, it is important to gather as much fission data as possible to continue testing and refining the current models. In this dissertation, the study of several new isotopes of berkelium and neptunium, some of which undergo electron-capture delayed fission (ECDF) decay, is presented.

The renewed interest in fission and advances in detection technology have brought to light new methods for studying the fission process. Delayed fission techniques have made possible the determination of the fission properties of nuclei which have ground state fission branches too small to otherwise permit detailed study of the fission properties. Delayed fission as well as the technique of multiple target arrays [Hall, 1989A] have allowed the fission properties of nuclei such as ^{234}Am [Hall, 1990A], and ^{232}Am [Hall, 1990B] to be studied in detail. It is believed that delayed fission techniques can be used to study details of the fission barrier in an out-of-beam environment and in unprecedented detail [Gregorich, 1991]. Many of the electron-capture, (EC), half-lives are of the order of minutes. These half-lives are sufficiently long to allow transport of the EC parent out of the target system for chemical separation and subsequent measurement of the nuclear properties. This significantly reduces the problems associated with in-beam studies. The K-

vacancy lifetime of 10^{-17} seconds [Scofield, 1974] for emission of K x-rays following EC can be used in ECDF to measure the time scale of the subsequent fission [Kreek, 1992B].

1.3 History of ECDF

ECDF is an exotic nuclear decay process in which a nucleus decays via electron-capture to excited states in its daughter nucleus which then fission. These excited states can be above the fission barrier(s) of the daughter (yielding prompt fission), inside the second well of the potential energy surface (a fission shape isomer) or within the first well of the potential energy surface (an electromagnetic isomer). This is illustrated in Figure 1-2.

For ECDF to become an important mode of deexcitation, the electron-capture Q-value (Q_{EC}) (the energy released during the electron-capture decay) must be comparable to the height of the fission barrier [Hall, 1990A]. If the precursor nuclide chosen for study has a Q_{EC} smaller than the fission barrier, the EC would be expected to predominantly populate levels in the first potential well (see Figure 1-2). Population of states in the second well would require a significant change in deformation to occur simultaneously with the EC decay.

The ECDF mode of decay is of interest because of its similarity to beta-delayed fission (BDF), which is believed to have an important role in determining the yields of heavy isotopes produced in multiple neutron capture processes such as nucleosynthesis in the r-process of supernovae and nuclear weapons tests [Burbidge, 1957] [Wene, 1974] [Wene, 75] [Klapdor, 1981] [Meyer, 1989]. In the r-process, the large neutron fluxes, coupled with the availability of heavy target material, leads to multiple neutron capture events. This can produce neutron-rich nuclei all the way out to the neutron

drip-line. These neutron-rich nuclei undergo beta decay which produces elements of higher atomic number. If this chain of beta decays were to continue, the very heavy actinides would be produced in relative amounts which are neither found in nature nor in nuclear weapons tests [Hoff, 1986] [Hoff, 1988]. It is believed that BDF depletes the beta decay chains. This reduces the production of higher atomic numbered elements [Burbidge, 1957] [Meyer, 1989]. The enhanced Q_{EC}s associated with the decay of odd-proton, odd-neutron nuclei may reduce the relative amounts of the resulting even-proton, even-neutron daughters relative to odd-even or even-odd nuclei. However, reexamination of the available data by Hoff [Hoff, 1986] [Hoff, 1988] has shown that the predicted influence of BDF has been overestimated but is not negligible. The influence of delayed fission (DF) processes on the production and isotopic abundances of the actinide cosmochronometers can give important information applicable to determination of the age of the galaxy [Theilemann, 1983] [Yokoi, 1983] [Meyer, 1986] and its chemical evolution [Meyer, 1986] [Reeves, 1976].

DF also has the potential to greatly expand the number of nuclei whose fission properties can be measured; the nuclei in the actinide region have ground state fission half-lives which are too long compared to their overall half-lives to allow detailed study. This is illustrated in Figure 1-3. The spontaneous fission half-lives in regions where ECDF is important are too long to make study practical.

Of the most significance, however, is the possibility for detailed study of the highly deformed shape isomer in an out-of-beam environment. Excited states in the daughter are populated with the half-life of the EC parent. These half-lives can be of the order of minutes and thus allow sufficient time for transport out of the target system for chemical separation and

determination of the nuclear properties. The study of the shape isomer will allow for examination of the fission barrier in unprecedented detail [Gregorich, 1991] (see Section 1.4).

As early as 1972, Skobelev et al. [Skobelev, 1972] claimed that fissions observed in the light americium and neptunium region by Kuznetsov et al. [Kuznetsov, 1966] [Kuznetsov, 1967] were the result of ECDF. Fission decay in ^{232}Am was confirmed by Habs et al. [Habs, 1978] in 1978. It was not until 1989, however, that Hall et al. [Hall, 1989B] provided direct evidence for ECDF in ^{232}Am by measuring the time correlation between the EC x-rays and the subsequent fission. In the measured coincidence spectra, other photopeaks appeared which may have resulted from transitions in the second potential well [Hall, 1992] (see Figure 1-2). However, sufficient statistics were not available to confirm such a claim. The limited number of events did not eliminate the possibility that the additional photopeaks were random coincidences with prompt γ-rays from the fission fragments. All reports of ECDF are summarized in Table 1–1.

1.4 Theory of ECDF

1.4.1 Delayed Fission Probability Calculations

The probability of delayed fission, P_{DF}, is defined experimentally as the number of electron-capture decays which result in a fission, N_{ECDF}, divided by the total number of electron-capture decays, N_{EC}. This is illustrated by equation 1-1.

$$P_{DF} = N_{ECDF}/N_{EC} \qquad \text{Equation 1-1}$$

Typical values of P_{DF} range from 10^{-2} to 10^{-8} (see Table 1-1). Any time the Q_{EC} approaches the height of the fission barrier, delayed fission becomes a possibility.

Table 1-1. List of all reports of electron-capture delayed fission. [a]P_{DF} is defined as the number of electron-capture decays which result in fission divided by the total number of electron-capture decays.

Nuclide	Half-life	P_{DF}[a]	Production Reaction	Reference
Md-250	52 sec	2×10^{-4}	$^{243}Am(^{12}C,5n)$	Gangrskii, 1980
Es-248	28 min	3×10^{-7}	$^{238}U(^{14}N,4n)$	Gangrskii, 1980
Es-246	8 min	3×10^{-5}	$^{238}U(^{14}N,6n)$	Gangrskii, 1980
Es-244	37 sec	$\approx10^{-4}$	$^{235}U(^{14}N,5n)$	Gangrskii, 1980
Es-242?	≈25 sec	1.4×10^{-2}	$^{205}Tl(^{40}Ar,3n)$	Hingmann, 1985
Bk-240	4 min	$\approx10^{-5}$	$^{232}Th(^{14}N,6n)$	Gangrskii, 1980
Am-236	3.7 min	2.5×10^{-8}	$^{237}Np(\alpha,5n)$	Hall, 1989D
Am-234	2.6 min	$\approx10^{-5}$	$^{230}Th(^{10}B,6n)$	Skobelev, 1972
	2.32 min	6.6×10^{-5}	$^{237}Np(\alpha,7n)$	Hall, 1990A
Am-232	1.4 min	$\approx10^{-2}$	$^{230}Th(^{10}B,8n)$	Skobelev, 1972
	0.92 min	1.3×10^{-2}	$^{237}Np(\alpha,9n)$	Habs, 1978
	1.31 min	6.9×10^{-4}	$^{237}Np(\alpha,9n)$	Hall, 1990B
Np-228	60 sec	$\approx10^{-3}$	$^{209}Bi(^{22}Ne,3n)$	Skobelev, 1972
Tl-180	0.7 sec	$\approx10^{-6}$	$^{144}Sm(^{40}Ca,p3n)$	Lazarev, 1987

Theoretically, P_{DF}, depends on several factors. These include the Q_{EC}; the excitation energy, E, of the levels populated in the daughter by the electron-capture; a transition probability function, $W_{EC}(E)$; and the ratio of the fission decay width, $\Gamma_f(E)$, to the total decay width of the excited daughter, $\Gamma_t(E)$. The total decay width is the sum of decay widths for all possible decay modes. In this dissertation, it is assumed that only gamma and fission decay

modes compete, therefore $\Gamma_t(E) = \Gamma_\gamma(E) + \Gamma_f(E)$ where $\Gamma_\gamma(E)$ is the gamma decay width. This is not completely correct because other factors including neutron emission should be considered, if the decay energy is larger than the neutron binding energy. To calculate the P_{DF}, these factors must be integrated over the total energy available for the decay, Q_{EC}, and normalized to the total number of electron-capture decays. The P_{DF} is given from theoretical considerations in functional form as equation 1-2.

$$P_{DF} = \frac{\int_0^{Q_{EC}} W_{EC}(E) \frac{\Gamma_f}{\Gamma_t}(E) dE}{\int_0^{Q_{EC}} W_{EC}(E) dE} \quad \text{Equation 1-2}$$

Approximations can be included in equation 1-2 for the transition probability function, and the decay widths in the following manner.

The gamma decay width term, $\Gamma_\gamma(E)$, can be approximated [Gangrskii, 1980] from the probability for gamma transitions, P_γ, as equation 1-3.

$$\Gamma_\gamma(E) = \frac{P_\gamma}{2\pi\rho(E)} = \frac{C_\gamma \Theta^4 e^{(E/\Theta)}}{2\pi\rho(E)} \quad \text{Equation 1-3}$$

In equation 1-3, $\rho(E)$ is the nuclear level density, C_γ is a constant with the value 9.7×10^{-7} MeV^{-4} and Θ is the nuclear temperature (0.5 - 0.6 MeV). The nuclear temperature can be calculated from formulas such as those in [Swiatecki, 1983].

The fission width term, $\Gamma_f(E)$, can be derived from the penetrability of the fission barrier. This yields equation 1-4.

$$\Gamma_f(E) = \frac{P_f}{2\pi\rho(E)} \quad \text{Equation 1-4}$$

In equation 1-4, P_f is the penetrability of the entire two humped fission barrier (see Figure 1-2).

Calculation of the penetrability of the fission barrier in the actinides is difficult because the fission barriers are complex [Habs, 1978] [Gangrskii, 1980].

It is common to simplify the problem by assuming all nuclear motion in the second potential well is damped (see Figure 1-2). This has the effect of allowing time for all states populated in the second potential well to gamma decay to the ground state in the second well before fission can occur. Calculating the penetrability of the outer barrier from this single level in the second well is reduced to a calculation involving a simple transmission coefficient. The penetrability of the inner barrier can be calculated using a parabolic barrier such as that used by Hill and Wheeler [Hill, 1953]. The penetrability of the fission barrier is then the product of the transmission coefficient from the lowest state in the second well through the outer barrier and the penetrability of the inner barrier. Including the Hill-Wheeler formalism, the fission decay width becomes equation 1-5.

$$\Gamma_f(E) = \frac{R_B}{2\pi\rho(E)}\left[1-\exp\left(\frac{2\pi(B_f-E)}{\hbar\omega_f}\right)\right]^{-1} \quad \text{Equation 1-5}$$

In equation 1-5, R_B is the transmission coefficient for decay from the lowest state in the second potential well through the outer fission barrier, B_f is the inner barrier height, $\hbar\omega_f$ is the energy associated with the curvature of the inner fission barrier, and E is the excitation energy. Because the lowest state in the second well can either fission or γ-decay back to the first well, the factor R_B is really comprised of the ratio of transmission coefficients for the lowest level in the second well for tunneling through the outer barrier to that for γ-decay back to the first potential well.

The transition probability function in equation 1-2, $W_{EC}(E)$, consists of the product of the integrated Fermi function (dictates the rate of the EC transition) and a beta strength function, ζ_β (dictates the distribution of states available for the EC to populate). This product accounts for population of excited states in the daughter. The Fermi function for allowed electron-

capture transitions can be approximated as $(Q_{EC} - E)^2$. Here, E represents the residual excitation energy in the daughter. The difference between Q_{EC} and E is the transition energy. The electron binding energy is ignored in this approximation.

Use of the beta strength function, ζ_β, to calculate the probability of population of states is justified because ζ_β is related to averaged properties of the nuclear decay which do not depend on the detailed structure of the levels. This treatment is only valid at relatively high excitation energies in the daughter, i.e. in the region where P_{DF} becomes important. Klapdor et al. pointed out that low lying structure may affect ζ_β and thus the P_{DF}. This can be illustrated with the following example.

> Example 1: If a nucleus has a large Q_{EC} relative to the height of the fission barrier in the daughter, the P_{DF} would be expected to be large. However, if decay to the ground state of the daughter is superallowed (no net change in spin or parity), no high-energy states would be populated from which delayed fission could occur. The beta strength to high energy states would be zero. The P_{DF} would be zero in this case.

The beta strength function has been approximated in several ways. It can be taken as proportional to the nuclear level density [Wene, 1974] [Shalev, 1977]; it can be generated from the gross theory of beta decay [Kodama, 1975]; or it can be taken as constant above a certain energy [Kratz, 1973] [Hornshøj, 1975]. Meyer et al. [Meyer, 1989] have presented a new method to calculate ζ_β which includes a specific treatment of nuclear deformation. This is important because the distribution of states is influenced significantly through mixing caused by deformation.

The model of Meyer et al. [Meyer, 1989] calculates beta strength functions by treating nuclear deformation explicitly using the random-phase

approximation to mix deformed states; the Gamow-Teller (GT) interaction mixes states and significantly alters the beta-decay properties. The GT interaction provides more low energy states for the beta-decay to populate and thus influences the P_{DF}.

To calculate effects such as that given in example 1 would require a knowledge of the low-lying structure of ζ_β. Equation 1-2 is applicable for a qualitative understanding of the factors involved in determining the delayed fission probability. A more comprehensive approach would include factors to account for detailed structure of the fission barrier, nuclear deformation, and a better expression for ζ_β which more realistically models the true level scheme of the electron-capture daughter.

It may be necessary to include additional factors in equation 1-2 which account for fission from levels not directly populated by the electron-capture but by low energy gamma transitions from higher energy states. Because the fission width decreases very rapidly with decreasing excitation energy, it is likely that this factor is extremely small, at least for transitions in the first potential well (see Figure 1-2). It becomes even less significant by realization that low energy gamma transitions to states where the fission width is still appreciable would be several orders of magnitude slower than high energy gamma transitions to states well inside the first potential well [Weisskopf, 1951].

With the use of the above approximations for W_{EC} and Γ_t, equation 1-2 becomes:

$$P_{DF} \approx \frac{\int_C^{Q_{EC}} (Q_{EC} - E)^2 \frac{\Gamma_f}{\Gamma_f + \Gamma_\gamma}(E)dE}{\int_C^{Q_{EC}} (Q_{EC} - E)^2 dE} \qquad \text{Equation 1-6}$$

This expression for the delayed fission probability includes the cut-off energy approximation, C, of Kratz et al. [Kratz, 1973] for the beta strength function below which the P_{DF} is zero. Because the beta strength function above the cut-off energy is assumed to be constant and is present in both the numerator and denominator of equation 1-6, it is simply divided out of the expression. The cut-off energy below which the beta strength function is zero is given by $C = 26A^{-1/2}$ MeV [Kratz, 1973], where 'A' is the mass number of the fissioning species.

The denominator of equation 1-6 is easily evaluated yielding equation 1-7. This equation has an exponential dependence on the difference between the Q_{EC} and the fission barrier, illustrating the requirement that the Q_{EC} must be of the same order as the height of the fission barrier for delayed fission to become a significant mode of decay.

$$P_{DF} \approx \frac{\int_C^{Q_{EC}} (Q_{EC} - E)^2 \frac{\Gamma_f}{\Gamma_f + \Gamma_\gamma}(E)dE}{\frac{1}{3}(Q_{EC} - 26A^{-1/2})^3} \qquad \text{Equation 1-7}$$

Equation 1-7 includes factors for the barrier height and curvature in the $\Gamma_f(E)$ term given in equation 1-5, but it is not possible to calculate either of these quantities explicitly without specific information about the shape isomer. As a general model, however, equation 1-7 is quite useful. A possible use of delayed fission to study the details of the shape isomer is presented in later sections.

1.4.2 Fission Modes in ECDF

It is well established that mass-yield distributions of fragments from fission are strongly influenced by shell effects [Hoffman, 1989]. The mass distributions in the region $^{235}U < ^{A}Z < ^{255}Fm$ are highly asymmetric with the

heavy-mass fragment having a near spherical, closed nuclear shell structure. The light fragment increases in mass and Z with increasing mass and Z of the fissioning nucleus [Vandenbosch, 1973]. However, in the region of ^{257}Fm (Z = 100) the mass split becomes highly symmetric. This is presumably due to both fission fragments having near spherical, closed nuclear shell structure (Z=50 and N=82) [Balagna, 1971].

In the Ra region, near neutron number 136, the mass-yield distribution becomes three-humped [Itkis, 1988]. This was the first evidence for a separate symmetric and asymmetric mode involved in the fission process [Jensen, 1958]. Studies which impart different amounts of excitation energy to the fissioning nucleus in the Ra region have shown that the mass-yield distribution becomes more broadly symmetric with increasing excitation energy of the system [Konecny, 1969]. The change from asymmetric to broadly symmetric mass-yield distributions in the Ra region with increasing excitation energy is a result of the damping of shell effects by the excitation. The increased excitation energy causes the fission to proceed more like that predicted by the Liquid Drop Model [Vandenbosch, 1973]. The effects have been seen with excitation energies as low as 7 MeV in studies of ^{227}Ac and ^{228}Ac produced by means of direct reactions of ^{3}He on a ^{226}Ra target [Konecny, 1973].

ECDF can impart excitation energy to the fissioning system up to nearly the entire electron-capture Q-value. The EC Q-values in the region of ^{228}Np and ^{238}Bk are of order 4-5 MeV [Möller, 1988]. Given that the residual excitation energy after the EC decay may be as high as about 4 MeV in the region of ^{228}Np and ^{238}Bk and because the fission barriers are known to decrease significantly from Rn to Th [Habs, 1978], a small symmetric component might be expected to contribute to the overall mass-yield

distribution from ECDF in the region of ^{228}Np and ^{238}Bk. According to the static scission point model of Wilkins et al. [Wilkins, 1976], the symmetric mode will have a significantly lower total kinetic energy than the asymmetric mode. This is presumably due to larger fragment deformation at scission.

1.4.3 ECDF and the Fission Barrier

1.4.3.1 Origin of Shape Isomers

As is illustrated in Figure 1-2, and as was discussed briefly in the preceding sections, shape isomers occur as a result of a second minimum in the nuclear potential energy as a function of deformation. It was not until 1967 that Strutinsky [Strutinsky, 1967] proposed a theoretical explanation which yielded a second minimum in the plot of potential energy versus deformation. The following is a brief description of the origin of the shape isomer concept.

As early as 1962, a spontaneously fissioning species, which had an unusually short half-life [Polikanov, 1962], was produced in bombardments of U and Pu targets with ^{16}O and ^{22}Ne. This 14-msec half-life did not fit with any of the fission half-life systematics available at the time. The explanation for this unusually short-lived fissioning species was decay from an isomeric state which did not have to penetrate the entire fission barrier. Schematically, this is the same as the fission occurring from inside the second potential minimum shown in Figure 1-2. States in the second potential well have a significantly smaller barrier to fission than states in the first potential well, for the same excitation energy. The 14-msec activity was later identified as an isomer of ^{242}Am by the crossed reaction technique.

Other explanations for the short spontaneous fission half-lives included the possibility that the isomers may be high spin metastable states

which are highly gamma hindered, which allowed fission to become a significant mode of deexcitation. This explanation was eliminated by Bjørnholm et al. in 1967 [Bjørnholm, 1967] with the determination that a threshold energy of about 3 MeV was required to populate the isomeric state. Unless the spins involved are very high, this excitation energy is too large for highly hindered gamma decay. If the gamma transition is of a small multipolarity, the Weisskopf gamma transition estimates [Weisskopf, 1951] yield a lifetime of about 10^{-18} seconds for such a state. This is many orders of magnitude shorter lived than the observed ^{242}Am isomeric lifetime of 14-msec. The isomeric states were later demonstrated to possess little angular momentum by Flerov et al. [Flerov, 1968] in studies of reactions in which different amounts of angular momentum were brought in by the incident particle. A consequence of these studies is that the isomeric levels must be associated with a second minimum in the potential energy surface which was not adequately explained by the Liquid Drop Model (LDM).

Theory did not fit the experimental results until Strutinsky applied a shell correction with a uniform single particle energy level distribution to the LDM of fission [Strutinsky, 1967]. This correction produced a second minimum in the plot of potential energy versus deformation and removed the previous inadequacies of single particle models at large deformation. A typical two-dimensional potential energy surface is illustrated in Figure 1-2 and is now used as the standard shape of the fission barrier in the actinides.

The Strutinsky Hybrid Model [Strutinsky, 1967] accounts for nucleon shell effects. These shell effects are treated as small deviations from the LDM energies and are used as a correction factor to the LDM. The LDM is primarily composed of Coulomb and surface energy terms. The LDM treatment of fission produces a smooth barrier with increasing deformation. This is

illustrated in Figure 1-4. There is no second potential minimum in the LDM treatment of the fission barrier. The shape of the curve arises from a difference between the dominant surface and Coulomb terms in the LDM. Shell corrections are small compared to either the surface or Coulomb terms individually. However, the shell effects become large enough to yield a second minimum when compared to the difference between the surface and Coulomb terms. The inclusion of a shell and pairing correction produces a deviation from the smooth LDM potential (see Figure 1-4) and yields the well known double-humped fission barrier shown in Figure 1-2 which is applicable in the actinide region.

As is illustrated in Figure 1-2, population of states in the second well are associated with significantly larger deformation than the ground state. Confirmation that the isomer has a much larger deformation than the ground state was first obtained by Specht et al. in 1972 [Specht, 1972]. Specht et al. detected conversion lines of the rotational band built upon the shape isomeric state in ^{240}Pu. The moment of inertia was determined to be more than twice that of the ground state. In the simple rigid rotor approach, the energy difference between the ground state and the first rotational state is related to the moment of inertia as follows:

$$E = (h/2\pi)^2/2\,I\,J(J+1) \qquad \text{Equation 1-8}$$

In equation 1-8, E is the energy difference between the ground and first rotational state; J is the spin of the first excited state; I is the moment of inertia; h is Plank's constant. This energy difference between the lowest level and the first excited state in the shape isomer showed the moment of inertia of the species to be more than twice that of the ground state. The isomeric deformation (ratio of major to minor axis) was more than twice the ground state deformation.

1.4.3.2 Shape Isomer Studies with ECDF

The recent observation of a time correlation between the electron-capture x-rays and the subsequent fission [Hall, 1989B] has shed new light on the study of shape isomerism in the actinides. Because population of states in the fissioning species occurs with the half-life of the electron-capture parent, it is possible to separate the activity from the high background associated with typical in-beam studies. If excited states in the second well are populated and motion in the second well is damped, it should be possible to detect specific gamma transitions occurring inside the second well. With the availability of high-geometry γ-ray detector arrays, delayed fission may be used as a sensitive probe of the inner and outer fission barriers [Gregorich, 1991] (see Figure 1-5).

To accomplish a detailed analysis of the fission barrier the level scheme in the second potential well must be determined. This can be accomplished by measuring γ-rays in coincidence with delayed fissions. The large γ-ray multiplicity associated with the highly excited fission fragments will produce a background problem. However, with sufficient statistics, any transitions in the second well should be observable above this γ-ray continuum. The recently published results on the ECDF of ^{234}Am [Hall, 1990A] and ^{232}Am [Hall, 1990B] show these isotopes as promising candidates for such a study.

Information about the levels in the first potential well can be obtained through an x-ray–γ-ray coincidence experiment. Data from a γ-ray–γ-ray coincidence experiment between a transition γ-ray in the second well and a γ-ray from the second to the first potential well will yield the probability for gamma decay back to the first well. It may also yield the excitation energy associated with the ground state in the second potential well. Studies by Bjørnholm et al. have shown that the excitation energy associated with the

ground state of the second well is of order 3 MeV [Bjørnholm, 1967] in the Pu region.

Other information about the second well, such as the fission probability from the ground state in the second well, may be obtainable through the x-ray–fission coincidence technique. With this information, it is possible to calculate the relative height and widths of both the inner and outer fission barriers from the ratio of the fission probability to the probability for γ-decay back to the first potential well.

If the Q_{EC} is sufficiently large, it may be possible to populate a K-isomeric state in the second potential well. (Gamma transitions between different rotational bands are hindered. If the states are sufficiently hindered, a K-isomer results.) These levels are about 1-2 MeV above the lowest state and are typically several orders of magnitude longer lived than the timing resolution of a Ge γ-ray detector, which is about 10-20 nsec. Determination of the K-isomeric lifetime and the probability for fission from this level will yield the penetrability of the outer barrier at the K isomer energy. The lifetime of the ground state in the shape isomer may be obtained with techniques such as decay in flight. Determination of the gamma transition probability from the K isomer back to the first potential well and the K-isomeric lifetime will permit calculation of the penetrability of the inner barrier at the K isomer energy. These studies can be accomplished with γ-ray–fission and γ-ray–γ-ray coincidence techniques. The energy of the K-isomeric state can be determined by measuring its decay to either the lowest level in the shape isomer or to the ground state in the first potential well.

The absolute heights and widths (curvature) of the inner and outer barriers can be determined from the ratios of the penetrabilities of the inner and outer barriers from the lowest level in the shape isomer and the K-

isomeric level. This is critical to the refinement of the existing nuclear models because absolute measurements of the fission barrier have never been achieved.

1.5 Requirements for Study of ECDF

For the purposes of this study, three separate experiments must be performed to show that the ECDF process is indeed occurring and to study the process in detail. First, fissions must be detected in a region where the spontaneous fission branch is expected to be small (see Figure 1-3). This gives an indication that the ECDF mode is present in the nucleus under study. Second, an x-ray–fission coincidence experiment must be performed to show that x-rays resulting from an electron-capture are coincident with fission. Third, chemical separations of the electron-capture parent and detection of fissions in this fraction give the atomic number of the parent as well as allowing for the determination of the overall production rate of the isotope; this is accomplished by measuring the x-rays from the electron-capture decay or alpha-pulse-height spectroscopy. Because the isotopes in this dissertation, ^{238}Bk and ^{228}Np, have yet to be discovered, a correlation between the parent and a known daughter will be required in order to assign the mass number of the isotope and determine the electron-capture branch.

The berkelium and neptunium regions were chosen for several reasons. First, ECDF branches have been reported in the americium [Habs, 1978] [Hall, 1990A,B] [Liu, 1983], einsteinium [Gangrskii, 1980], berkelium [Gangrskii, 1980] and neptunium [Skobelev, 1972] regions, previously. Second, as stated above, the Q_{EC} must be of the same order as the height of the fission barrier for ECDF to become an important decay mode. Fission barriers in the actinide region have been shown to be of the order of 5 MeV

[Habs, 1978]. Therefore, isotopes with a Q_{EC} value larger than about 4 MeV should begin to have measurable ECDF branches. Nuclides with sufficient Q_{EC}s are found in the very, neutron-deficient odd-proton, odd-neutron nuclei. Odd-odd nuclei are preferable because of the enhanced electron-capture Q-values associated with decay to their more stable even-even daughters. Very light even mass number berkelium and neptunium isotopes which are odd-odd fit these criteria. Some isotopes for which delayed fission probabilities have been reported as well as other potential candidates are shown in Figure 1-6. The Light Ion Multiple Target system (LIM) [Hall, 1989A] makes it possible to use many targets, thereby increasing the production rates sufficiently to make study of isotopes in this region practical using reactions of light ions with actinide targets. Light ion bombardments are preferable over heavy ions because of the generally larger reaction cross sections, and higher available beam intensities.

In these experiments, targets were bombarded in the LIM system (see Section 3.2.2) at the Lawrence Berkeley Laboratory 88-Inch Cyclotron. The reaction products were ejected from the target because of the recoil momentum imparted to the system for the incoming projectile, swept from the target chamber with a He/KCl aerosol jet and transported to various locations depending on the experimental objective. See Section 3 for a detailed description of the procedures involved.

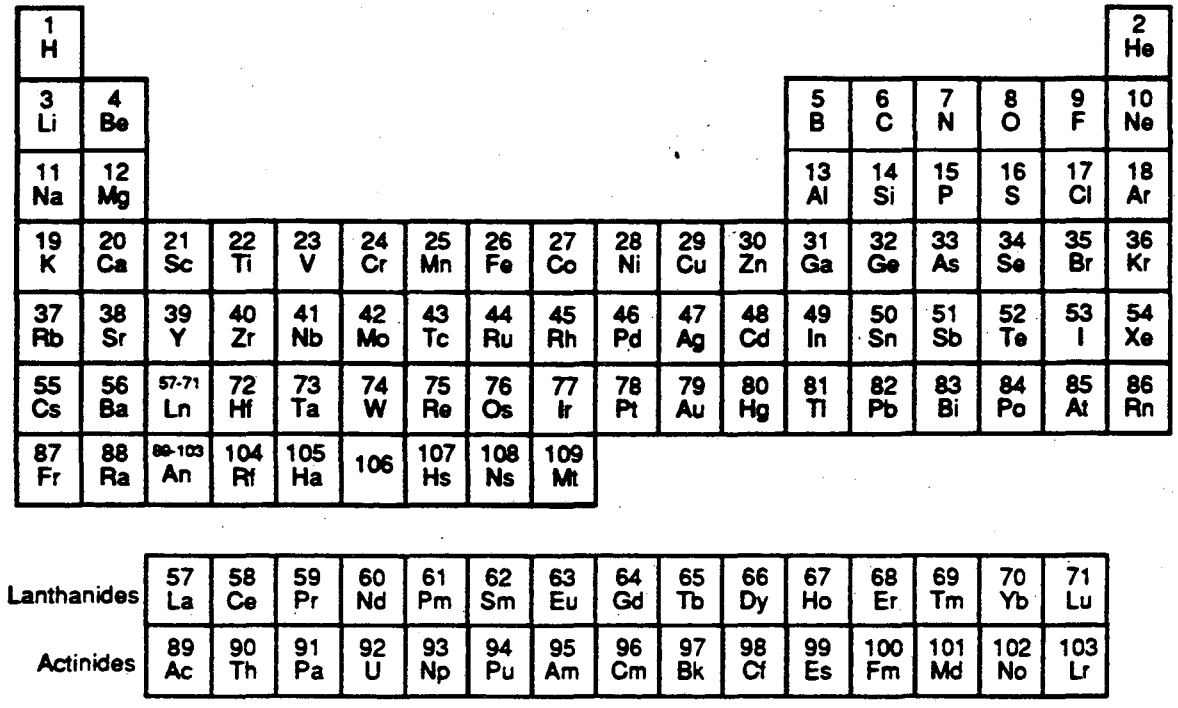

Figure 1-1. Periodic Table of the Elements. The periodic table shown is the currently accepted version illustrating the filling of a 4f and 5f electronic shell in the region of the lanthanides and actinides.

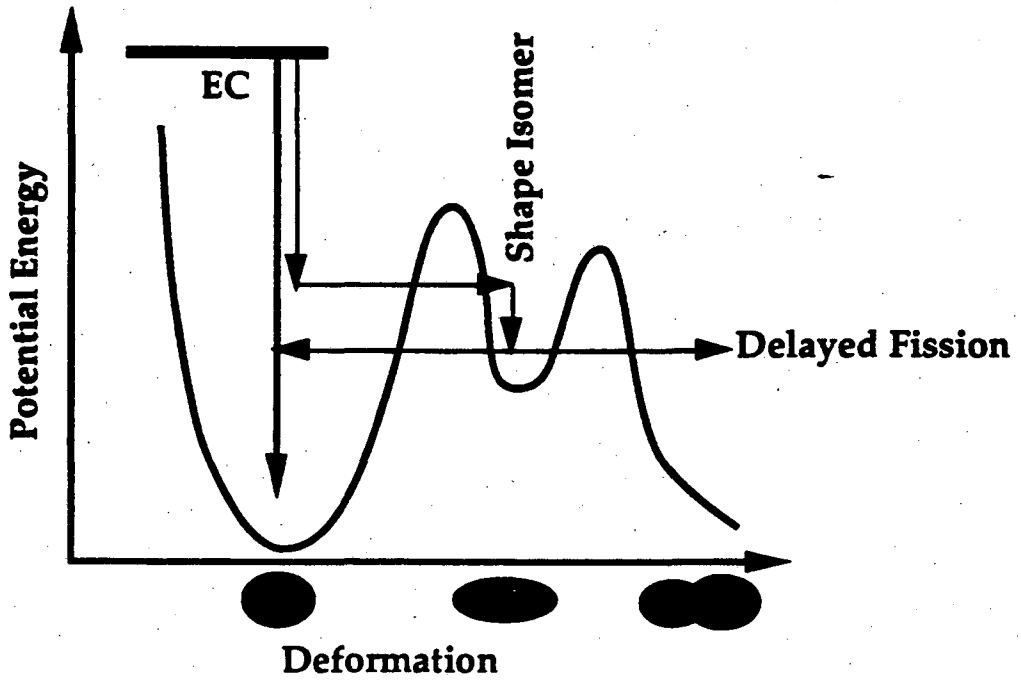

Figure 1-2. Two-dimensional illustration of the delayed fission process.

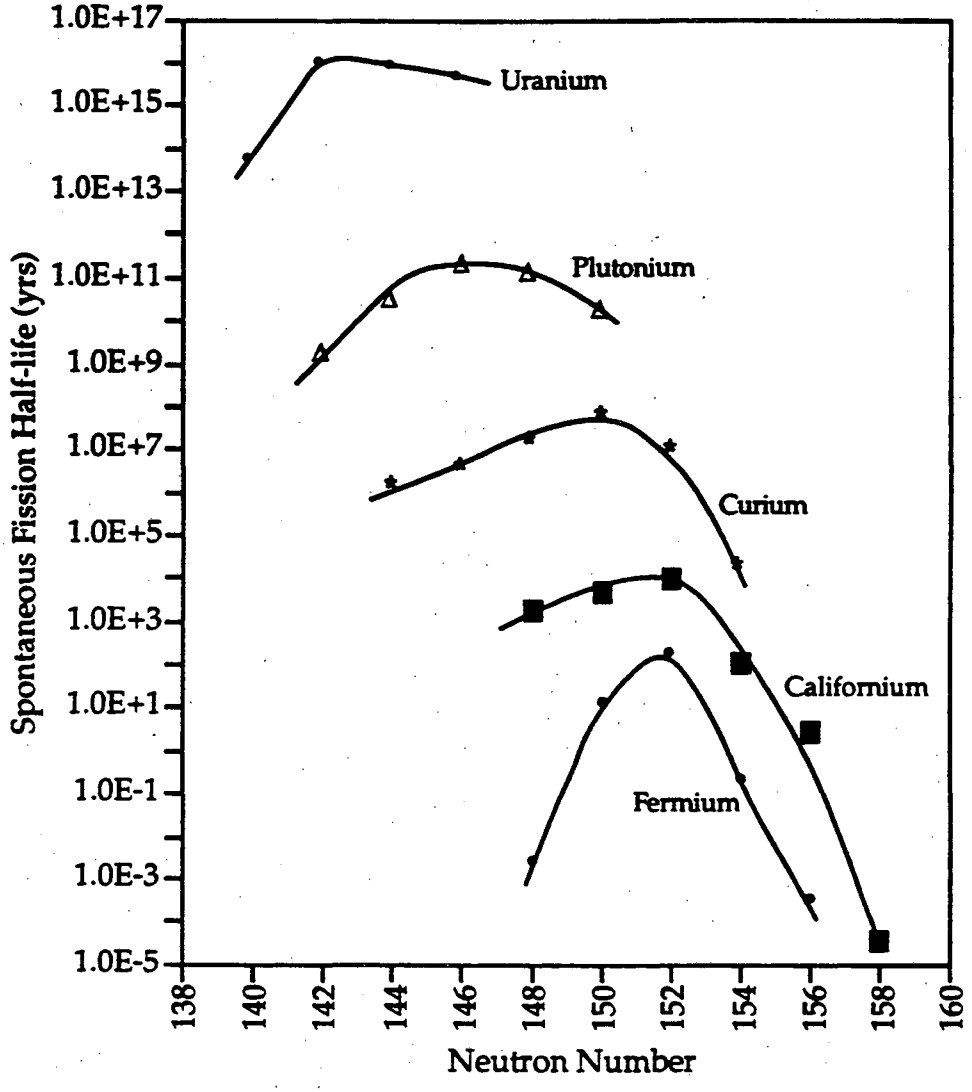

Figure 1-3. Plot of spontaneous fission half-lives for even-proton, even-neutron isotopes versus neutron number.

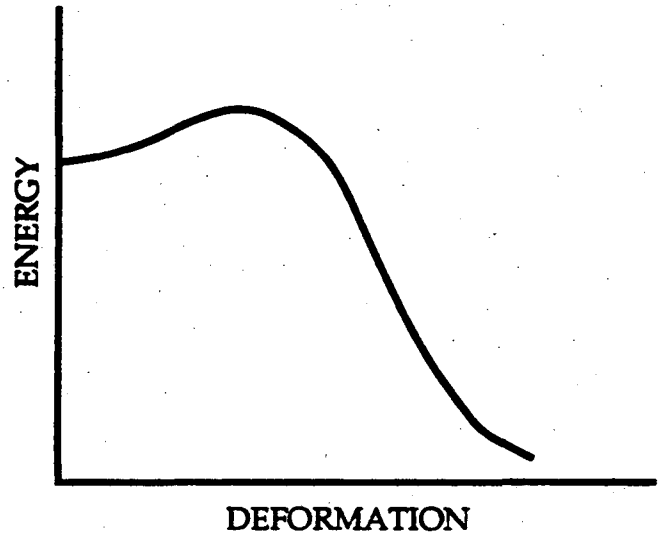

Figure 1-4. Liquid Drop Model potential energy with increasing deformation.

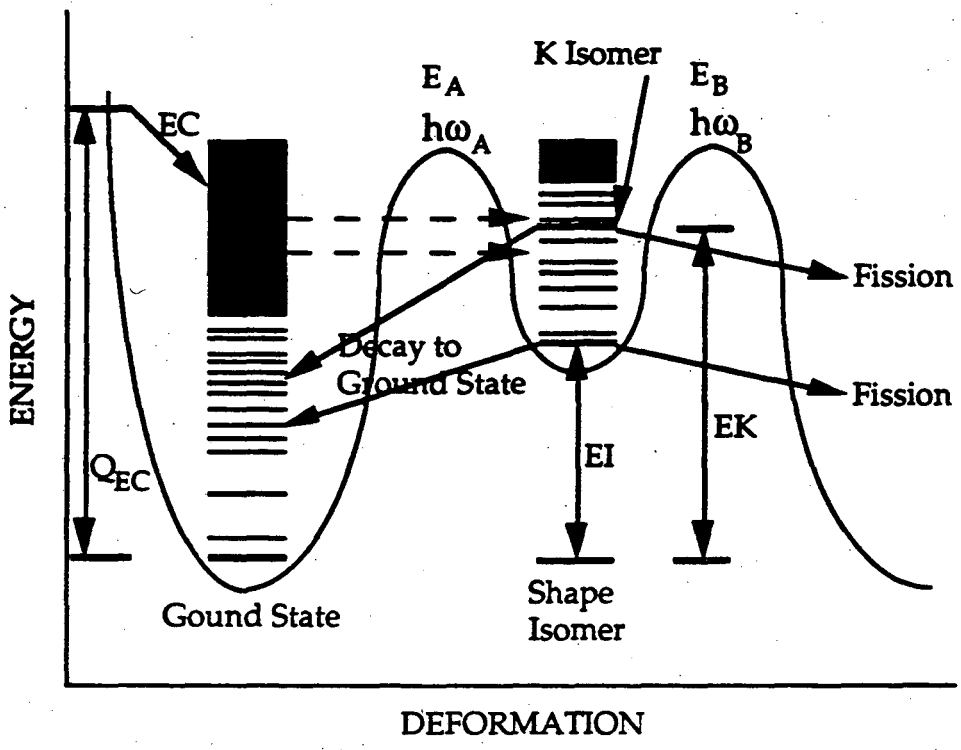

Figure 1-5. Schematic of how ECDF can be used to probe the fission barrier. EI is the energy of the lowest level in the shape isomer; EK is the energy of the K-isomeric level in the second well; Q_{EC} is the electron capture Q-value.

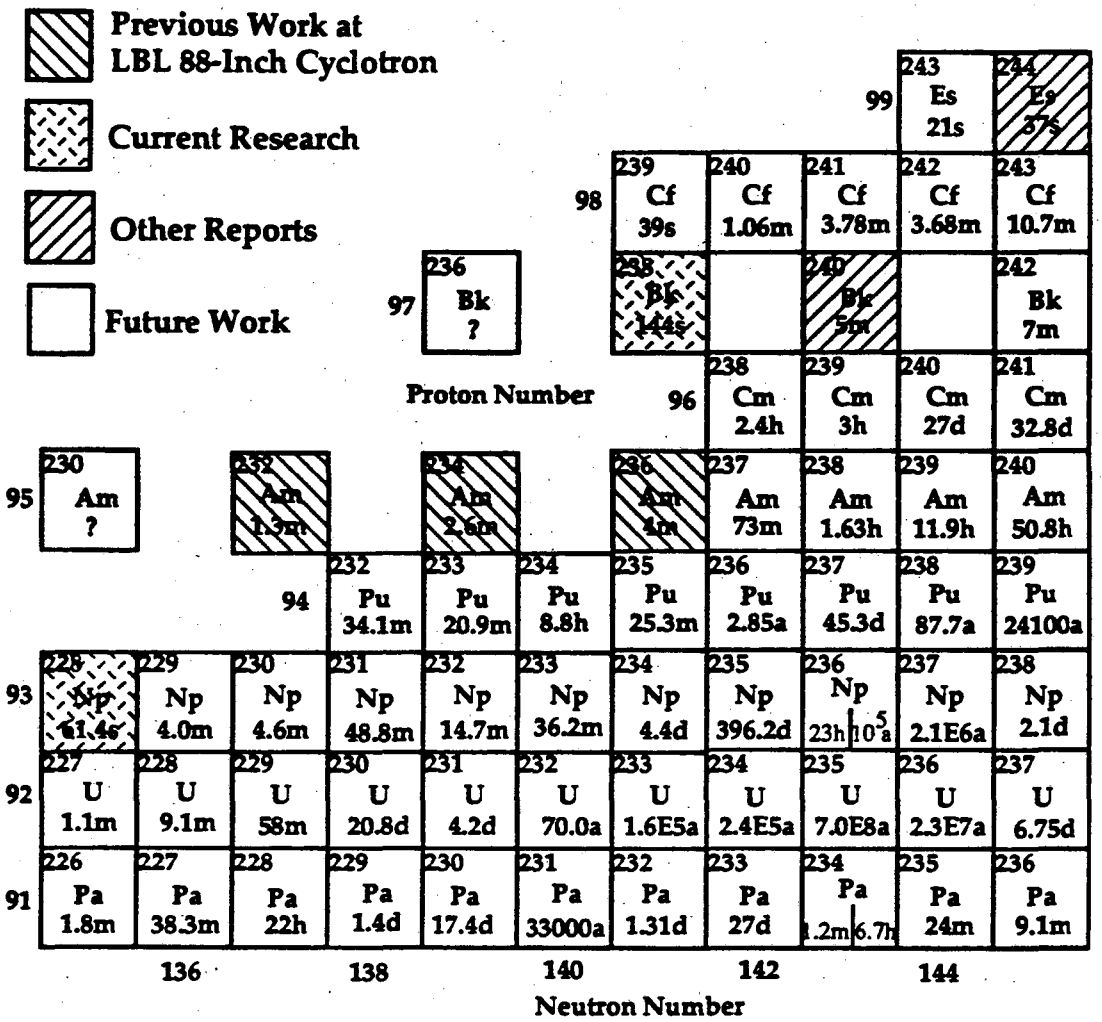

Figure 1-6. Actinide region where isotopes may have significant delayed fission probabilities.

2 Previous Work

2.1 Bk Studies

2.1.1 Previous Delayed Fission Studies

Electron-capture delayed fission in the Bk region was first examined by Gangrskii et al. in 1980 [Gangrskii, 1980]. Along with other elements, the delayed fission probabilities of ^{240,242}Bk were reported which were produced in the ^{232}Th(93-MeV ^{14}N, 6n)^{240}Bk and ^{232}Th(75-MeV ^{14}N, 4n)^{242}Bk reactions, respectively. The isotopes were identified by observation of the alpha decay of the known ^{240,242}Cm EC daughters. Gangrskii et al. assumed that the contribution from Cm isotopes produced by proton emission from the compound nucleus is small and could be neglected in the reactions involving ^{14}N projectiles. This is acceptable for a mere estimation of the delayed fission probability. Gangrskii also assumed that the isotopes of interest decayed exclusively by electron-capture. This is a poor estimate as examination of the Chart of the Nuclides† in this region shows that alpha decay begins to dominate with decreasing neutron number. To determine the true delayed fission probability, as was illustrated by Hall et al. [Hall, 1990A], chemical separation and direct measurement of the ECDF parent is preferable.

The products were produced and studied via an inclined target technique. The Th targets were prepared with an unspecified technique, plated onto a water cooled Cu support, and irradiated with up to 50 eμA of beam at the U-300 cyclotron at the Joint Institute for Nuclear Research,

† General Electric Company, Chart of the Nuclides, 13 th edition, 1984.

Dubna. The fission fragments were detected, after suitable irradiation, by positioning the target in the immediate vicinity of a solid-state track detector consisting of 15 micron lavsan polyester films. The films were replaced at known time intervals during the decay so that half-life information could be obtained. The films were etched and the half-life of the species determined from the number of fission tracks, measured with an optical microscope, per detection film.

Fission backgrounds in the track detectors were attributed to the following sources:

1. Delayed neutrons from fragments of prompt fission of the target material, which can produce fission of target nuclei during the measurement time.
2. Fission induced by energetic gamma-rays emanating from fission fragments produced in the bombardments.
3. Fission induced by energetic gamma-rays emanating from species produced by the interactions of the beam with the target support material (Cu).
4. Fission from the target material and incidental daughter products of the reactions.

The fission backgrounds associated with 1 and 2 were removed by a sufficient delay time between the end of the bombardment and the beginning of the track detector measurements (10 minutes). The half-lives of the ^{240}Bk and ^{242}Bk are relatively long so as to allow this delay. The contribution from 3 was eliminated by replacement of the Cu target support material with Al, which produced significantly less high energy gamma-ray activity. Item 4 was estimated by analysis of the alpha spectra of the activity from the target, and shown to be insignificant (when the time of the measurements is taken into account). Comparison of the number of fissions remaining above the background with the alpha activity of the ^{242}Cm and ^{240}Cm daughters

allowed Gangrskii et al. to estimate the delayed fission probability for ^{240}Bk to be approximately 10^{-5} [Gangrskii, 1980]. Gangrskii et al. did not report the delayed fission probability for ^{242}Bk.

As may be obvious to the reader, this technique does not yield positive Z or A identification of the ECDF precursor. It also does not allow for the determination of the fission properties of the EC daughter. It was not until 1989 that a better technique for determining the delayed fission probability was developed [Hall, 1990A].

2.1.2 Previous Searches for ^{241}Bk and ^{252}Bk

To this date, no direct evidence for the existence of either ^{241}Bk or ^{252}Bk has been published.

Recently, in the case of ^{241}Bk, a paper of deduced levels and their spin/parity assignments of states populated by the alpha decay of ^{245}Es has been published [Hatsukawa, 1989]. The Es was produced via several reactions. The production reactions are ^{249}Cf(p, 5n)^{245}Es, ^{238}U(^{14}N, 7n)^{245}Es, ^{237}Np(^{12}C, 3n)^{245}Es, and ^{233}U(^{14}N, 2n)^{245}Es. No data yielding the direct observation of the decay of ^{241}Bk have been published. It should be possible to determine the ^{241}Bk half-life with a technique such as that used in the discovery of ^{253}Md [Kadkhodayan, 1991]. In the technique of Kadkhodayan et al., a growth curve of the known daughter of the isotope under study is constructed by varying the time of irradiation and determining the activity of the daughter as a function of the irradiation time. Chemistry is performed to isolate the element of interest. With several irradiation times, determination of the daughter activity yields a growth curve for the daughter. If the amount of beam impinging on the target(s) is known, and if the irradiation times were chosen such that saturation was achieved, and if sufficient statistics are

available, it is possible to determine the half-life of the parent and the production cross section. This was first achieved by Kadkhodayan et al. in 1991 in the discovery of ^{253}Md [Kadkhodayan, 1991].

Two recent works have been published concerning ^{252}Bk. The work of Kupriyarov [Kupriyarov, 1984] included information pertaining to the fission cross-section with fast neutrons as calculated with a statistical approach using a double-humped fission barrier. In the work of Magda [Magda, 1987], the expected production cross-section in cluster transfer reactions between ^{248}Cm and ^{238}U at 7.4 MeV/A was calculated. No data on the direct observation of the decay of ^{252}Bk have been published. This is difficult because ^{252}Bk is likely to be a beta emitter. It should be possible to determine the ^{252}Bk half-life with a technique such as that used in the discovery of ^{253}Md [Kadkhodayan, 1991].

2.2 Np Studies

2.2.1 Previous Delayed Fission Studies

Electron-capture delayed fission in the Np region was first examined by Kuznetsov et al. in 1967 [Kuznetsov, 1967] and Skobelev in 1972 [Skobelev, 1972]. Further studies of the fissioning species were done by Somerville et al. in 1978 [Somerville, 1976], [Somerville, 1978].

Kuznetsov et al. [Kuznetsov, 1967] produced a 60-second fissioning activity, presumably ^{227,228}Np, in reactions of 110-MeV ^{22}Ne with a ^{209}Bi target. The production reaction is ^{209}Bi(^{22}Ne, 3n or 4n)^{227,228}Np. The isotopes were produced using an inclined target technique of 2 mg/cm^2 Bi with detectors above and below the target.

The target was bombarded at an angle of 12° for 4 minutes with a ^{22}Ne beam current of 160 μA. The beam was turned off and fissions measured by

positioning four glass-plate, fission-fragment detectors over the target, each for a period of 60-seconds. The detectors began measuring fission events 3 seconds after the end of bombardment. The delay eliminated the observation of short-lived fission activities. A species with a half-life of 60 ± 5 seconds was observed. The fission background in the track detectors was measured by determining the number of fission tracks observed at the surfaces on which the fission fragments from the nuclei produced could not impinge.

The isotopic identification as either ^{227}Np or ^{228}Np came from excitation function and cross bombardment reaction techniques. The shape of the excitation function of the fissioning species provided evidence that the reaction proceeded via a compound nucleus and neutron evaporation mechanism. The excitation function was determined with a thin target and the production cross section determined to be 0.45 ± 0.08 nb. The possibility of producing fissioning U isotopes by the ^{209}Bi(^{22}Ne, p3n) or ^{209}Bi(^{22}Ne, p2n) reactions was eliminated by studies of the ^{208}Pb(^{22}Ne, 3n) and ^{208}Pb(^{22}Ne, 4n) reactions. The fissioning species was not produced in these reactions. Other reactions of the type ^{209}Bi(^{22}Ne, α3n) were eliminated as the source for the fissioning activity in studies of ^{209}Bi reactions with ^{18}O projectiles. The fissioning species was not produced in these reactions. Therefore, Kuznetsov et al. concluded that the fissioning species must be ^{227}Np or ^{228}Np.

In the studies by Somerville et al. [Somerville, 1976] [Somerville, 1978], ^{227,228}Np were produced in two reactions. The production reactions are ^{209}Bi(115-MeV ^{22}Ne, xn) and ^{233}U(55-85 MeV ^{10}B, xn). They produced a fissioning species with a half-life of 51-seconds. Again, however, no positive evidence for Z and A assignment by correlations with known progeny activities was offered.

The technique of cross bombardment reactions, while useful, does not yield positive Z or A identification of the ECDF precursor. The technique of fission track detectors does not allow determination of the fission properties of the EC daughter. It was not until 1989 that a better technique for determining the delayed fission probability and giving proof of the ECDF mechanism was developed [Hall, 1989B]. This method used thin sources on polypropylene to measure the fission properties, an x-ray–fission coincidence technique to give direct evidence for the ECDF mechanism, and chemical separations to give positive proof of the Z and A of the ECDF precursor [Hall, 1990A], [Hall, 1990B].

3 Experimental

3.1 Target Preparation

3.1.1 Americium Targets

The ^{241}Am targets were prepared by electrodeposition [Bedov, 1956], [Evans, 1971], [Aumann, 1974], [Müllen, 1975] on 0.5-mil (2.32 mg/cm^2) Be foil. Beryllium was chosen because it was necessary to use target backings that would withstand large beam intensities, minimize beam energy degradation, and would be mechanically strong.

A sample containing 150 mg ^{241}Am was obtained in the form of Am_2O_3. It was dissolved in about 3 mL concentrated HCl and dried. The $AmCl_3$ was redissolved in 1 mL 0.1 M HCl and extracted into 1 mL 0.5 M HDEHP in heptane [Knauer, 1968], [Higgins, 1960], [Peppard, 1957A]. The Am^{3+} is extracted into the HDEHP while other impurities such as Na^+ remain in the aqueous phase. The HDEHP phase was removed and Am^{3+} back extracted into 1 mL concentrated HCl. The Np^{5+} daughter remained in the HDEHP phase. The solution of $AmCl_3$ was dried and converted to $Am(NO_3)_3$ by adding 1.0 mL concentrated HNO_3 and drying. This process was repeated several times. The conversion to the nitrate form was required because the Be foil is subject to chemical attack by chloride. This would reduce the effectiveness of the plating procedure and make the resulting target unsafe for bombardment in the accelerator. An aliquot of the final Am^{3+}–HNO_3 solution was dried and the $Am(NO_3)_3$ dissolved in 1.0 mL isopropanol (IPA). An aliquot of the IPA solution was dried on Pt foil and

assayed by alpha-pulse-height analysis. A flow diagram of the procedure is given in Figure 3-1.

The electroplating cell was prepared by placing about 1 mL of clean IPA in the Teflon chimney (see Figure 3-2). An appropriate amount of the $Am(NO_3)_3$–IPA solution was added so that a target of about 100 $\mu g/cm^2$ would be produced. The Teflon chimney had an i.d. of 0.95 cm, which yields a 0.71 cm^2 target. The Am was electroplated from the IPA at 0.8 mA and 300 volts for 30 minutes on the 2.32 mg/cm^2 Be backings. The Be foil was kept at a negative potential by attaching the negative pole of the power supply to the base of the electroplating cell. The positive electrode was a Pt wire which also served as a mixer. The electroplated sample was then baked in an oven at 400 °C for 30 minutes to convert it to the oxide. The targets were glued to Al supports for use in the target system (see Section 3.2). Figure 3-2 is a schematic of the electrodeposition cell.

The thicknesses of the ^{241}Am targets were determined by gamma-ray analysis with a Ge detector. The efficiency of the Ge detector for detecting 60 keV photons from the ^{241}Am was determined with a National Bureau of Standards (NBS) linked ^{241}Am γ-ray source at a distance of 25 cm. The activity of this source was 449.8 dps. To obtain sufficient statistics, the standard was measured for 45 minutes. The efficiency of the Ge detector was 5.33×10^{-4}. The 60 keV γ-ray of the sealed ^{241}Am targets was measured in the same geometry as the ^{241}Am standard. Ten targets were prepared and assayed in this manner. Table 3-1 lists the thicknesses of the ^{241}Am targets.

3.1.2 Uranium Targets

The ^{233}U targets were electroplated in the same manner as the ^{241}Am targets (see Section 3.1.1). However, the following procedure was used to

Table 3-1. Thicknesses of the ^{241}Am targets as determined by γ-ray analysis.

Sample Number	Activity (cpm)	Thickness (μg/cm^2)
^{241}Am Standard	5.1	n/a
^{241}Am-4	9.43×10^4	91.45
^{241}Am-5	9.85×10^4	95.56
^{241}Am-7	9.95×10^4	96.54
^{241}Am-8	1.03×10^5	99.72
^{241}Am-9	9.34×10^4	90.62
^{241}Am-10	9.72×10^4	94.25
^{241}Am-11	1.04×10^5	100.93
^{241}Am-12	1.04×10^5	100.90
^{241}Am-13	9.71×10^4	94.19
^{241}Am-14	8.13×10^4	78.87

purify the U prior to electrodeposition.

Approximately 10 mg of ^{233}U was obtained from the Nuclear Chemistry Division (Batch ORNL-27, 4.2 ppm ^{232}U) at Lawrence Livermore National Laboratory and purified by anion exchange chromatography. The ^{233}U was dissolved in concentrated HCl and sorbed onto an anion exchange column (AG 1-X8 resin, 1 cm x 15 cm) from concentrated HCl. Several column volumes of concentrated HCl were passed through the column followed by several column volumes of 2 M HCl to elute contaminants as well as the ^{233}U progeny activities. The column was converted to the nitrate form by elution with several column volumes of 6 M HNO_3. The ^{233}U was eluted from the column with several column volumes of 0.1 M HNO_3 into a

glass centrifuge cone and dried. The dried uranium was dissolved in isopropanol (IPA) to yield a solution of approximately 1 mg/mL ^{233}U.

Approximately 50 μL of the ^{233}U solution was placed in the Teflon chimney of the electroplating cell with about 1 mL IPA (see Figure 3-2). The Teflon chimney had a 0.95 cm i.d. which yields a 0.71 cm^2 target. The uranium was electroplated on 4.65 mg/cm^2 Be foil at 400 volts for 30 minutes. The resulting target was dried and heated in an oven at 400 °C for 30 minutes to convert it to the oxide. Twenty-three targets were prepared in this manner. The targets were assayed using a low geometry surface barrier detector with a 0.6245-inch collimator operated in He with a detection efficiency of 8.2×10^{-4} The thicknesses of the targets were calculated and are listed in Table 3-2.

3.1.3 Curium Target

The ^{248}Cm (97.44% ^{248}Cm, 2.53% ^{246}Cm, 0.025% ^{245}Cm, 0.010% ^{247}Cm, and 1×10^{-4}% ^{244}Cm) was electroplated on a 2.09 mg/cm^2 Be backing in the same manner as the ^{241}Am targets (see Section 3.1.1). Figure 3-1 is a flow diagram of the chemistry used to purify the Cm before electrodeposition. The target was produced by electroplating and then baking layers approximately 50 $\mu g/cm^2$ each. The Teflon chimney used had a 0.6 cm i.d. of which yields a 0.28 cm^2 target. The target was dried and baked to convert it to the oxide after the application of each layer to avoid flaking and keep the target uniform. The Cm_2O_3 target was assayed by alpha-pulse-height analysis using a low-geometry surface barrier detector in the same manner as the ^{233}U targets and determined to contain 0.65 mg/cm^2 ^{248}Cm.

Table 3-2. Thicknesses of the ^{233}U targets as determined by low geometry alpha-pulse-height analysis.

Target Number	Activity (dpm)	Thickness ($\mu g/cm^2$)
A-1	2.06×10^6	75.7 ± 0.03
A-2	2.12×10^6	78.2 ± 0.03
A-3	1.39×10^6	51.1 ± 0.03
A-4	1.47×10^6	54.1 ± 0.03
A-5	1.43×10^6	52.6 ± 0.03
A-6	1.49×10^6	54.9 ± 0.03
A-7	1.43×10^6	52.6 ± 0.03
A-8	1.46×10^6	53.9 ± 0.03
A-9	1.44×10^6	52.9 ± 0.03
A-10	1.48×10^6	54.5 ± 0.03
A-11	1.32×10^6	48.5 ± 0.03
A-12	1.45×10^6	53.4 ± 0.03
A-13	1.50×10^6	55.1 ± 0.03
A-14	1.42×10^6	52.4 ± 0.03
A-15	1.42×10^6	52.5 ± 0.03
A-16	1.49×10^6	54.8 ± 0.05
A-17	1.52×10^6	55.8 ± 0.05
A-18	1.42×10^6	52.3 ± 0.05
A-19	1.49×10^6	54.9 ± 0.05
A-20	1.51×10^6	55.4 ± 0.05
A-21	1.37×10^6	50.6 ± 0.05
A-22	1.50×10^6	55.4 ± 0.05
A-23	1.51×10^6	55.7 ± 0.05

3.2 Irradiations

3.2.1 Lawrence Berkeley Laboratory 88-Inch Cyclotron

All ion beams used in this work were provided by the 88-Inch Cyclotron located at the Lawrence Berkeley Laboratory (LBL). The 88-Inch Cyclotron is a sector-focused cyclotron capable of generating relatively large beam currents of many different ions. Beams ranging in mass from protons to ^{238}U have been achieved at moderate intensities.

Beam energies are given in the laboratory system and refer to the energy in the target material unless otherwise stated. Two types of target systems were used. A multiple target array was used in the light ion bombardments to produce ^{238}Bk, ^{241}Bk, and ^{228}Np. A single target was used in the ^{18}O bombardments to produce ^{252}Bk and ^{253}Bk. The targets in all the bombardments were radioactive requiring a 4.65 mg/cm^2 Be foil as the vacuum window to isolate the targets from the rest of the cyclotron. A Faraday cup was used to measure target beam current throughout all experiments and the integrated charge was recorded periodically.

3.2.2 Single Target Bombardments

A schematic of the single target arrangement used in the ^{18}O irradiations is given in Figure 3-3. The beam enters the target system through a 6 mm collimator, passes through an 8 mm Be vacuum window, which is cooled by N_2, through the target, and into the recoil chamber (see Figure 3-3). The beam stop composed of graphite. The vacuum window is used to isolate the radioactive targets from the rest of the cyclotron. The collimator and beam stop are composed of graphite to reduce neutron production and make the irradiation area less hazardous to the experimenter. The beam stop and collimator are cooled by water. A He/KCl transport system, with the He

flowing at 2 liters/minute, is attached to the recoil chamber to sweep the produced activities out of the target system to the collection site through a 1.2-mm i.d. polyvinyl chloride capillary. The KCl aerosols are generated by passing the He stream over a small quantity of fresh KCl heated in an oven which is maintained at 650°C. The maximum recoil collection yield and optimum KCl oven temperature were determined using 4.8-min ^{221}Fr recoils from a ^{225}Ra/^{225}Ac source in-line with the He/KCl transport system. The yield varied between 50% and 80% depending on the length of the capillary.

3.2.3 The Light Ion Multiple Target System

For the production of neutron-deficient actinide isotopes at reasonable rates, light ion bombardments are desirable because of the relatively large production cross sections. Light ions, however, produce products with small recoil ranges. To avoid using complicated and time consuming thick-target techniques, it was desirable to use the Light Ion Multiple Target system (LIM) [Hall, 1989A]. This system allows the bombardment of up to 23 targets simultaneously in an array. Using the recoil products from many thin targets increases the effective target thickness over that of a single thick target. The recoiling products are continuously swept from between the targets, and out of the target chamber by a He/KCl aerosol jet with the He flowing at 2 liters/minute. The KCl aerosols are generated in the same manner as in the single target bombardments. The activity laden KCl aerosols are collected for chemical separation or direct analysis. Figure 3-4 is a schematic of the LIM system.

The targets can be stacked at a distance of roughly twice the recoil range of the compound nucleus in He. In the case of the ^{4}He bombardments of ^{241}Am, the targets were positioned about 2-cm apart. In the case of the proton

bombardments of ^{233}U, the targets were placed about 1-cm apart. The compound nucleus product ranges can be estimated with tables provided in [Hubert, 1980] or others. Fission products produced during the irradiation have significantly larger production cross sections and recoil ranges in He than the compound nucleus. Separating the targets by twice the compound nucleus recoil range results in the majority of the fission products being deposited in the back of the next target in the array [Hall, 1989A]. This has the effect of reducing the amount of beta–gamma activity at the KCl aerosol collection site. The beam stop and collimator are graphite and water cooled (see Figure 3-4). Graphite was chosen to reduce the neutron levels in the experimental areas and to reduce activation of the target system. Because many of the chemical operations are performed manually, it is important to minimize the radiation exposure of the persons involved in the experiments.

3.2.4 Isotope Production

To produce the neutron-deficient Bk isotopes, ^{241}Am was chosen as the target material because it was both readily available and yielded relatively large production cross sections for ^{238}Bk and ^{241}Bk in bombardments by alpha particles. For similar reasons, ^{233}U was chosen as the target material to produce neutron-deficient Np isotopes in bombardments by protons. The appropriate bombarding energies and estimated production cross sections were calculated by the neutron evaporation code, SPIT [Haynes, 1988]. We have determined experimentally that the production cross sections calculated by SPIT are accurate to within an order of magnitude [Haynes, 1988] and are usually within a factor of 2 for 7- and 9-neutron-out reactions. Table 3-3 gives the maximum calculated production cross sections for ^{238}Bk and ^{241}Bk from the reactions of ^{241}Am with alpha particles and ^{228}Np from the reactions of

^{233}U with protons. Figure 3-5 shows the SPIT calculated excitation functions for the production of ^{238}Bk, ^{241}Bk, and ^{228}Np. Table 3-4 gives the production reactions, bombarding energies, and beam intensities used to produce ^{238}Bk, ^{241}Bk, and ^{228}Np.

Table 3-3. Calculated Bk and Np production cross sections.

Projectile Energy (MeV)	^{238}Bk σ (cm^2)	^{241}Bk σ (cm^2)	^{228}Np σ (cm^2)
76	0.25E-30		
46 or 48		0.10E-26	
51			0.25E-28

Table 3-4. Production information for ^{238}Bk, ^{241}Bk and ^{228}Np. a) The Bk isotopes were produced in bombardments of ^{241}Am targets via $^{241}Am(^4He, 7n)\ ^{238}Bk$, and $^{241}Am(^4He, 4n)^{241}Bk$ reactions. The Np isotopes were produced in bombardments of ^{233}U targets via the $^{233}U(p, 6n)^{228}Np$ reaction.

Isotope	Production Reaction	Beam Energy (MeV)	Intensity (pμA)	# of Targets in LIM
$^{238}Bk^a$	$^{241}Am(\alpha,7n)^{238}Bk$	73	3-4	9
$^{241}Bk^a$	$^{241}Am(\alpha,4n)^{241}Bk$	48	4-5	4
$^{228}Np^b$	$^{233}U(p,6n)^{228}Np$	49	4-6	23

The targets used in the production of ^{238}Bk, ^{241}Bk, and ^{228}Np were positioned in the LIM system. The LIM was installed in the beam line in Cave 0 at the 88-Inch Cyclotron at LBL and connected to the He/KCl aerosol

jet system. Beam degradation through the target stack was not important because alpha particles and protons lose less than about 300 keV and 150 keV/target, respectively, in the thin Be backings. The alpha and proton beam energies were degraded through the cyclotron and vacuum windows by about 2 MeV and 1 MeV, respectively. This was estimated from the range tables of Hubert et al. [Hubert, 1980]. The recoils and KCl aerosols were transported through the 1.4 mm i.d. polyvinyl chloride capillary to the mezzanine hood above Cave 0 for chemical separation and analysis or to an x-ray–fission apparatus or to a rotating wheel system (see Section 3.4).

For the production of ^{252}Bk and ^{253}Bk, the ^{248}Cm target was bombarded in the single target system with 125-MeV $^{18}O^{5+}$ (machine) from the 88-Inch Cyclotron at LBL at an intensity of 500 pnA. This corresponded to about 107 MeV after passing through the target. The recoils were transported through a 1.4 mm polyvinyl chloride capillary to the mezzanine hood above Cave 0 for chemical separation and alpha-pulse-height analysis or placement into a beta–L x-ray coincidence apparatus (see Section 3.3.1.1.3).

The transfer reactions in the production of ^{252}Bk and ^{253}Bk involve the respective transfer of a ^{4}H or ^{5}H from the projectile to the target. The projectile energy was chosen after an analysis of the ^{1}H, ^{2}H and ^{3}H transfer reaction cross sections and heavy product excitation energies given in [Leyba, 1990] and [Hoffman, 1990A].

3.3 Chemical Procedures

3.3.1 Manual Separations

3.3.1.1 HDEHP Separations of Bk

The well known $3^{+}/4^{+}$ redox couple in Bk is of particular use in the separation of Bk from all trivalent actinides. Samples containing Bk can be

oxidized with aqueous oxidants such as $KBrO_3$ in concentrated HNO_3 and the Bk^{4+} extracted with an organic complexing agent such as HDEHP. This complexing agent is well known for its ability to extract all 3^+ and higher charge ions from dilute acid solutions and all 4^+ and higher charge ions from concentrated acid solutions [Knauer, 1968], [Higgins, 1960], [Peppard, 1957], [Peppard, 1957A]. The HDEHP phase can be isolated and the Bk^{4+} reduced to Bk^{3+} with an appropriate reducing agent such as H_2O_2 in dilute acid. The Bk is back extracted into the dilute acid phase while all other species of higher oxidation state remain in the organic phase. Figure 3-6 is a flow chart of the chemistry used to isolate Bk from all trivalent actinides. Cerium is not separated from Bk in this procedure because of its similar $3^+/4^+$ oxidation state couple. The chemical formula and structure of HDEHP is given below.

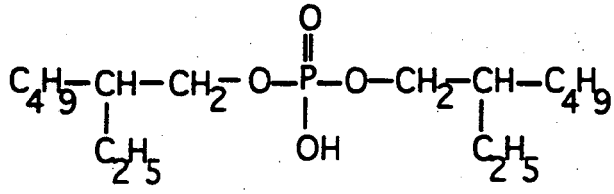

The HDEHP behaves as an acid with one acidic hydrogen. It has been shown that the HDEHP is probably dimerized [Knauer, 1968], [Higgins, 1960], [Peppard, 1957], [Peppard, 1957A] in the organic phase. This yields the following likely complexing reaction with the metal ion.

$$Bk^{4+}_{aq} + 4\,(HDEHP)_{2org} \longleftrightarrow Bk[H(DEHP)_2]_{4org} + 4H^+$$

The deprotonated form of HDEHP is designated as DEHP.

3.3.1.1.1 Daughter Milking Technique for ^{241}Bk, ^{252}Bk and ^{253}Bk

To discover ^{241}Bk, ^{252}Bk and ^{253}Bk, a growth experiment similar to that found in [Kadkhodayan, 1991] was performed. This technique involves varying the irradiation time and separating the Bk from all trivalent actinides using an HDEHP separation. The half-lives of the ^{241}Bk, ^{252}Bk and ^{253}Bk can

be determined from the growth of the ^{241}Cm, ^{252}Cf and ^{253}Es, daughters of ^{241}Bk, and ^{252}Bk and grand-daughter of ^{253}Bk, respectively, as a function of the irradiation interval. In the case of ^{253}Bk, the ^{253}Cf alpha branch was too small to make observation practical. The ^{253}Es grand-daughter has a 6.6-MeV alpha which should be well separated from all other alpha activities in the sample.

In the search for ^{252}Bk and ^{253}Bk, the collection times were 1, 3, 10, and 20 minutes. The samples were dissolved in 25 λ of HNO_3 and 25 λ of a saturated $KBrO_3$ solution and the Bk extracted into 50 λ of a 0.5 M HDEHP solution in heptane in a procedure similar to that shown in Figure 3-6. The reduction and back extraction step, however, was not performed. Instead, the organic phases were stored according to the irradiation interval. A tracer containing ^{243}Am was used in the HNO_3 to ensure that the daughters observed later were a result of the Bk decay and not contamination from trivalent actinides. After about 1 hour, the Bk daughters were back extracted with 3 M HCl. No H_2O_2 was necessary because the Bk daughters are 3+ ions. Without the reduction, the amount of ^{250}Cf and ^{248}Cf in the samples is reduced, because not enough time is allowed for all of the ^{250}Bk and ^{248}Bk to decay.

The samples were later electroplated via the method of [Hoffman, 1990B] on Pt for alpha-pulse-height analysis of the known ^{252}Cf and ^{253}Es. Figure 3-7 is a flow diagram of the procedure used to purify the samples before electrodeposition. This was necessary because evaporated samples proved to be too thick to yield good alpha resolution. The samples were thick, and did not allow resolution of the alpha peaks of ^{252}Cf, ^{250}Cf and ^{248}Cf. The ^{248}Cm target used in the bombardment was coated with a layer of ^{nat}Gd, for use in another experiment. No attempt to remove the Hf, made from the

interactions of the ^{18}O projectiles with the ^{nat}Gd coating on the ^{248}Cm target, was attempted because the Hf is a 4+ ion and was not back extracted from the HDEHP. Also, the Hf isotopes produced are short lived compared to the Cf. A small amount of a beta activity will not interfere significantly with the alpha-pulse-height analysis.

The electrodeposition procedure used in the ^{252}Bk and ^{253}Bk studies involved the aqueous deposition of the sample on Pt from a dilute NH_4Cl solution [Hoffman, 1990B]. The pH of the solution, adjusted with dilute HCl to be slightly acidic to methyl red, was placed in the electroplating cell shown in Figure 3-2, and the sample plated at a potential of 6.2 Volts and a current of about 60 mA for 30 minutes. The sample was washed several times with water and isopropanol, dried, flamed and mounted on a counting card for alpha-pulse-height analysis.

In the search for ^{241}Bk, the collection times were 1, 3, 5, and 10 minutes. The Bk was isolated and the organic phase stored as described earlier. The Cm^{3+} daughters were back extracted from the HDEHP with 3 M HCl. The 3 M HCl phases from the back extractions were later dried and flamed on Pt for alpha-pulse-height analysis of the known 32.8-day ^{241}Cm daughter. Because the quality of the flamed samples was poor, the activity was removed from the Pt and purified with a cation exchange technique prior to electrodeposition as shown in Figure 3-8.

In this purification procedure, the samples, after removal from the Pt, were dried in 1 mL plastic centrifuge cones under a heat lamp. The samples were dissolved in several drops of concentrated HCl and dried. This step was repeated several times because residual fluoride would interfere with the cation exchange chemistry. The samples were then dissolved in 0.5 M HCl and sorbed on a column (2 mm i.d. by 4.5 cm long) of AG MP-50 cation

exchange resin, 200-400 mesh. The free column volume (FCV) was 60 μL. The column was washed with several FCVs of 0.5 M HCl followed by several FCVs of 4.0 M HCl. The Cm was stripped from the column with 8 FCVs of concentrated HCl and dried. The samples were dissolved in 1 mL IPA and electroplated on Pt in the same manner used to prepare the ^{241}Am targets (see Section 3.1). The electroplated samples were dried, flamed and counted by alpha-pulse-height analysis.

3.3.1.1.2 ^{238}Bk Separation for ECDF Studies - Z and A Assignment

Determination of the electron-capture branch as well as a positive identification of the Z and A of the ECDF precursor requires a chemical separation of the Bk from all other potentially fissioning activities (actinides) produced in the bombardment. Detection of fissions in the Bk fraction as well as analysis of the ECDF x-ray–fission coincidences will positively assign the ECDF precursor to an isotope of Bk. Identification of the known ^{238}Bk EC and alpha daughters, 2.4-hour ^{238}Cm and 2.32-minute ^{234}Am, respectively, would assign the mass number as 238. This also yields the EC/alpha branching ratio. Knowledge of the EC/alpha branching ratio is required for determination of the delayed fission probability. The isolation procedure for Bk is shown in Figure 3-6. The final aqueous phase containing the Bk was removed, dried on Ni foils and flamed. Ni foil was chosen because it is relatively inexpensive and is also tolerant to the flaming required to make the source 'safe' for removal from the chemistry hood. Flaming also destroys any residual organic material and produces thin sources suitable for alpha-pulse-height analysis. The sample was counted for both alpha and fission activities by pulse-height analysis.

3.3.1.1.3 Beta–L x-ray Experiment - Study of ^{252}Bk

In previous studies [Fields, 1973] of ^{252}Cf, the beta-decay daughter of ^{252}Bk, it was noted that the electron-capture decay of ^{252}Es populates levels about 900 keV above ground in ^{252}Cf which all (>98%) deexcite through the 2^+ rotational state built upon the K=0 ground state. In the study by Fields et al., it was noted that the 45.7-keV gamma-ray associated with the deexcitation of this 2^+ state in ^{252}Cf was highly L converted (>93%) and produced Cf L x-rays.

It was thought that the beta decay of ^{252}Bk to ^{252}Cf might follow a similar path. The Q-value associated with ^{252}Bk beta decay was estimated to be approximately 2.21 MeV from the 1986-87 mass evaluation found in Atomic and Nuclear Data Tables, 39, 289 (1987). Because the lighter Bk isotopes have Q-values for beta decay which are significantly lower than the expected 2.21 MeV for ^{252}Bk, and assuming the deexcitation of the ^{252}Cf daughter produces L x-rays, a possible means of detecting the ^{252}Bk would be to configure a beta–L x-ray coincidence system to detect beta particles in coincidence with Cf L x-rays.

The Bk was isolated with an HDEHP extraction similar to that shown in Figure 3-6, dried on a thin backing, and placed between a beta detector and a thin window Ge x-ray detector. As described in Section 3.3.1.1.1, the ^{248}Cm target was coated with a layer of ^{nat}Gd which produced various Hf isotopes that are very beta active and also would be extracted into the HDEHP phase. As a result, it was imperative that the Bk separation be performed so as to remove the Hf impurities from the final Bk fraction. Otherwise, the amount of beta activity from background activities would mask activities from the ^{252}Bk beta decay. To remove Hf, an additional extraction step was added to the procedure illustrated in Figure 3-6.

The KCl aerosols and activity were dissolved in 20λ of 1 M HNO_3 without an oxidizer. The Hf^{4+} was extracted into 20λ of the HDEHP phase leaving the Bk^{3+} in the aqueous phase. The organic phase containing the Hf was removed. To the aqueous phase 20λ of concentrated HNO_3 and 20λ of a saturated $KBrO_3$ solution were added. An HDEHP extraction was performed with 40λ and the organic phase dried on Al foil. It is important to note that the samples were dried on Al for placement in the beta–L x-ray correlation apparatus. Aluminum was chosen because a foil with a higher K shell edge might mask the L x-rays from the ^{252}Bk beta decay, and a low Z material was also needed so as to transmit as much of the L x-rays as possible. Pertinent data about the K-conversion energies in Al were obtained from [Browne, 1986] and the L x-ray stopping in Al was estimated from the table of photon interactions given in [Lederer, 1978].

A schematic of the beta–L x-ray detector system is shown in Figure 3-9. A schematic of the beta–L x-ray system electronics is illustrated in Figure 3-10. The beta particles were detected with a standard plastic scintillator (5 cm diameter), covered with aluminized mylar and connected to a photomultiplier. The L x-rays were detected with a thin window Ge x-ray detector. The Ge detector consisted of two thin, 3-mm, Ge crystals housed in the same cryostat. This allowed two samples to be counted simultaneously with the same scintillator. The system was configured so that when a beta particle was detected in the scintillation detector, any signal in the Ge detectors was recorded. The system also recorded γ-ray–γ-ray coincidences, but because of the unusual detector geometry, it was expected that these would be rare. A threshhold of about 1 MeV for incident beta particles was set to reduce the signal associated with beta decay of the lighter Bk isotopes. Assuming that sufficient statistics are obtained, it should be possible to extract a half-life for

the ^{252}Bk above the reduced background of the lighter Bks which are produced with much larger cross sections.

3.3.1.2. TTA Separation of ^{238}Bk - X-ray–Fission Analysis

The x-ray–fission correlation procedure used to study ^{238}Bk required an initial separation of all activities from monovalent Na produced in the interaction of the beam with the aluminum target holders due to a slight target system misalignment. The Bk and other activities were removed from the Na by extraction with 0.5M thenoyltrifluoroacetone (TTA) in benzene. This complexing agent is known to complex 3+ and higher oxidation state species quite readily from aqueous solutions between pH 4 and 5 [Poskanzer, 1961]. The produced activities were dissolved in a buffered solution of acetic acid and sodium acetate maintained at pH 5 and then extracted into the TTA. The organic phase was removed and evaporated on Ta foil for analysis. A typical separation time was 30 seconds.

3.3.1.3. ^{228}Np Chemistry

Neptunium was separated from uranium using an anion exchange procedure [Browne, 1973]. The samples from our He/KCl transport system were dissolved in 50 μL of concentrated HCl and sorbed on a 1-cm long by 2-mm i.d. anion column of Bio-Rad AG-1, X-8, 200-400 mesh anion exchange resin which had been pretreated with concentrated HCl. The column was washed with several column volumes of concentrated HCl and the Np fraction was eluted with 2.7 M HCl and collected and dried on Ta foil. The Np sample was flamed and counted for alpha and fission activities. The uranium was eluted from the column with 0.1 M HCl and saved for another experiment.

3.3.2. Automated Separations

3.3.2.1 Development of ACCESS

The Automated Chromatographic Chemical Element Separation System (ACCESS) [Kreek, 1992A] and Automated Injection System (AIS) [Kreek, 1992A] were designed for repeated high precision chemical separations of short-lived radionuclides.

These computer-controlled ion chromatography and injection systems are designed to provide a rapid and reproducible separation using established methods such as α-hydroxy isobutyrate (α-HIB) elutions from cation exchange resins or HDEHP reverse phase extraction chromatography. The system is modular, and can be used in either an off-line (manual injection) or on-line (AIS interfaced) configuration. ACCESS-AIS [Kreek, 1992A] is controlled by an IBM PC running a BASIC program. An analog to digital and digital to analog interface (Data Translation DT-2801) board in the PC provides 16 digital I/O ports, 8 ADC inputs and 2 DAC outputs. The digital outputs control two chemically inert pumps (Cheminert Kel-F Precision Pumps, model number CMP-1VK), another pump (Eldex Laboratories Dual Piston Pump, Kel-F Heads, model number AA-100-S), a 6-way valve (Eldex Laboratories Selector Valve, model number 1200), the pneumatically actuated slider valves used to direct the flow of solution through the system and the AIS. Chemical fractions of separated elements are collected with a fraction collector (Gilson Scientific, model number FC-203), which is controlled by the PC through a RS-232C serial interface. Figure 3-11 is a schematic of the ACCESS control-system.

Solvents are introduced by controlling the positions of pneumatic actuators (Rainin Instruments Tefzel Actuators, model number 201-57) which control slider valves (Rainin Instruments Tefzel 4-way slider valves, model

number 201-52). The sliders are chemically inert materials such as Delrin and the tubing between the valves is Teflon. Bores in the slider are positioned such that the solvents are forced to follow different paths as dictated by the user. The Teflon tubing has an i.d. of 0.5 mm. The tubing used to supply the N_2 to the pneumatic actuators is also Teflon with an i.d. of 0.8 mm. Teflon was chosen over other materials because of its relative resistance to aqueous chemical attack and the ease with which it can be connected to the system. All of the Teflon tubes are as short as possible to minimize dead volume and hence increase resolution and speed. The separation columns are constructed from precision-bore glass tubing and chemically inert column end fittings (Rainin Instruments Tube End Fittings, 1/16-inch inside diameter, model number 200-00). This permits optimization of the separation by varying the column length and solvent flow rates. A typical 2-cm length x 2 mm i.d. column has a free column volume of about 5 drops (13 μL/drop). The entire system has a void volume of about 50 drops, but is dependent on the configuration in use. Figure 3-12 is a schematic of the ACCESS configuration for a chromatographic separation employing a single column and the AIS.

ACCESS has been used in several experiments, including the identification of the previously unknown ^{253}Md [Kadkhodayan, 1991], and separation of Lr for study of the decay properties of ^{261}Lr [Henderson, 1990]. In both cases, ACCESS separated the elements by α-HIB elution.

The chemical yield through ACCESS is dependent on the chemistry used in the separation and the separation time (for short-lived species). The chemically inert surfaces of ACCESS provide nearly 100% transport efficiency of the activity. Using the lanthanides ^{171}Tm, ^{152}Eu, and ^{166m}Ho, we observed separation factors for α-HIB separations that were consistent with previous work [Choppin, 1956], [Smith, 1956]. The resolution of the measurements,

over those of previous work, was improved by using smaller drops (13 μL vs. 45 μL).

The implementation of ACCESS-AIS maximizes the use of accelerator time and allows for the collection of as much data as possible during the course of one experiment. This system also reduces the labor intensive nature of these experiments and increases the reproducibility over repeated rapid manual chemical separations.

3.3.2.2 Development of the Automated Injection System

The AIS is a pneumatically actuated device for automated collection of the products from a He/KCl gas jet transport system and injection of these products into ACCESS. Figure 3-13 is a schematic of the AIS. The reaction products from bombardments at the 88-Inch Cyclotron at Lawrence Berkeley Laboratory are transported out of the target system by KCl aerosols carried in He. The jet deposits the activity laden aerosols in one of two small collection sites on the surface of the Delrin bar (see Figure 3-13). An advantage of ACCESS-AIS is that while chemistry is being performed on one sample, another is being collected. After a preset collection time, the Delrin bar is pneumatically positioned so that the aerosol deposit is in-line with one of the two Delrin plugs which have solvent lines leading to and from ACCESS. The aerosol deposit is dissolved in the solvent and transported into ACCESS. The Delrin bar is pneumatically secured against o-rings by two plungers at the bottom so that solvent leakage is avoided. A vacuum pump connection at the collection site is perpendicular to the direction of the incoming He jet.

The AIS has been successfully interfaced with ACCESS and experiments have been performed to determine chemical yield through the AIS. The yield was determined using 4.8 m ^{221}Fr recoils from a $^{225}Ra/^{225}Ac$

source in-line with our He/KCl transport system. For yield normalization, the ^{221}Fr laden KCl aerosols were transported via a polyvinyl chloride capillary (1.2 mm i.d.) and collected on Ta foils for counting by alpha-pulse height analysis with a surface barrier detector. The He/KCl was then directed into AIS and collected for various time intervals. The collected KCl was positioned in-line with ACCESS by the AIS and solvent flow initiated. The sample was completely dissolved in about 60 λ of H_2O and deposited on a Ta foil for drying and activity determination. Several experiments were performed and the average yield, corrected for the decay of the ^{221}Fr, was determined to be 80 ± 9 %. Because the KCl can deposit anywhere on the Ta foil in the initial activity determination and only a 5 mm space is provided in AIS, it was necessary to install a capillary guide (see Figure 3-13) to ensure that the activity was deposited properly in the AIS. Any misalignment of the capillary will significantly reduce the efficiency of the system.

3.3.2.3 Automated Search for ^{241}Bk

A glass column (2-mm i.d. by 2-cm long) was filled with an HDEHP coated Matrex resin. This resin was prepared by dissolving 1 mL of 99% HDEHP in 200 mL of acetone and adding 50 g Matrex MP-50 cation exchange resin. While stirring, the acetone was allowed to evaporate leaving a resin coated with HDEHP. The column was installed in ACCESS and Ce/Eu tracers were used to determine the yield of the system.

The activity laden aerosols from the He/KCl transport system were dissolved in 10 μL of saturated $KBrO_3$ and 10 μL of conc. HNO_3. The sample was injected into the sample loop of ACCESS with a syringe (see Figure 3-12). The activity was directed onto the column with the LDC pumps and eluted with several column volumes of 3 M HNO_3. The Bk was eluted with a 1%

H_2O_2 solution in 3M HCl. The column was regenerated before each experiment with several column volumes of 3M HNO_3. Problems arose from the formation of air bubbles, presumably from the peroxide reductant, in the column reacting with residual oxidizing agent remaining on the column and this method was abandoned because the separations were not reliable. The formation of air bubbles in the column caused channeling of the solvents through the column and reduced the separation effectiveness. ACCESS proved very useful, however, for performing repeated chemical separations, which utilized other separation schemes on a rapid time scale.

3.4 Instrumentation

3.4.1 MG-RAGS - Fission Detection

Fissions were counted with the "Merry-Go-round Real-time Data Acquisition and Graphics System" (MG-RAGS) [Hoffman, 1980], [Leres, 1987]. The "Merry-Go-round" (MG) is composed of a wheel on which 80 polypropylene foils can be positioned around the periphery. Each foil is approximately 40 $\mu g/cm^2$ thick and is in turn rotated between six detector stations. Each station is composed of a pair of silicon detectors which can register alpha particles and fission fragments. This system has the advantage that while one sample is being collected, six others are being counted. The detector stations are illustrated in Figure 3-14. The "Real-time Data Acquisition and Graphics System" (RAGS) is then used to record and analyze the data from the twelve individual detectors. Figure 3-15 is a schematic of the MG-RAGS.

The activity-laden aerosols from the LIM system were collected for preset time intervals on the polypropylene foils and rotated between the six pairs of silicon detectors. One foil was removed from the wheel to allow time

to reset RAGS. A long collection on one polypropylene foil is hazardous because of the possibility of KCl and activity flaking off the foil upon removal of the wheel. After the wheel rotated so that the remaining 79 foils were used, the wheel and corresponding foils were replaced to avoid build up of the KCl and any long-lived activities.

Neutron-deficient Bk isotopes were produced at the Lawrence Berkeley Laboratory 88-Inch Cyclotron as described in Section 3.2. The recoiling products were carried on KCl aerosols swept in He to the MG. The foils were stepped at a preset interval of 2 minutes and positioned successively between the six pairs of silicon detectors which were held directly above and below the wheel. This arrangement gave an efficiency of approximately 60% for detection of coincident fission fragments. Energy and time information for each detected alpha and fission fragment were recorded in list mode with RAGS. The system was calibrated using ^{252}Cf fission sources on thin polypropylene foils and ^{249}Cf and ^{212}Pb alpha sources. Subsequent sorting and histogramming were performed on the data to extract fission-fragment energy spectra, coincidence data and half-life information. The off-line fission fragment energy calibrations were obtained by the method of Schmitt, Kiker and Williams [Schmitt, 1065] using the constants of Weissenberger et al. [Weissenberger, 1986]. Observation of a significant number of fissions would establish that further investigation was warranted. See Section 1 for details of the experimental requirements for the study of ECDF.

Neutron-deficient Np isotopes were produced at the Lawrence Berkeley Laboratory 88-Inch Cyclotron as described in Section 3.2. The recoiling products were carried on KCl aerosols swept in He to the MG. The sources were stepped at a preset interval of 1 minute and positioned successively between six pairs of passivated ion-implanted silicon (PIPS) detectors. Energy

and time information for each event were recorded in the same manner as above. The system was calibrated as described above, and subsequent sorting and histogramming were performed on the data to extract fission-fragment energy spectra, coincidence data and half-life information. The off-line fission fragment energy calibrations were obtained as described for the neutron-deficient Bk isotopes.

3.4.2 X-Ray–Fission Correlation - Study of ^{238}Bk and ^{228}Np

An x-ray–fission coincidence apparatus was used to determine whether the fissions observed in the ^{238}Bk and ^{228}Np MG experiments arise from the ECDF mechanism. The activity and KCl aerosols were deposited onto a support which was placed between two Ge x-ray detectors and one silicon surface barrier detector. A schematic of the system is shown in Figure 3-16. A schematic of the system electronics is illustrated in Figure 3-17. The detection system was configured so that when a fission was detected, any signal in the Ge detectors, time-to-amplitude converters or solid state detector were recorded.

Measurements of the time correlation between the electron-capture x-rays and the subsequent fission confirms that the observed fissions seen with the MG-RAGS arise from ECDF.

Major interferences can arise from the 8-10 prompt γ-rays emitted during de-excitation of the fission fragments [Hoffman, 1974]. Too large a detector geometry would reduce the number of true x-ray–fission coincidences due to summing between the prompt γ-rays from the fission fragments and the x-rays. Too small a geometry would reduce the number of coincident x-rays detected. To alleviate this problem, a calibration with a ^{252}Cf source was used to appropriately position the Ge detectors so that an

approximate 50% rejection limit for prompt γ-rays from fission fragments was obtained. As long as the number of prompt γ-rays from the fission fragments in the fission of ^{252}Cf is not dramatically different than that occurring in the ECDF of ^{238}Bk or ^{228}Np, the detector configuration should be appropriate for the detection of x-ray–fission coincidences.

The 50% rejection limit for prompt γ-rays from fission fragments is an approximation. The best detector geometry can be calculated in the following manner. For each ECDF event, assume that one K x-ray, and N prompt γ-rays are emitted. The efficiency for the x-rays impinging on the detector is simply the solid angle subtended by the detector, S. In addition, all prompt γ-rays from the fission fragments have the same probability of interacting in some manner with the detector as the K x-ray. The efficiency for detecting the x-ray and none of the prompt γ-rays is given as ε in equation 3-1.

$$\varepsilon = S(1-S)^N \qquad \text{Equation 3-1}$$

The mathematics associated with calculating the best detector solid angle is simpler if we define ε in terms of a dummy variable M, where M=1-S. This yields equation 3-2.

$$\varepsilon = (1-M)M^N = M^N - M^{N+1} \qquad \text{Equation 3-2}$$

In equation 3-2, M is the probability that any single photon misses the detector. To maximize the efficiency, equation 3-2 is differentiated with respect to the number of prompt γ-rays, N, and set equal to zero, yielding equation 3-3.

$$0 = NM^{N-1} - (N+1)M^N = M^{N-1}(N-(N+1)M) \qquad \text{Equation 3-3}$$

Solutions to equation 3-3 are $M^{N-1} = 0$ or $(N-(N+1)M) = 0$. The M^{N-1} part of equation 3-3 yields the uninteresting root M=0, and S=1. The (N-(N+1)M) part of equation 3-3 yields roots such as M=N/(N+1).

The prompt γ-ray summing probability is defined as (S-ε)/S in equation 3-4.

$$(S-\varepsilon)/S = \frac{(1-M-\varepsilon)}{(1-M)} = \frac{(1-M)-(1-M)M^N}{(1-M)} = (1-M)^N \quad \text{Equation 3-4}$$

It should be noted that N in equation 3-4 is the fraction of prompt γ-rays which interact with the detector. If the prompt γ-ray multiplicity is 10 and only 40% of those will interact in a 10-mm thick Ge detector, if they hit the detector, then N is 4. For a large γ-ray multiplicity, the best value of (S-ε)/S is 63%. However, because of spacing constraints, the best detector geometry that was achieved yielded a value of 50%.

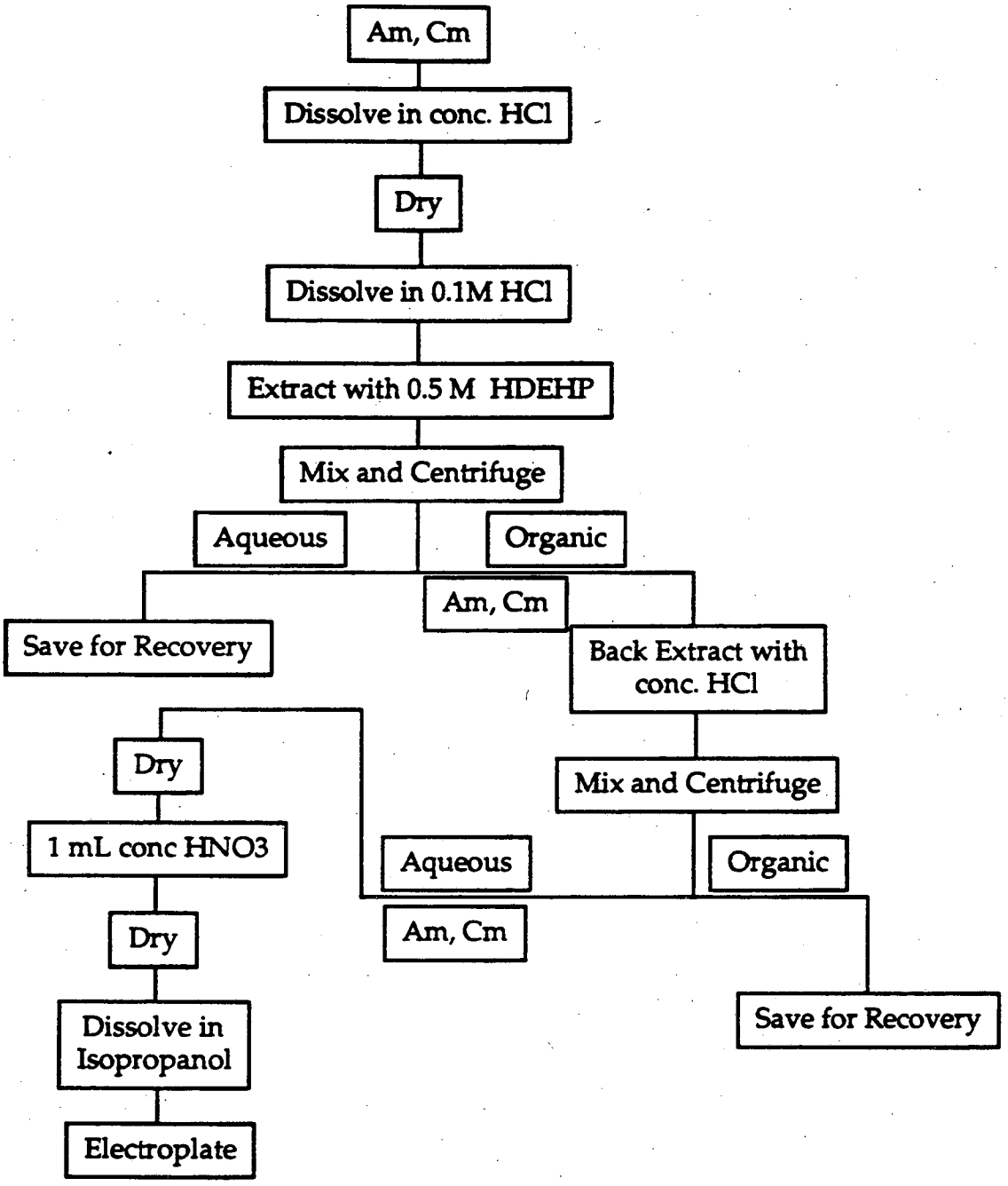

Figure 3-1. Flow diagram of Am and Cm purification procedure for target preparation. The drying step with HNO_3 was repeated three times to ensure that all chloride was removed.

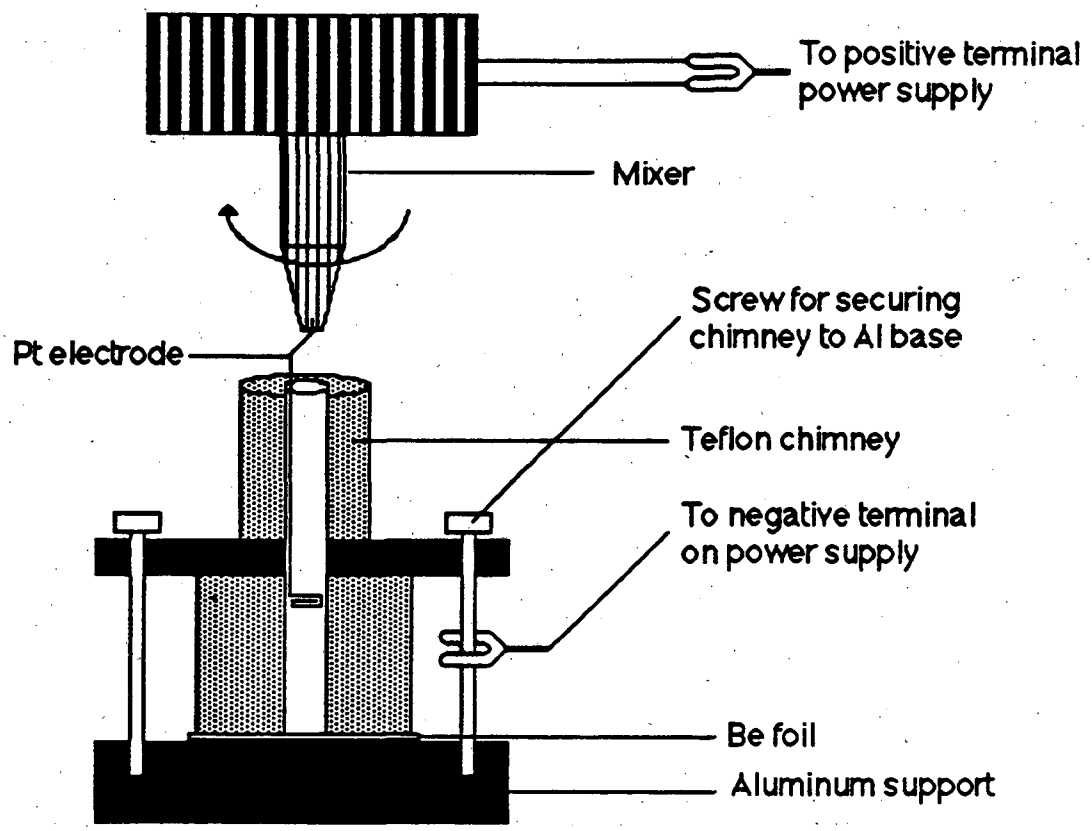

Figure 3-2. Schematic of electrodeposition cell used in production of targets. The Teflon chimney has a length of about 5-cm and an i.d. of 9.5 mm for the ^{241}Am and ^{233}U targets and 6 mm for the ^{248}Cm target. The isopropanol solution containing the target material is placed in the chimney and the cell connected to a power supply for electrodeposition. The negative pole of the power supply is attached to the base.

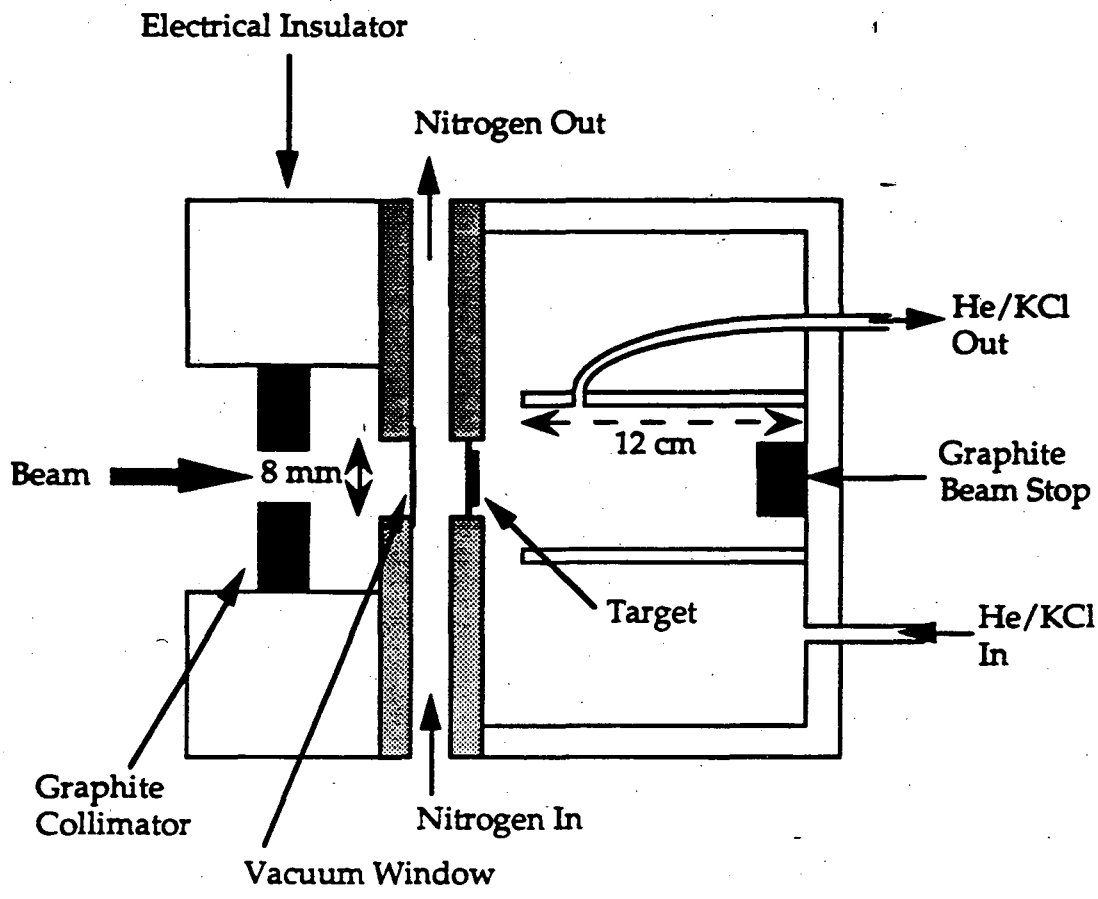

Figure 3-3. Schematic of single target system used in ^{18}O irradiations to produce ^{252}Bk and ^{253}Bk (not to scale). The ^{248}Cm target has a 6-mm diameter. The recoil chamber insert is 12 cm long. The vacuum window has an 8-mm diameter.

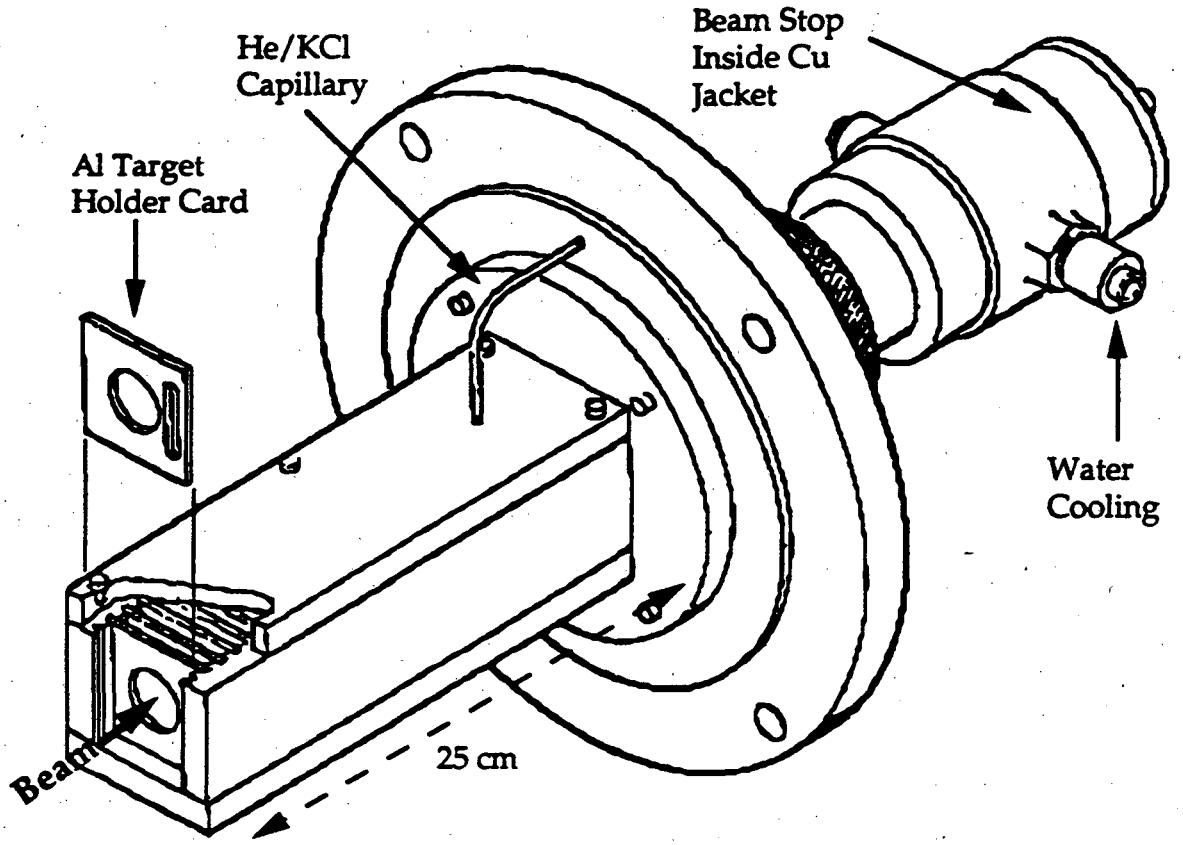

Figure 3-4. Schematic of LIM system. Targets are placed in a continuous array. The targets are appropriately spaced, depending on the accelerator beam and energy, to about twice the recoil range of the compound nucleus in 1 atmosphere He. The fission products recoil into the back of the next target, while the recoiling compound nucleus products are swept from the system by a He/KCl aerosol transport system.

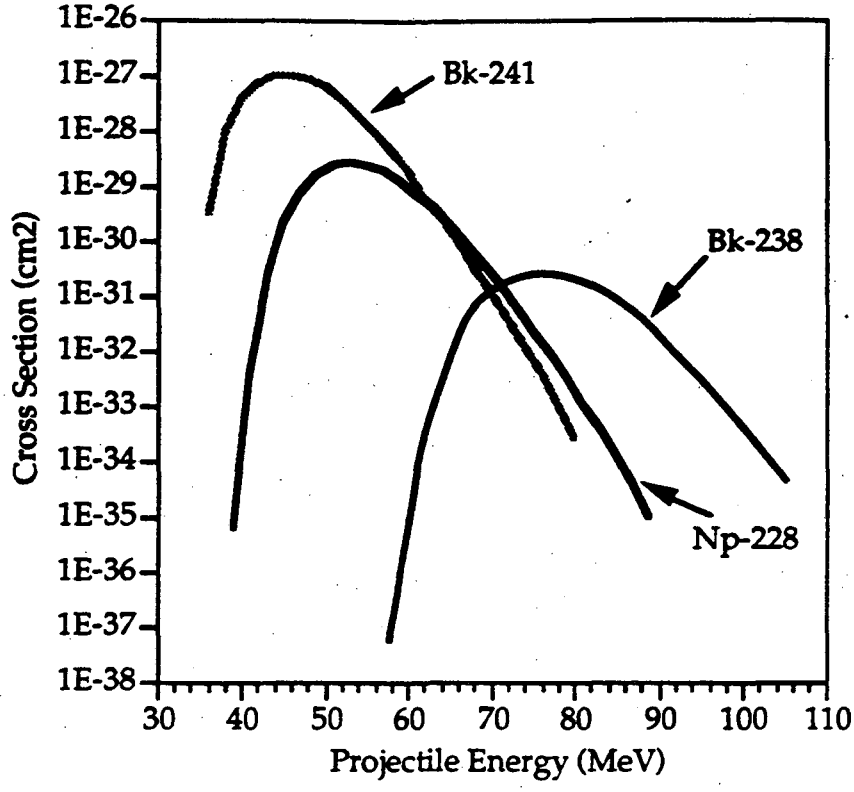

Figure 3-5. Plot of production cross sections for ^{241}Bk, ^{238}Bk and ^{228}Np calculated by SPIT [Haynes, 1988]. The production reactions for ^{241}Bk, ^{238}Bk and ^{228}Np are: ^{241}Am(α,4n)^{241}Bk; ^{241}Am(α,7n)^{238}Bk; and ^{233}U(p,6n)^{228}Np.

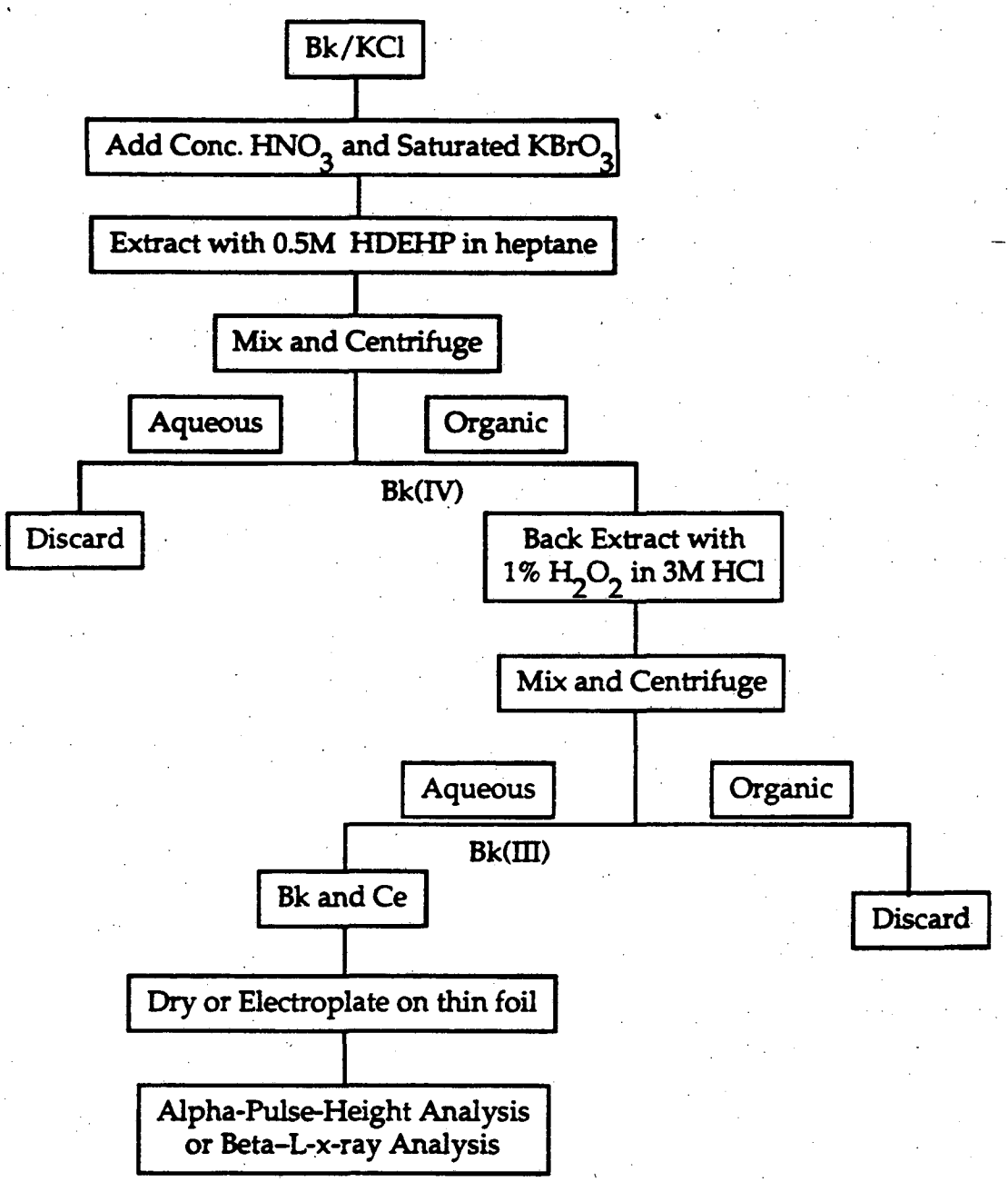

Figure 3-6. General HDEHP separation of Bk from trivalent actinides.

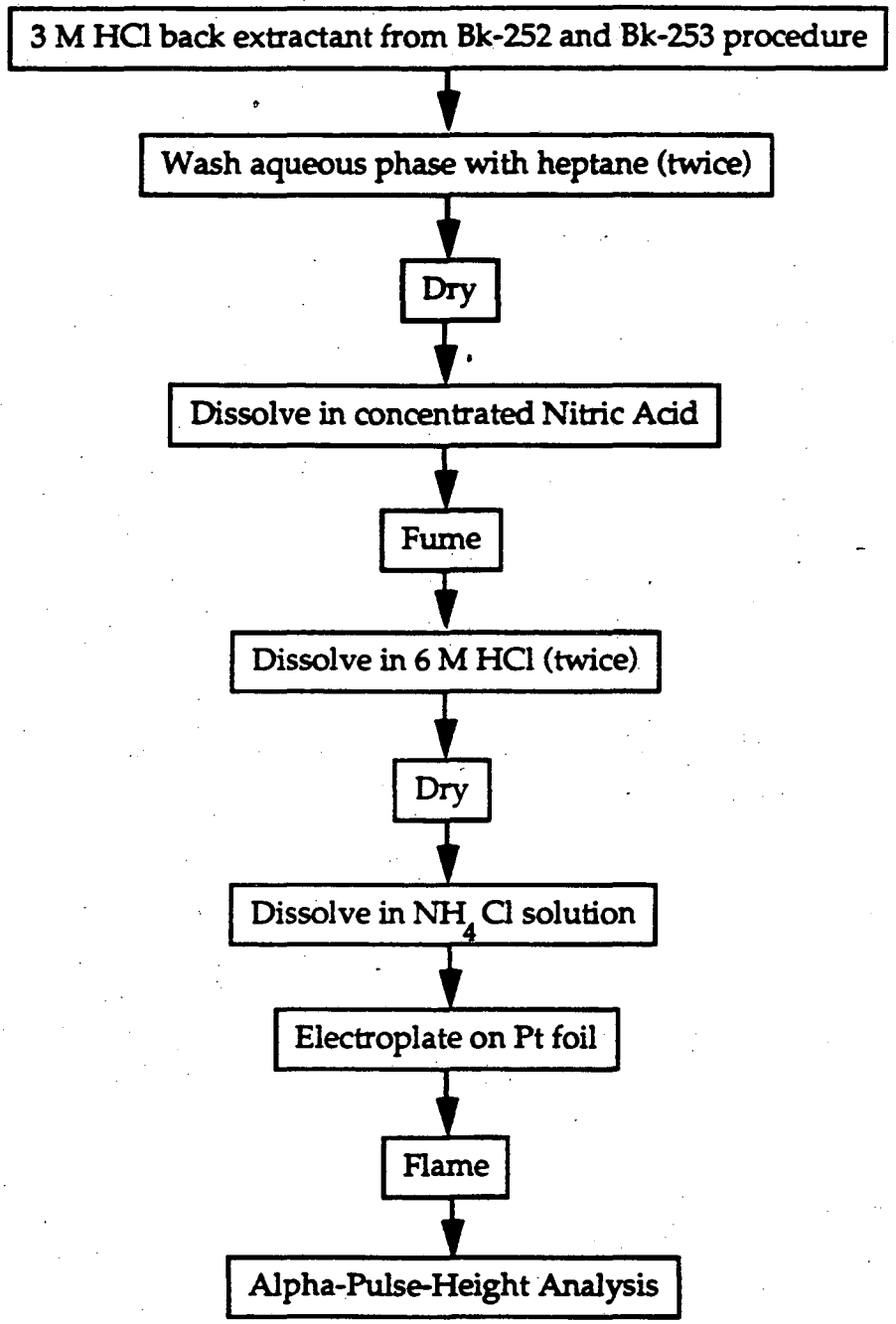

Figure 3-7. Flow diagram of purification procedure used in ^{252}Bk and ^{253}Bk experiments. After back extraction into 3 M HCl, the sample was first washed with heptane and then dried. Any resulting residue is destroyed by fuming in concentrated HNO_3 heated in an oil bath. After fuming, the sample was completely dried, redissolved in 6 M HCl to remove any nitrate, and dissolved in an NH_4Cl solution for electrodeposition on Pt foil.

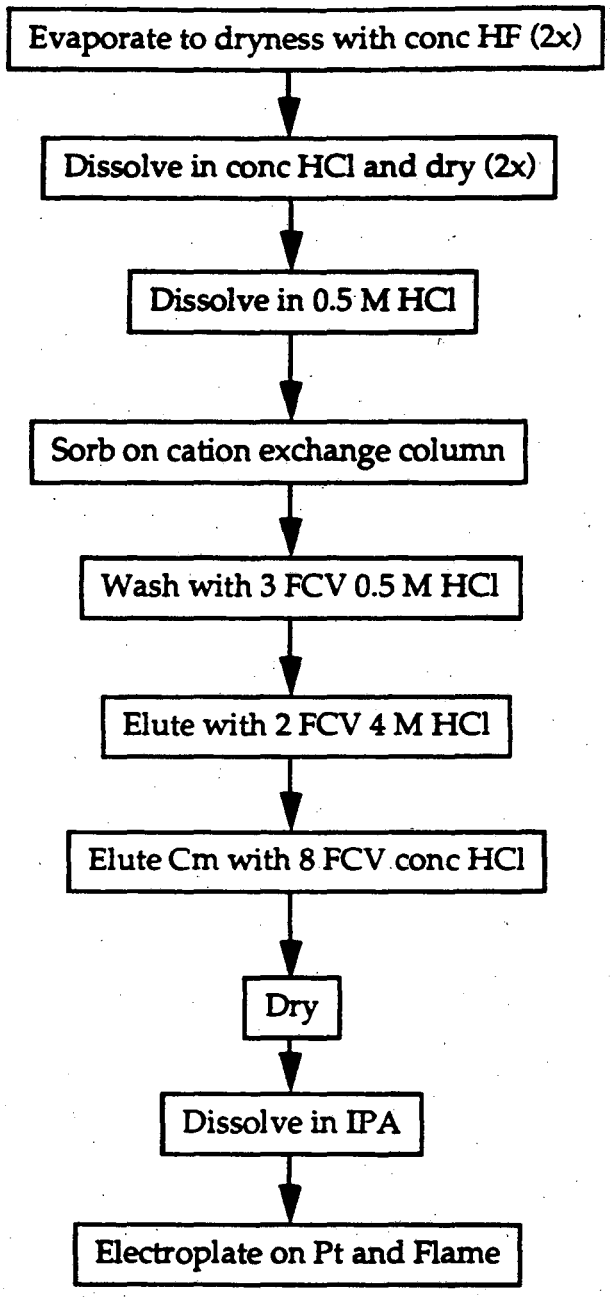

Figure 3-8. Cleanup procedure for ^{241}Bk experiment. In this procedure the column was pretreated with conc. HCl followed by water.

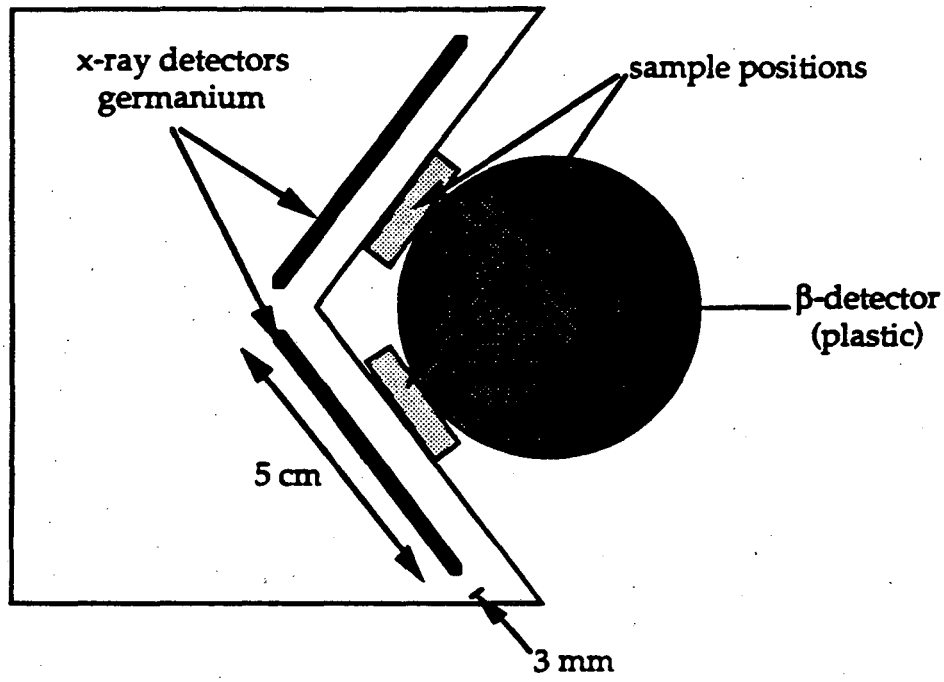

Figure 3-9. Schematic of beta–L x-ray detector apparatus. The beta particles were detected with a standard plastic scintillator, covered with aluminized mylar and connected to a photomultiplier. The Ge detector consisted of two thin Ge crystals housed in the same cryostat.

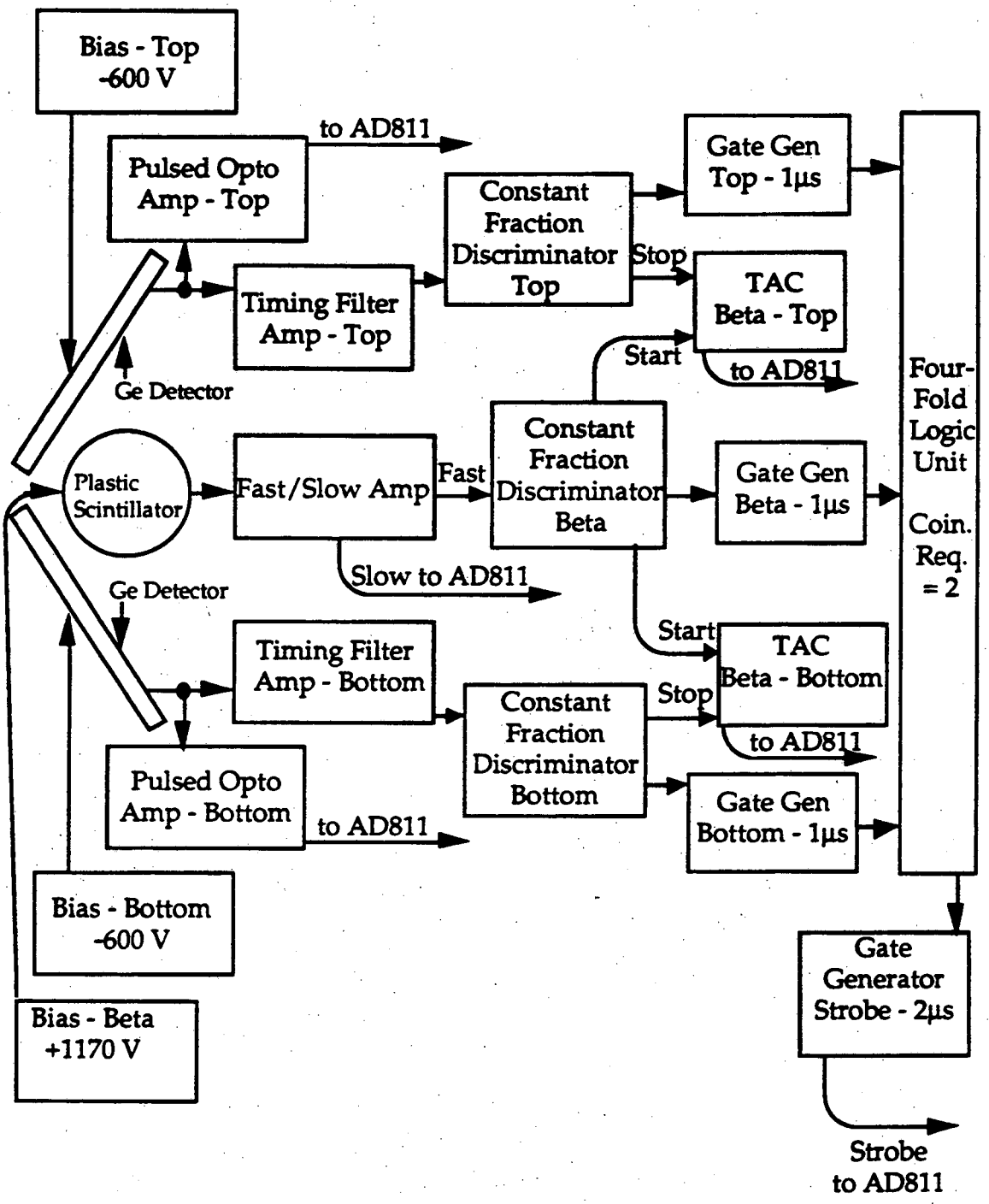

Figure 3-10. Schematic of beta–L x-ray detection electronics. The data were recorded in list mode with RAGS (see section 3.4.1).

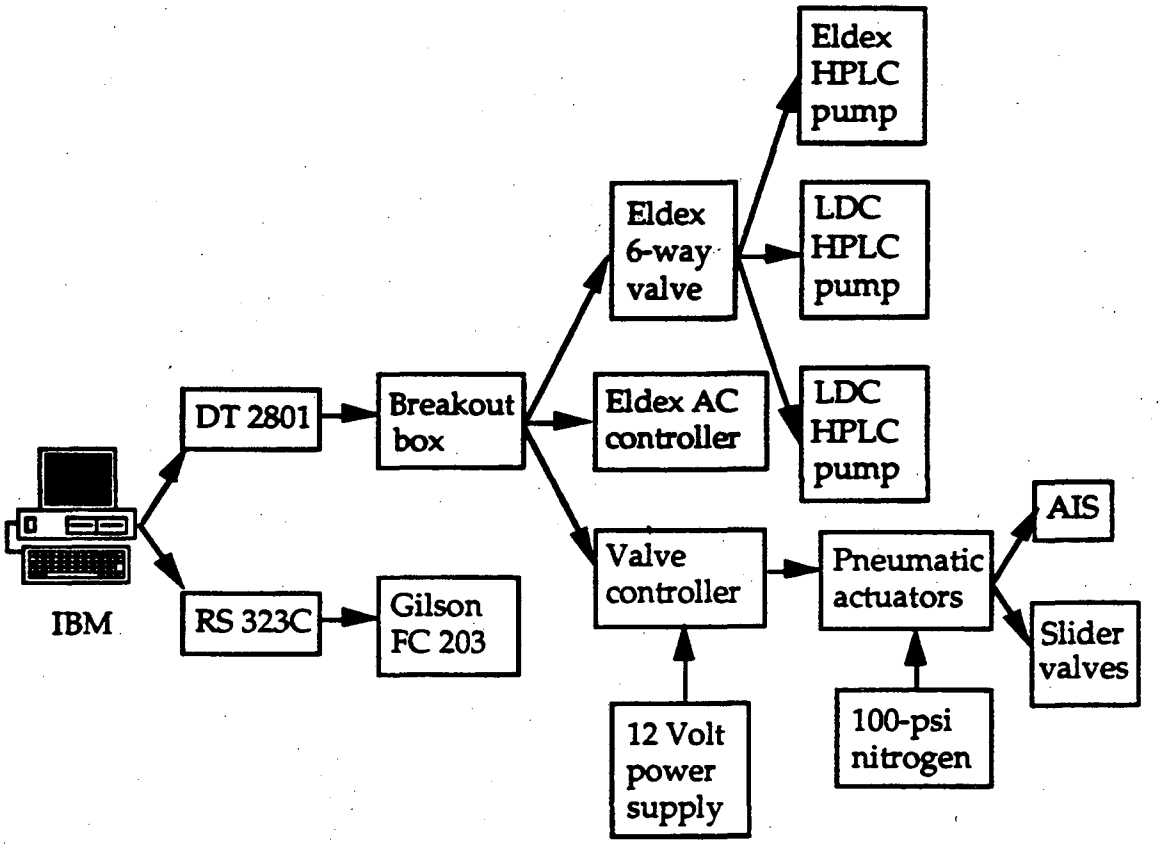

Figure 3-11. Automated control-system diagram for ACCESS.

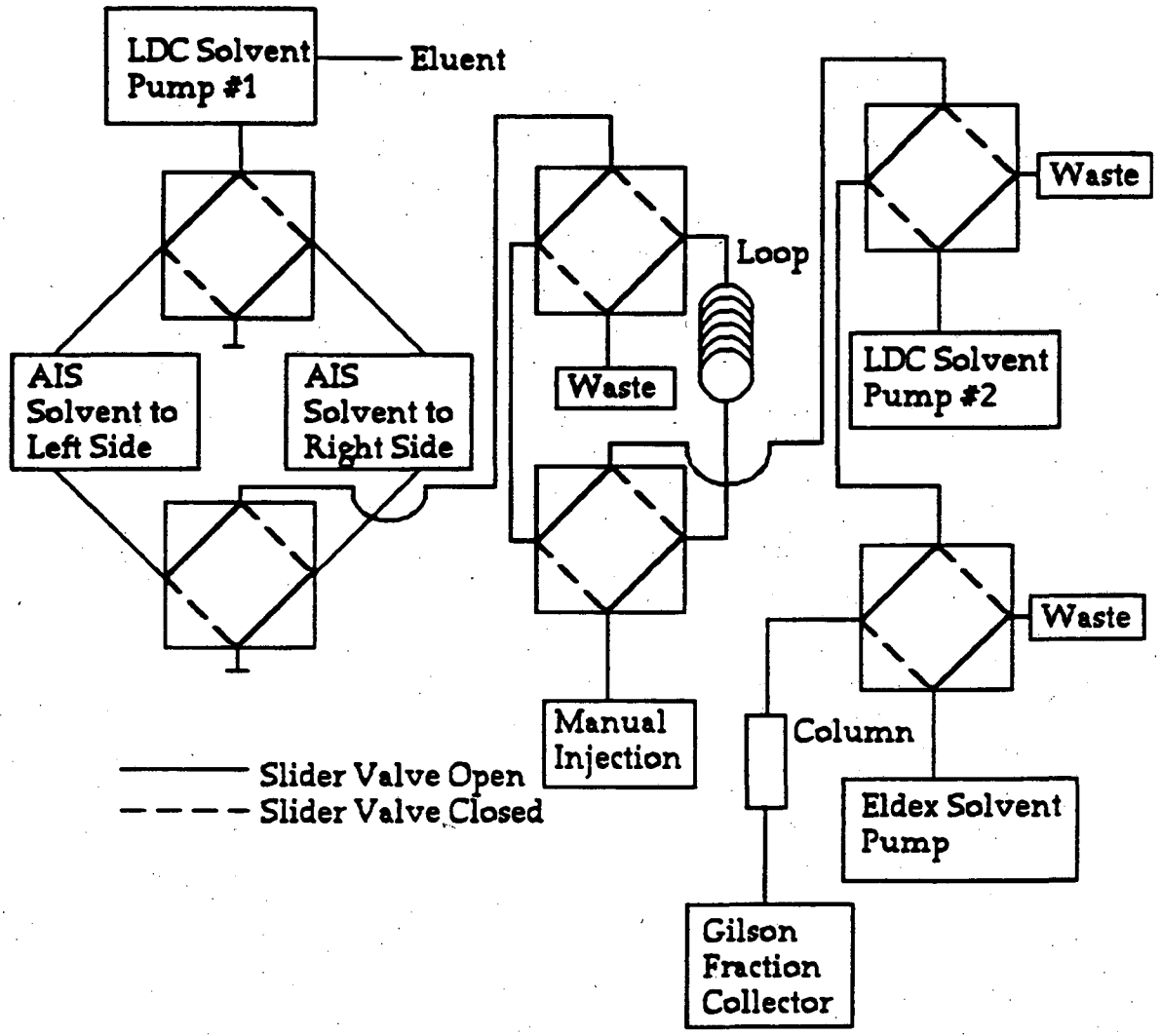

Figure 3-12. Schematic of ACCESS. The boxes with dashed and solid lines represent 4-way valves. When the slider is in the open position, solvent is directed via the solid path through the valve. When the slider is in the closed position, solvent is directed via the dashed path.

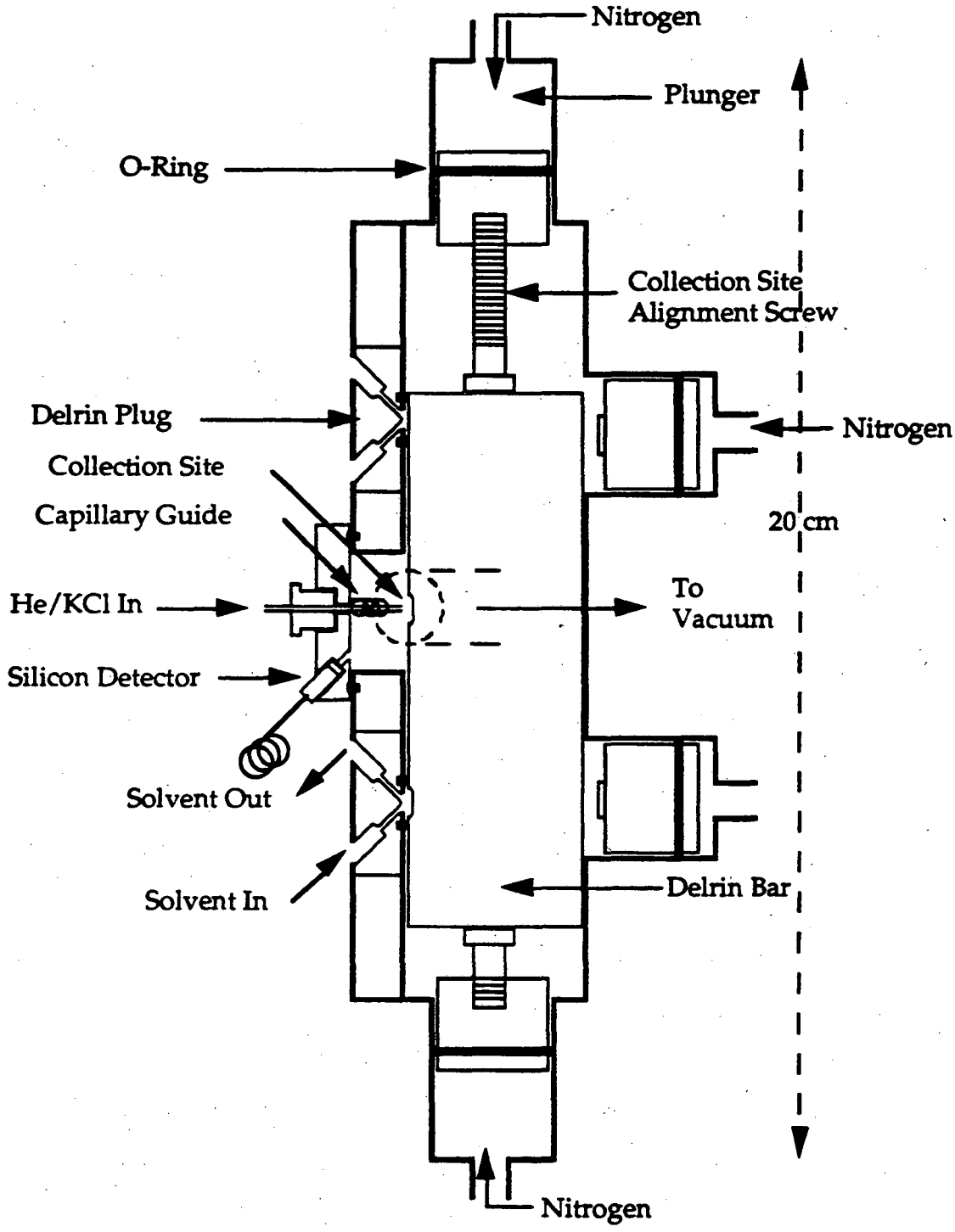

Figure 3-13. Schematic of AIS. Activity is being collected from the He/KCl jet on the right side of the Delrin bar while the previously collected sample is being dissolved and washed into ACCESS on the left side of the Delrin Bar.

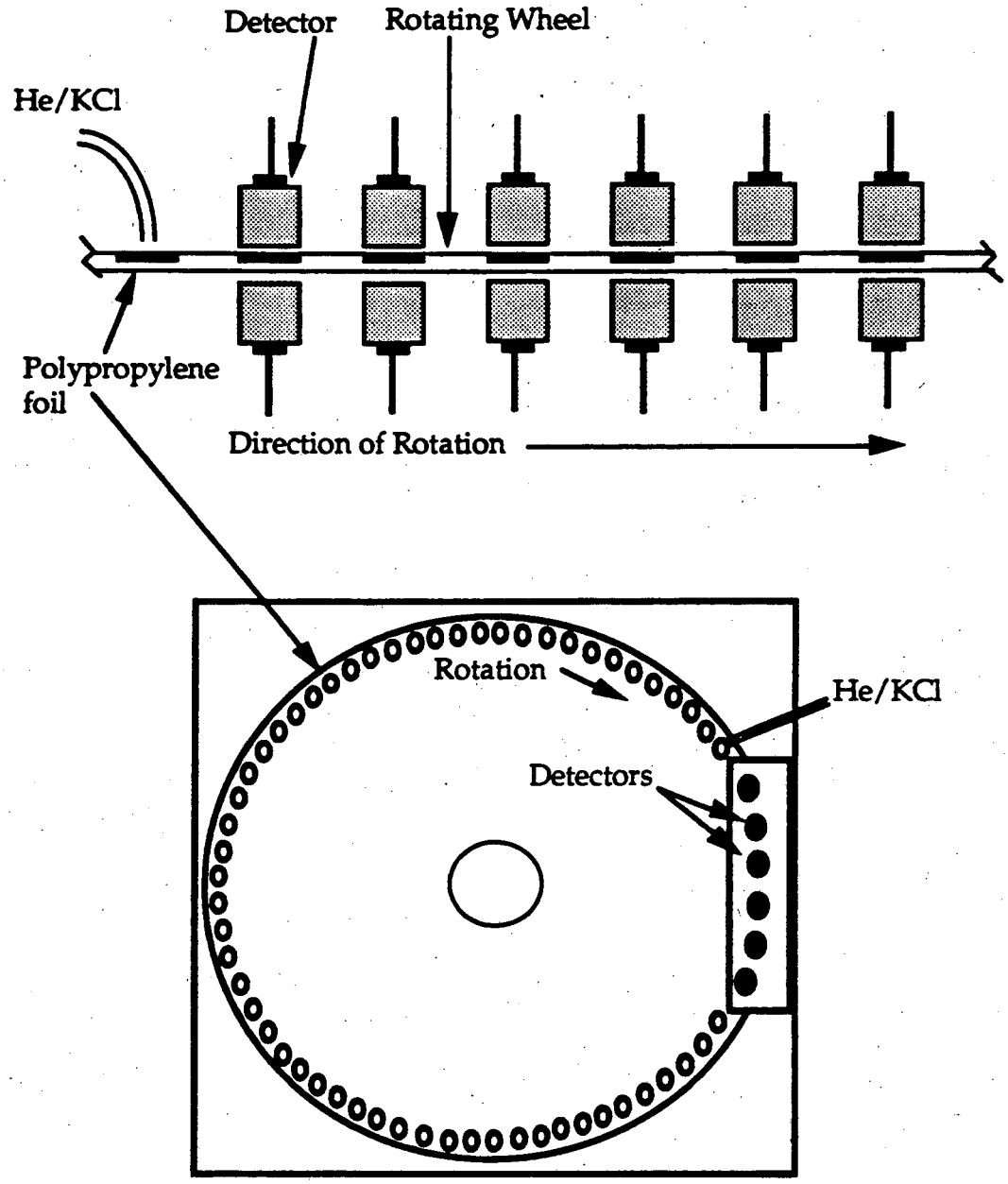

Figure 3-14. Diagram of MG detector set-up. Pairs of silicon detectors are positioned above and below the wheel. The sources are deposited on 40±10 $\mu g/cm^2$ polypropylene foils which are around the periphery of the wheel and stepped sequentially between six pairs of detectors.

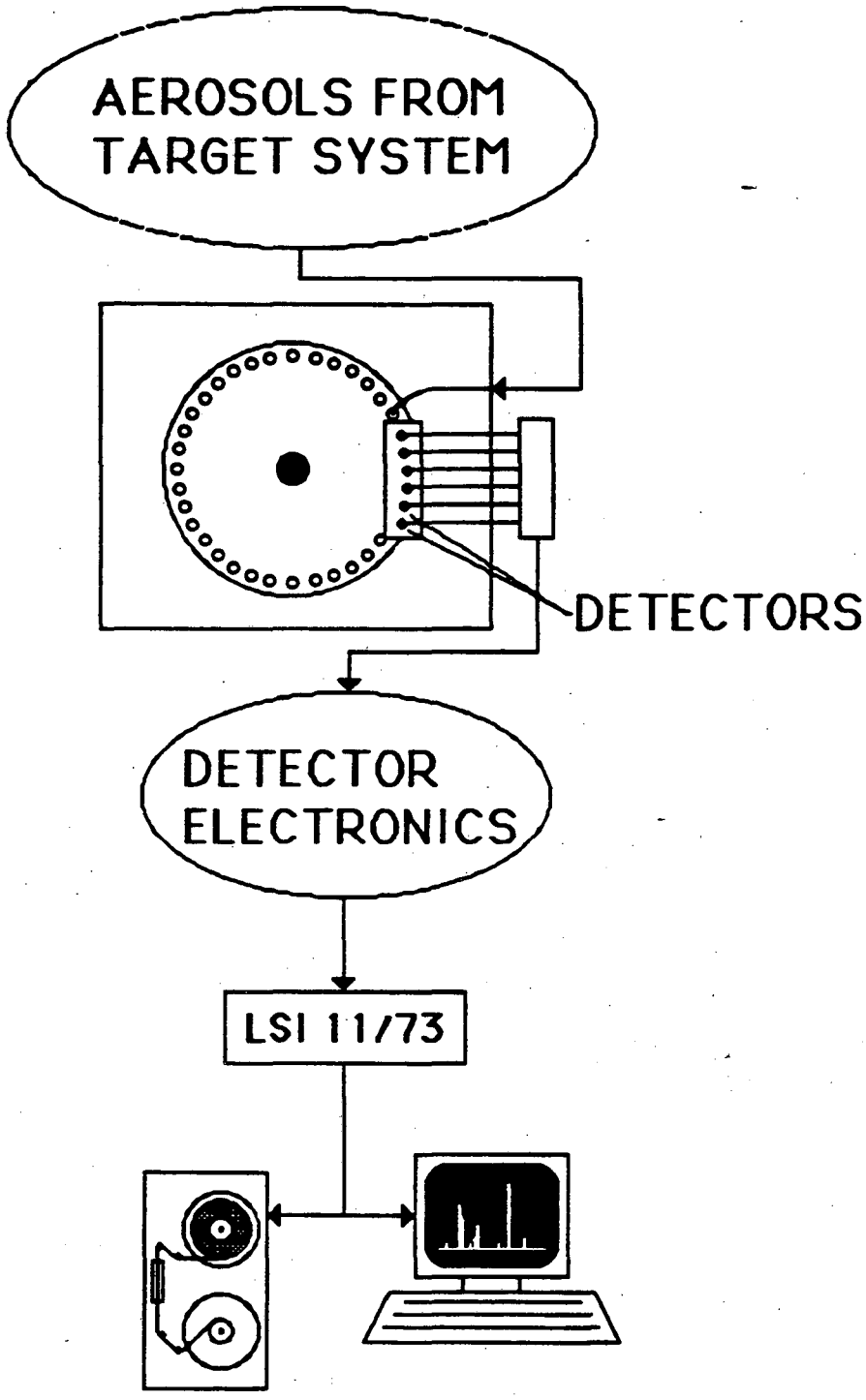

Figure 3-15. Schematic diagram of MG-RAGS. The MG and corresponding electronics are controlled by an LSI 11/73 computer. The data are written in list mode to a hard disk or a magnetic tape.

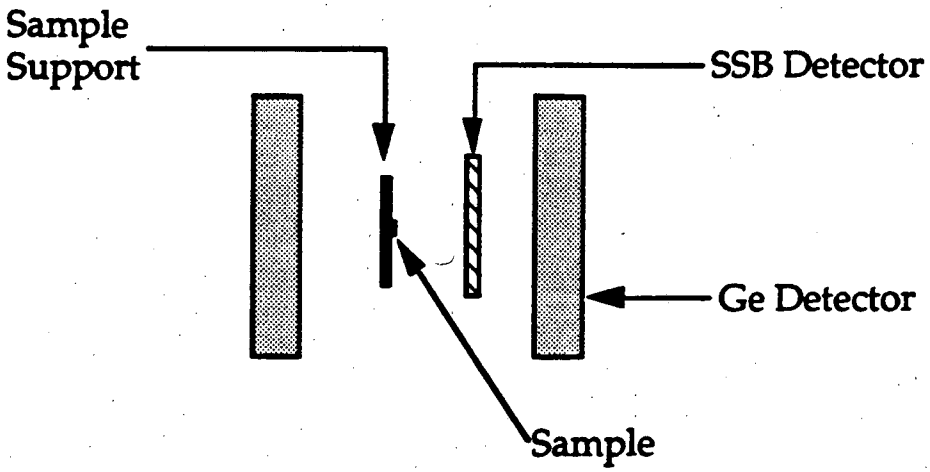

Figure 3-16. Schematic of x-ray–fission coincidence experiment. In the case of ^{238}Bk, the sample support was a Ta foil taped to a 1-mm thick fiberglass stick. In the case of ^{228}Np the support was a Ni foil attached to the fiberglass.

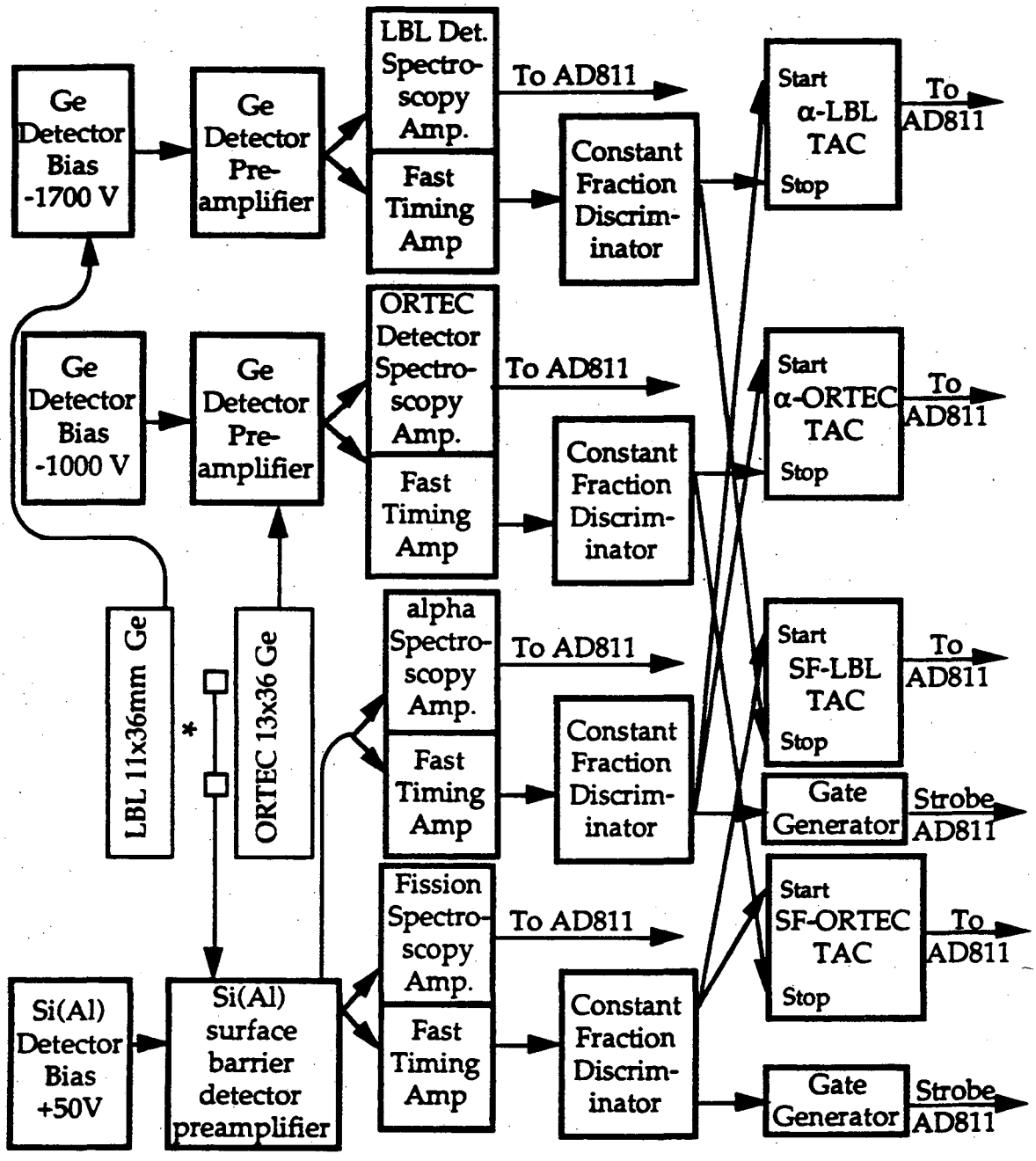

Figure 3-17. Schematic of ECDF electronics. This system will detect x-rays in coincidence with fissions as well as alphas. The alpha coincidence is used to calibrate the system.

4 Results and Discussion

4.1 Electron-Capture Delayed Fission

4.1.1 ^{238}Bk

4.1.1.1 Fission Properties

Berkelium-238 was produced and transported to the MG as described in Section 3. Samples resulting from 2.0-minute collections of the KCl aerosols on polypropylene foils were stepped consecutively between the six pairs of PIPS detectors in the MG system. After one complete revolution of the MG wheel (80 positions, 79 samples), the wheel was replaced with a clean one to prevent the buildup of KCl and any long-lived fission activities.

During the course of 3 experiments, 739 pairs of coincident fission fragments were detected. Because of damage to a calibration file, one set of data was not usable; the period of time between the individual experiments did not permit the use of one of the two remaining calibration files from the other experiments. A total of 382 pairs of coincident fission fragments were detected in the two remaining experiments. The half-life was determined to be 144 ± 5 seconds by a maximum likelihood technique [Gregorich, 1991A] using all 739 events. The decay curve is shown in Figure 4-1. Each point in the fit was normalized to represent the same number of samples. This is necessary since before the data acquisition is stopped, detector station one measures 79 samples, station two measures 78 samples, station three measures 77 samples, and so on.

Appropriate detector gains for fission fragments were determined from ^{252}Cf sources evaporated on Ni foils. Coincident fission fragment calibrations

were obtained using ^{252}Cf sources on 40 $\mu g/cm^2$ polypropylene foils. Approximately 10000 pairs of coincident fission fragments from the ^{252}Cf were detected per detector station.

The 382 remaining coincident fission fragment pairs from ^{238}Bk ECDF were sufficient, along with the ^{252}Cf calibration information, to determine the kinetic energies of the fragments. The off-line fission fragment energy calibrations and corrections for neutron emission were obtained by the method of Schmitt, Kiker and Williams [Schmitt, 1965] using the constants of Weissenberger et al. [Weissenberger, 1986]. The average neutron emission function, $\bar{\nu}(A)$, was taken as similar to that of ^{252}Cf, normalized to an average neutron emission $\bar{\nu}_t = 2.40$ (estimated from systematics in [Hoffman 1974]). The most probable pre-neutron TKE was determined to be 174 ± 5 MeV. This value is somewhat lower than predicted by the systematics of Viola [Viola, 1966]. Figure 4-2 is a plot of the average or most probable TKE, $\overline{TKE}$, vs. $Z^2/A^{1/3}$ for all known spontaneous fission and delayed fission isotopes. As illustrated in Figure 4-2, the TKEs from ECDF are generally lower than from spontaneous fission. This may result from the 4-5 MeV excitation energy imparted to the fissioning nucleus from the EC. The shell effects may be somewhat reduced by this excitation. The TKE versus mass fraction (MF) contour diagram for the ECDF of ^{238}Bk is given in Figure 4-3. The actual MF versus TKE data are given in Figure 4-4. (MF is defined as $MF = A_H/A_F$ where A_H is the mass number of the heavy fragment; A_F is the mass number of the fissioning nucleus.) The TKE distribution shown in Figure 4-5 shows a low energy tail. This may be partially a result of straggling due to sample thickness. Large collection intervals lead to large KCl deposits, resulting in fission fragment kinetic energy degradation. The FWHM of the TKE distribution is 40 MeV. According to the static scission point model by

Wilkins et al. [Wilkins 1976], the asymmetric mode in the ECDF of ^{238}Bk should have one spherical (β_s=0.1, Z=52, N=80) and one deformed fragment (β_d=0.4, Z=44, N=62). The symmetric mode should have either two near spherical fragments (β_s=0.2, Z=48, N=71) or two highly deformed fragments (β_d=0.7, Z=48, N=71), depending on the deformation chosen for N=71. The neutron contour diagram in [Wilkins, 1976] shows two possible deformations for N=71. A high and low TKE component at symmetric mass splits is possible because of the significantly different deformations possible for fragments with N=71. The deformation parameters, β_d and β_s, are estimated from the proton and neutron contour diagrams given in [Wilkins, 1976]. The parameter β_d refers to the deformation associated with a deformed fragment and β_s refers to the deformation associated with a spherical fragment.

The mass-yield distribution for the ECDF of ^{238}Bk is given in Figure 4-6. The mass-yield distribution shows a yield at symmetry of nearly 1.5%. However, because of the poor ^{238}Bk statistics and energy degradation due to source thickness, whether or not there is an enhanced yield of symmetric mass splits cannot be determined. It does appear that two grouping of events at mass fraction 0.50 correspond to the two different fragment configuration in the symmetric fission discussed previously (see Figure 4-4). Twenty-three events were observed in the MF region between 0.50 and 0.52 which constitutes 6% of the 382 total events. The average TKE for ^{238}Bk at each mass fraction, shown in Figure 4-3, indicates a drop near symmetric mass splits.

4.1.1.2 X-ray–Fission Correlation

Samples were collected for 2 minutes, separated and dried on Ta foil as described in Section 3.3.1.2. The Ta foil was taped to a 1-mm thick fiberglass stick. The diameter of the evaporated source was approximately 2-mm. The

activity was placed in the x-ray–fission coincidence apparatus shown in Figure 3-16.

The overall curium K_α x-ray–SF coincidence detection efficiency was determined to be 11.8% by measuring the 5.81-MeV alpha particles from a ^{249}Cf source in coincidence with the K_α x-rays of the ^{245}Cm daughter. The Cm K_α x-ray intensities from the ^{249}Cf alpha decay are given in [Lederer, 1978]. The ratio of the total number of coincident Cm K_α x-rays to the total number of ^{249}Cf alpha events yields the K_α x-ray–SF efficiency. Appropriate amplifier gains for fission fragments were determined with a ^{252}Cf source on an 11.5 mg/cm^2 Ni foil. Prompt γ-ray summing effects were estimated by measuring the γ-rays in coincidence with fission fragments from a ^{252}Cf source. The ratio of the number of γ-ray–fission coincidences to the total number of detected fissions yields the fraction of x-ray–fission coincidences lost by summing. It is assumed that any difference in the γ-ray multiplicities between the SF of ^{252}Cf and the ECDF of ^{238}Bk are negligible.

The signal from the SSB detector provided a common start for two time-to-amplitude converters (TACs). The stop signals were provided by the first and second germanium γ-ray detectors. The time window on the TACs was $\pm$ 500 nsec. The timing resolution of the germanium detectors was approximately 9 nsec FWHM, and the energy resolution of each detector was less than 1.5 keV FWHM in the Cm K x-ray region. Upon detection of a fission fragment in the SSB detector, the amplitudes of the pulses in the SSB detector, the γ-ray detectors, and the TACs were recorded.

Approximately 800 samples were prepared with the TTA chemistry described in Section 3.3.1.2 and 208 fission fragments were observed in the x-ray–fission coincidence system shown in Figure 3-16. From previous work [Hall, 1990A], [Hall, 1990B] and the determined detection efficiencies and

summing rates, it was expected that 18 ± 4 x-rays in the curium K_α x-ray energy region would be detected. Table 4-1 gives the efficiency and summing

Table 4-1. Efficiency and summing information for the germanium and the solid state detectors used in the study of ECDF in ^{238}Bk.

Experiment 1	Gamma 1	Gamma 2	SSB
Fission Efficiency			80%
X-ray Efficiency	8.6%	9.6%	
γ-ray Summing	30%	40%	
Fissions Detected			208
Expected Number of Correlations	12	12	
Correction for absorption by Ta		6	
Total Expected X-ray–Fission Correlations	18 ± 4		

information for the germanium detectors and the efficiency of the solid state detector (SSB) for the experiment. The expected number of x-ray–fission correlations in each detector is calculated from equation 4-1.

$$\#\text{correlations} = \sum_{\substack{\text{all} \\ \gamma\text{-detectors}}} (\#\text{fissions})(\text{x-ray efficiency})(1-(\gamma\text{-summing})) \qquad \text{Equation 4-1}$$

Equation 4-1 assumes that only K-electron-capture contributes, no gamma transitions are K converted, and a K fluorescence yield of 100%.

It should be noted that a correction of approximately a factor of 2 was applied to the number of expected x-ray–fission correlations in the Gamma 2

detector to account for the x-ray events lost due to absorption in the Ta foil. The correction to the number of expected events in the Ge detector, which was positioned on the opposite side of the Ta foil, was obtained from the tables of photon ranges in matter in [Lederer, 1978].

The Cm $K_{\alpha 2}$ and $K_{\alpha 1}$ peaks appear at 104.4 and 109.3-keV and the $K_{\beta 1+3}$ and $K_{\beta 2}$ peaks at 123 and 127-keV, respectively [Lederer, 1978]. The observed x-ray–fission correlation data are shown in Figure 4-7. We observed 17 ± 4 x-rays in the Cm K x-ray energy region. No more than 1 or 2 of these are likely due to prompt γ-rays which leaves approximately 15 ± 4 of the expected 18 x-rays.

The observed number of prompt γ-rays relative to the ^{238}Bk EC x-rays indicates that the prompt γ-ray multiplicity from ^{238}Bk ECDF is similar to that from the SF of ^{252}Cf. The pile-up rate was less than about 2% because the γ-ray singles rate was less than 10^4 sec^{-1}. This was monitored occasionally during the experiment with an oscilloscope.

It is assumed that the fissioning states populated by the EC decay are high in excitation energy. For ^{238}Bk, electron-capture from the K-shell cannot populate states larger in excitation energy than about 4.5 MeV (the Q_{EC} minus the K-shell binding energy). Because of the small EC transition energy, it may be possible that L-capture plays a significant role in the ECDF process. The possibility that the ECDF proceeds via L-capture was ruled out because Cm L x-rays were not detected in the x-ray–fission correlation experiment (see Figure 4-7). Using the same technique involved in the calculation of the expected number of K x-ray–fission correlations, the total number of L_β and L_γ x-ray–fission correlations was expected to be 4 ± 1. This number includes the significantly lower fluorescence yield of L x-rays compared to K x-rays. One L x-ray correlation was detected (see Figure 4-7). It was estimated that

about 1 L x-ray correlation would result from conversion after K-capture based on data from the table of x-ray intensities given in [Browne, 1986]. This may explain the single event in the L x-ray region. It is likely that the absence of L x-ray–fission correlations indicates that fission occurs primarily from levels populated by EC-transition energies larger than the K-shell edge. If the fission occurred at excitation energies that would energetically forbid K-capture, only L x-ray–fission correlations could occur.

The observation of 15 ± 4 K x-rays compared to the expected 18 ± 4 indicates that the K-vacancies filled before fission of ^{238}Cm occurred. This may indicate that ECDF in ^{238}Bk proceeds via a fission shape isomer in the EC daughter and that the shape change associated with tunnelling through the first barrier is faster than 10^{-17} to 10^{-15} seconds. If the shape change to the second potential well were slower than 10^{-15} seconds, gamma decay would dominate and the P_{DF} would be zero. The limit on the fission lifetime is 10^{-15} to 10^{-9} seconds. If the fission occurred faster than 10^{-15} seconds, fewer than expected K x-ray–fission coincidences would have been detected. If the fission occurred slower than 10^{-9} seconds, a delay would have been observed in the TAC spectrum.

4.1.1.3 Mass and Element Assignment

The mass and element assignment utilized the well known 3+/4+ oxidation state couple for Bk [Thompson, 1950], [Thompson, 1950A] and an HDEHP extraction as described in Section 3.3.1. No evidence for an alpha branch in the decay of ^{238}Bk with a 144 ± 5 second half-life was observed. No activity could be attributed to the 8.8-MeV alpha decay of ^{214}At, genetically related via multiple alpha decays to ^{238}Bk, in chemically separated Bk samples. The electron-capture decay was measured by observation of the 2.4-

hour ^{238}Cm 6.52-MeV alpha decay, EC daughter of ^{238}Bk, in chemically separated Bk fractions. The alpha-decay chains for ^{238}Bk and ^{238}Cm are shown in Figure 4-7. The ^{238}Cm decay was consistent with its known 2.4-hour half-life. Because no alpha branch was observed in the decay of ^{238}Bk, it was assumed that the isotope decays primarily by EC. It is difficult to conclude that ^{238}Bk has no alpha branch, because the daughter ^{234}Am decays only 0.4% by alpha emission. If the ^{238}Bk also has a small alpha branch, detection of the daughters further down the decay chain is difficult.

4.1.1.4 σ and P_{DF}

The ^{238}Bk was produced by the reaction ^{241}Am(75 MeV α, 7n)^{238}Bk. The production cross section was 150 ± 10 nb. This cross section is based upon and estimated effective target thickness of 75 $\mu g/cm^2$/target, an estimated 80% He-jet yield and 80% chemical yield. This value is consistent with the cross section calculated by SPIT [Haynes, 1988] (see Table 3-3).

A delayed fission probability of $(4.8 \pm 2) \times 10^{-4}$ was calculated from the assumed electron-capture branch of 100%, the production cross section, and the fission rate of 5 ± 1 fission fragment pairs/hour/eμA observed in the rotating-wheel experiments. This value is consistent with the values of 6.6×10^{-5} and 6.9×10^{-4}, respectively, determined for ^{234}Am and ^{232}Am by Hall et al. [Hall, 1990A], [Hall, 1990B] given the differences in the estimated EC Q-values. The ^{238}Bk delayed fission probability of $(4.8 \pm 2) \times 10^{-4}$ is the first reported for this previously unknown isotope. Using the half-life of 144 seconds, and the estimated Q_{EC} of 4.65 MeV [Möller, 1988], the log(ft) is estimated as 5.2 using the systematics in [Lederer, 1978].

4.1.2 ^{228}Np

4.1.2.1 Fission Properties

Neptunium-228 was produced and transported to the MG as described in Section 3. Samples resulting from 1.0 minute collections of the KCl aerosols on polypropylene foils were stepped consecutively between the six pairs of PIPS detectors in the MG. After one complete revolution of the MG-wheel (80 positions, 79 samples), the wheel was replaced with a clean one to prevent the build-up of KCl and any long-lived fission activities.

A total of 2373 pairs of coincident fission fragments was detected. The half-life was determined to be 61.4 ± 1.4 seconds by a non-linear least-squares technique. The decay curve is shown in Figure 4-9. Each point on the decay curve was normalized to represent the same number of samples. This is necessary since before the data acquisition is stopped, detector station one measures 79 samples, station two measures 78 samples, station three measures 77 samples, and so on.

Appropriate detector gains for fission fragments were determined from ^{252}Cf sources on Ni foils. Coincident fission fragment calibrations were obtained using ^{252}Cf sources on 40 μg/cm^2 polypropylene foils as described for ^{238}Bk.

The 2373 coincident fission fragment pairs from ^{228}Np ECDF were sufficient, along with the ^{252}Cf calibration information, to determine the fission properties. The off-line fission fragment energy calibrations and corrections for neutron emission were obtained as described for ^{238}Bk. The average neutron emission function, $\bar{\nu}(A)$, was taken as similar to that of ^{252}Cf, normalized to an average neutron emission $\bar{\nu}_t$ = 2.40 (estimated from systematics in [Hoffman, 1974]). The most probable pre-neutron TKE was determined to be 165 ± 5 MeV. This value is somewhat lower than predicted

by the systematics of Viola [Viola, 1966]. However, based on the discussion in Section 4.1, this is not surprising. Figure 4-2 is a plot of the average or most probable TKE, $\overline{TKE}$, vs. $Z^2/A^{1/3}$ for all known spontaneous fission and delayed fission isotopes. Evidence for a small number of symmetric mass splits can be seen in the TKE vs. MF data shown in Figure 4-10. The mass split associated with the symmetric mode is illustrated by the relatively large number of events with MF = 0.500-0.520. The number of events associated with the symmetric mode was taken as the sum of all events with MF values between about 0.500 and 0.520. This constitutes 59 of the 2373 events. Figure 4-11 is a TKE–MF contour plot. Plotting of the individual events, however, illustrates the smooth transition from the small symmetric mass split to the dominant asymmetric mass split which is not as easily seen in the contour plot. The overall TKE distribution, Figure 4-12, is nearly symmetric, but shows a low energy tail which is associated with the small symmetric fission component. The full-width-at-half-maximum (FWHM) of the TKE distribution is 30 MeV. The mass-yield distribution is shown in Figure 4-13a. The decreased yield of symmetric events in the ECDF of ^{228}Np versus ^{238}Bk is likely a result of the smaller Q_{EC} in ^{228}Np (4.2 MeV) versus ^{238}Bk (4.65 MeV) [Möller, 1988]. (The symmetric mode in the ECDF of ^{238}Bk was about 6% of the 382 total events. However, the poor statistics did not allow for positive assignment of a symmetric component.)

According to Wilkins et al. [Wilkins, 1976], the symmetric mode in the ECDF of ^{228}Np should have a smaller TKE than the asymmetric mode [Konecny, 1969] because the symmetric fission fragments are expected to be highly deformed. Based on the static-scission point model, the symmetric mode can be interpreted as consisting of two fragments with β_d=0.5, Z=46, N=68, each. The asymmetric mode should have one spherical β_s=0.1, Z=52,

N=78 and one deformed fragment β_d=0.4, Z=40, N=58 [Wilkins, 1976]. Here the deformation parameters, β, are estimated from the proton and neutron contour diagrams given in [Wilkins, 1976] and are defined as in the studies of ^{238}Bk.

Previous studies in the Ra region show that the ratio of symmetric to asymmetric fission increases with excitation energy [Konecny, 1969], [Weber, 1976], [Itkis, 1989], [Perry, 1971], [Zhagrov, 1973], [Jensen, 1958]. Jensen et al. bombarded ^{226}Ra with 11 MeV protons and clearly observed a three-humped mass-yield distribution [Jensen, 1958]. Studies of Perry et al. [Perry, 1971] showed triple-humped mass yield distributions in bombardments of ^{226}Ra with 12.5 and 15.5 MeV protons and 16.0 and 19.0 MeV deuterons. In the same study, Perry et al. showed that the fission of ^{228}Ac at excitation energies around 24 MeV had a broadly symmetric mass-yield distribution. This illustrates that the asymmetric mode disappears with increasing excitation energy. The work of Zhagrov et al. [Zhagrov, 1973] illustrated the appearance of a symmetric fission component in the bombardment of ^{226}Ra with 5 - 15 MeV neutrons. At neutron energies of about 15 MeV, the symmetric component increased in intensity to a maximum of about 30% of the asymmetric component. Even at neutron energies of about 7 MeV, the symmetric component is distinguishable from the asymmetric component.

If DF is to compete with gamma deexcitation in ^{228}U, the residual excitation after the EC of ^{228}Np must be several MeV. It is, therefore, not surprising that a small symmetric fission mode exists in the DF of ^{228}U. The associated excitation energies in the previous studies of Ra fission were larger than the estimated 4 MeV in the case of ^{228}U, but the fission barrier is also known to decrease rapidly with increasing Z in this region. With the mass resolution of our experiments, little evidence for the symmetric mode can be

seen in the mass-yield distribution, Figure 4-13a, because the symmetric mass division is only a few percent of the total.

According to Wilkins [Wilkins, 1992], the ECDF of ^{228}Np may not be influenced by shell effects to nearly the extent found in ^{252}Cf. The neutron correction applied in the analysis may not be appropriate. Figure 4-13b shows the mass-yield for ECDF of ^{228}Np without a neutron correction. The peak to valley ratio does not appear to change significantly.

4.1.2.2 X-ray–Fission Correlation

The activity laden KCl aerosols were collected on 23 mg/cm^2 Ni foils. The samples were flamed on the Ni foils prior to placement in the x-ray–fission detection system as described in Section 3.4.2. The activity was placed before a light-tight transmission-mounted 300 mm^2 silicon surface barrier (SSB) detector operated in air which was sandwiched between two germanium x-ray detectors as shown in Figure 3-16.

The overall uranium K_α x-ray–SF coincidence detection efficiency was determined to be 22% in the same manner as described for ^{238}Bk (see previous section). Appropriate amplifier gains for fission fragments were obtained as described for ^{238}Bk. Prompt γ-ray summing effects were estimated as described for ^{238}Bk. It is assumed that any difference in the γ-ray multiplicities between the SF of ^{252}Cf and the ECDF of ^{228}Np are small.

The signal from the SSB detector provided a common start for two time-to-amplitude converters (TACs). The stop signals were provided by the first and second germanium γ-ray detectors. The time window on the TACs was ± 500 nsec. The timing resolution of the germanium detectors was approximately 12 nsec FWHM, and the energy resolution of each detector was less than 1.3 keV FWHM in the U K x-ray region. Upon detection of a fission

fragment in the SSB detector, the amplitudes of the pulses in the SSB detector, the γ-ray detectors, and the TACs were recorded.

During the course of two experiments, approximately 1200 samples were measured and 416 fission fragments were observed in the x-ray–fission coincidence system shown in Figure 3-16. From previous work [Hall, 1990A], [Hall, 1990B] and the determined detection efficiencies and summing rates, it was expected that 32 ± 6 x-rays in the uranium K_α x-ray energy region would be detected. Table 4-2 gives the efficiency and summing information for the germanium detectors and the efficiency of the SSB for each of the two experiments. The expected number of x-ray–fission correlations in each detector is calculated from equation 4-1. The Gamma 3 germanium detector was inoperative for part of the experiment (see Table 4-2). The calculated number of expected correlations for this detector was corrected.

The U $K_{\alpha 2}$ and $K_{\alpha 1}$ peaks should appear at 94.7 and 98.4 keV, respectively and the $K_{\beta 1+3}$ peaks at 110.4 and 111.3 keV and the $K_{\beta 2}$ peak at 114.4 keV [Lederer, 1978]. Ten total events were detected in the U K x-ray region. No more than 1 or 2 of these are likely due to prompt γ-rays which leaves 8 U x-ray–fission coincidences. The x-ray–fission correlation data are shown in Figure 4-14.

The 8 possible coincident K x-rays correspond to only about 25% of the expected number (see Table 4-2). The missing K x-rays cannot be attributed to a significant difference in the γ-ray multiplicity between the SF of ^{252}Cf and the ECDF of ^{228}Np. From the number of prompt γ-rays relative to the ^{228}Np EC K x-rays, the prompt γ-ray multiplicity from ^{228}Np ECDF appears to be similar to that from the SF of ^{252}Cf. Also, the "missing" K x-rays cannot be attributed to pile-up effects. The pile-up rate was less than about 2% because

the γ-ray singles rate was less than 10^4 sec^{-1}. This was monitored occasionally during the experiment with an oscilloscope.

Table 4-2. Efficiency and summing information for the germanium and the solid state detectors used in the study of ECDF in ^{228}Np.

Experiment 1	Gamma 1	Gamma 2	SSB
Fission Efficiency			80%
X-ray Efficiency	2.12%	10.83%	
γ-ray Summing	10.3%	47.5%	
Fissions Detected			332
Expected Correlations	6.3	18.9	
Experiment 2	Gamma 3	Gamma 4	SSB
Fission Efficiency			80%
X-ray Efficiency	9.79%	13.8%	
γ-ray Summing	58.8%	57.3%	
Fissions Detected			84
Expected Correlations	2.0	4.9	
Total Expected X-ray–Fission Correlations	32 ± 6		

For reasons explained in the previous section, the possibility that the ECDF proceeds via L-capture was eliminated based on the absence of U L x-rays in the x-ray–fission correlation data (see Figure 4-14). The U L_β and L_γ x-ray energies are 17.2 and 20.2-keV, respectively [Browne, 1986]. Using the same technique involved in the calculation of the expected number of K x-

ray–fission correlations, the total number of L_β and L_γ x-ray–fission correlations was expected to be 7 ± 2. This number includes the significantly lower fluorescence yield of L x-rays compared to K x-rays and the reduced detection efficiency. One possible L x-ray correlation was detected (see Figure 4-14). It was estimated that 1 L x-ray correlation would result from conversion after K-capture from the table of x-ray intensities given in [Browne, 1986]. This may explain the single event in the L x-ray region. It is likely that the absence of L x-ray–fission correlations indicates that fission occurs from levels populated by EC transition energies larger than the K-shell edge, which leaves approximately 4 MeV as excitation energy of the daughter, well below the estimated fission barrier of 4.5 MeV [Habs, 1978].

The significantly fewer K x-ray–fission correlations than expected require an explanation. The possibility of a long-lived fission isomer was eliminated from analysis of trends in fission isomer lifetimes in the actinide region [Poenaru, 1989]. The estimated ^{228}U fission isomer lifetime is 10^{-12} - 10^{-10} seconds [Poenaru, 1989]. The time-to-amplitude converter window for the x-ray–fission measurements was ± 500 nsec. This would allow the detection of x-ray–fission correlation events for lifetimes shorter than about 1 μs. However, the fission isomer lifetime systematics and the observation of some, although a reduced number, of K x-ray–fission coincidences preclude the presence of a very long-lived fission isomer in ^{228}U. If a fission isomer in the ECDF of ^{228}Np was populated in the EC, then all of the expected x-ray–fission correlations should have been observed.

An interesting possibility is that the fission lifetime may be short compared to the 10^{-17} seconds required to fill the K-vacancy [Scofield, 1974]. If the fission occurs slightly faster than the electronic rearrangement, fewer U K x-rays than expected would be detected because the U would have already

fissioned before the K x-ray was emitted. As mentioned earlier, the fissioning states are assumed to have a high excitation energy. In the case of ^{228}Np, this could be as large as 4 MeV. As evidenced by the relatively small P_{DF} values observed in studies of ECDF (see Table 1-1), γ-decay from the high-energy states in the first potential well populated in the EC must dominate. Weisskopf estimates of lifetimes for 2 MeV, E1 gamma transitions are of order 10^{-17} seconds [Weisskopf, 1951]. It is assumed that deexcitation occurs via a series of high-energy, low multipolarity, gamma transitions such as E1.

In the ECDF of ^{234}Am [Hall, 1990A] and ^{232}Am [Hall, 1990B], the DF must have occurred fast enough to appear prompt to the x-ray–fission system electronics (<20 nsec), but slow enough for the K-vacancies to fill. This was indicated by the observation of the expected number of K x-ray–fission coincidences compared to the total number of fissions detected. If 1% of the EC decays populate the high-energy states (it cannot be larger than this because the rate to low-energy states is much faster) and the P_{DF} is 10^{-4}, then 10^{-2} of the populated high-energy states decay by fission. This would yield a partial fission half-life from these states of order 10^{-15} seconds (appears as prompt to the TAC). The 10^{-15} seconds is the partial half-life for ^{232,234}Pu to tunnel through the innner barrier to the shape isomer. The DF of ^{232,234}Am must have been slowed in the second well which allowed the K-vacancy to fill and indicates that the ECDF of ^{232}Am and ^{234}Am proceeds via a fission shape isomer in the EC daughters.

In the studies of ^{228}Np, only about 25% of the expected K x-ray–fission coincidences were observed. The fission must have occurred on a time-scale similar to the filling of the K-vacancy. The states populated by the EC must be below the top of the fission barrier because if the states populated are above the fission barrier, the P_{DF} should be much larger than 10^{-4}. For the ^{228}U

fission lifetime to be 10^{-17} seconds, ^{228}U cannot have a fission isomer, nor can it have any appreciable second minimum in the fission barrier (see Figure 1-2). This illustrates the importance of ECDF in determining details of the fission barrier (see Section 1).

It is likely the fission of ^{228}U from ^{228}Np ECDF proceeds at a rate comparable to the K-vacancy lifetime, indicating no significant second minimum in the fission barrier for this isotope (see Figure 1-2). This is consistent with the disappearance of fission isomers which is expected in the neutron deficient U/Th region [Poenaru, 1989] resulting from a significant decrease in the height of the first barrier. Because there does not appear to be a shape isomer in ^{228}U, the use of a double-humped fission barrier to calculate fission probabilities may not apply in this region.

4.1.2.3 Mass and Element Assignment

Neptunium was separated as described in Section 3.3.1.3. Evidence for an alpha branch in the decay of ^{228}Np with a 1 minute half-life was obtained by observing the decay of the ^{216}Fr great-granddaughter in the chemically separated Np samples. The electron-capture branch was measured by observation of the ^{212}Po resulting from the ^{228}U decay. The alpha decay chains for ^{228}Np and ^{228}U are shown in Figure 4-15. The ^{212}Po decay was consistent with the decay of 9-minute ^{228}U. The measurement of these activities yielded a ratio of EC to alpha decay of 1.5 ± 0.4 for ^{228}Np. This value has been corrected to include summing effects due to the short lifetimes of isotopes in the ^{228}U and ^{228}Np decay chains. The error limit reflects uncertainties in the magnitude of the summing effects.

4.1.2.4 σ and P_{DF}

The ^{228}Np was produced by the ^{233}U(p,6n)^{228}Np reaction with a total cross section of 35 ± 3 μb. This cross section is based upon an estimated effective target thickness or 50μg/cm^2/target, an estimated 80% He-jet yield and 80% chemical yield. A delayed fission probability of (2.0 ± 0.9) x 10^{-4} was calculated from the experimentally determined electron-capture branch of 0.60, the production cross section of 35 ± 3 μb, and the fission rate of 20 ± 4.5 fission fragment pairs/hour/eμA observed in the rotating-wheel experiments. This is similar to the values of 6.9 x 10^{-4} and 6.6 x 10^{-5}, respectively, determined for ^{234}Am and ^{232}Am by Hall et al. [Hall, 1990A], [Hall, 1990B], given the differences in the estimated EC Q-values. This delayed fission probability is about 5 times lower than indicated by the previous studies of ^{228}Np by Skobelev [Skobelev, 1972]. The results of Skobelev, however, did not provide either direct evidence for the production of ^{228}Np by chemical separation, correlations with the known alpha and EC daughters, or x-ray–fission correlations. Using the half-life of 61 seconds, and the estimated Q_{EC} of 4.17 MeV [Möller, 1988], the log(ft) is estimated as 4.9 using the systematics in [Lederer, 1978].

4.2 New Isotope Searches

4.2.1 ^{241}Bk

4.2.1.1 Production Cross Section Limit

A search was performed for the unknown isotope ^{241}Bk produced in the reaction ^{241}Am(^{4}He, 4n)^{241}Bk using the milking technique described in Section 3.3.1. Samples were collected as discussed in Section 3.3.1.1.1. Ten collections and separations were performed for each irradiation time. The 32.8-day ^{241}Cm was back extracted with 3M HCl. A known amount of ^{243}Am

was added to act as a tracer. The fractions containing the back-extracted Cm (Bk daughter) were dried and flamed on Pt for counting. Although the samples appeared thin, alpha-pulse-height analysis showed that the samples were not uniform based on large low-energy tailing in the ^{243}Am alpha peak. It was not possible to determine the amount of ^{241}Cm at 5.94 MeV because of the large tailing of the known ^{242}Cm (from ^{242}Bk) alpha peak at 6.11 MeV. A cation exchange column was employed to remove the impurities and the samples electroplated on Pt foil as discussed in Section 3.3.1. The overall yield through the initial chemistry (Figure 3-6), the purification chemistry (Figure 3-8) and the electroplating was determined to be 10%. The alpha decay branch for ^{241}Cm was taken as 1% from [Lederer, 1978].

The samples were counted at a geometry of 30% as determined with an alpha calibration standard. After 5 days of counting, no evidence for the 5.94 MeV ^{241}Cm alpha was observed. Approximately 30 events were recorded in this region, but were attributed to a small amount of tailing from the 6.11 and 6.06 MeV alpha groups of ^{242}Cm (daughter of ^{242}Bk). A limit was set for the ^{241}Bk half-life and production cross section based on requiring at least 2 standard deviations more counts in the region of interest than could be attributed to tailing from the slightly higher energy ^{242}Cm alphas. This is about 20 counts/5 days in the ^{241}Cm region above the 30 counts/5 days attributed to the ^{242}Cm tailing.

The limit on the ^{241}Bk half-life and production cross section can be calculated from the basic production equation as:

$$\lambda N_0 = N_t \sigma \phi (1-e^{-\lambda T_{irr}}) \qquad \text{Equation 4-2}$$

In equation 4-2, λ is the decay constant for ^{241}Bk, N_0 is the number of ^{241}Bk atoms produced after the irradiation, N_t is the number of ^{241}Am target atoms, σ is the production cross section of ^{241}Bk, ϕ is the beam current, and T_{irr} is

the length of irradiation. Factors must be included for decay during the initial chemical separation, the delay required for sample clean-up and plating, and the number of atoms of 32.8-day ^{241}Cm remaining after the sample is removed from the counter. Inclusion of these terms in equation 4-2 yields equation 4-3:

$$\lambda N_{det} = N_s N_t \sigma \phi (1-e^{-\lambda T_{irr}})(e^{-\lambda T_{chem}})(1-e^{-\lambda T_{count}})(e^{-\lambda_1 T_{plate}}) \quad \text{Equation 4-3}$$

In equation 4-3, N_{det} is the number of ^{241}Cm atoms detected (it is assumed that ^{241}Bk decays primarily by electron-capture so that there is a one-to-one correspondence between the number of atoms of ^{241}Cm and ^{241}Bk); N_s is the number of samples measured for a given irradiation interval; T_{chem} is the interval between end of irradiation and chemical separation; T_{count} is the counting interval; λ_1 is the decay constant for ^{241}Cm; T_{plate} is the delay due to sample clean-up and plating (30 days). Rearrangement of equation 4-3 yields equation 4-4. This gives the production cross section as a function of the decay constant, which is easily related to the half-life.

$$\sigma = \lambda N_{det} / [N_s N_t \phi (1-e^{-\lambda T_{irr}})(e^{-\lambda T_{chem}})(1-e^{-\lambda T_{count}})(e^{-\lambda_1 T_{plate}})] \quad \text{Equation 4-4}$$

Solutions to equation 4-4 are plotted in Figure 4-16. From Figure 4-16, if the estimated half-life of the ^{241}Bk is of order 40 minutes, the upper limit on the production cross section is about 3 μb. This half-life is estimated from the electron-capture systematics given in [Lederer, 1978] using an estimated Q_{EC} of 2.19 MeV [Möller, 1988] and a log(ft) of 6.

The calculations of SPIT [Haynes, 1988] estimate the production cross section of ^{241}Bk to be 1 mb. Because no evidence for the existence of ^{241}Bk was obtained in this experiment to the level of about 3 μb, either the ^{241}Bk half-life is significantly shorter than the estimated 40 minutes or SPIT is overestimating the cross section by several orders of magnitude. Because SPIT has been shown to be accurate within one order of magnitude

[Haynes, 1988], it is likely that the ^{241}Bk half-life is significantly shorter than 40 minutes. If the ^{241}Bk half-life is about 1 minute, the production cross section limit would be within one order of magnitude of that calculated by SPIT (see Figure 4-16). However, the estimated log(ft) would be 4.5. This is somewhat smaller than the known log(ft) values in this region and implies a nearly superallowed transition. In the case of ^{238}Bk described earlier, the log(ft) value was about 5.2. For ^{242}Bk, the half-life is known to be 7 minutes [Lederer, 1978] and the estimated Q_{EC} is 3 MeV [Möller, 1988]. The log(ft) for ^{242}Bk is 5.3. The log(ft) value for ^{241}Bk is expected to be somewhat larger than either ^{242}Bk or ^{238}Bk because of the significantly lower Q_{EC} and because the EC of ^{241}Bk involves conversion of an odd-proton, even-neutron isotope to an even-proton, odd-neutron isotope. Given the range of log(ft) values for ^{238}Bk and ^{242}Bk, it is marginally possible that ^{241}Bk has a log(ft) of 4.5. The log(ft) values excluded in this experiment are 5.4-7.3 for transitions to the ground state in the ^{241}Cm daughter. This log(ft) range was estimated using the systematics in [Lederer, 1978].

4.2.2 ^{252}Bk and ^{253}Bk

4.2.2.1 Manual Chemistry for ^{252}Bk and ^{253}Bk

The ^{252}Bk was produced and separated as described in Sections 3.2 and 3.3, respectively. The irradiation times of 1, 3, 10 and 20 minutes were alternated to eliminate the effects of fluctuating beam intensities and transport efficiencies. Eight samples were collected for each irradiation interval. The one-hour delay (see Section 3.3.1.1.1) prior to back extraction of the Bk should have allowed all of the ^{252}Bk and ^{253}Bk to decay to Cf while only a small fraction of the 3.2-hour ^{250}Bk and 23.7-hour ^{248}Bk decayed. This reduced the amount of ^{250}Cf (6.031 MeV alpha) and ^{248}Cf (6.26 MeV alpha) in

the samples, which might mask the ^{252}Cf (6.118 MeV) alpha group. After 2 days, the separated samples were electroplated on Pt foil and counted by alpha-pulse-height analysis as described in Section 3.3.1.1.1. The ratio of the amount of ^{243}Am tracer present in the separated samples to the total ^{243}Am tracer used in the initial separation indicates that the separation factor between the Bk^{4+} and the trivalent actinides is better than 8×10^5.

4.2.2.1.1 ^{252}Bk

The number of 13.1-year ^{250}Cf (from the decay of ^{250}Bk) and 2.6-year ^{252}Cf (from the decay of ^{252}Bk) atoms calculated from the observed activities in the samples is plotted in Figure 4-18 as a function of the irradiation interval. A growth curve was fitted to each set of data by a least-squares analysis program. The curves were generated from the expected number of atoms produced per irradiation interval from equation 4-2. A least-squares fit minimized the chi-squared values between the experimentally determined number of ^{252}Cf atoms and the calculated value based on an estimated half-life and production cross section at each irradiation interval. The ^{250}Cf growth curve was consistent with the known ^{250}Bk half-life of 3.2 hours. The amount of activity from the ^{250}Bk decay was consistent with a production cross section of 4 mb. This value is very close to the value of about 2 mb given by Lee et al. [Lee, 1983] at a ^{18}O beam energy of 104 MeV. The ^{252}Cf growth curve was consistent with a ^{252}Bk half-life of 1.8 ± 0.5 minutes and a production cross section of 47 ± 10 μb. The amount of ^{252}Cf in the samples does not increase beyond irradiation times of 3 minutes (see Figure 4-18). This observation and the ^{243}Am tracer results, indicate that the ^{252}Cf resulted from the beta decay of ^{252}Bk. The expected amount of ^{252}Cf and ^{250}Cf from contamination was more than 10^2 times lower than the observed activities.

The ^{252}Bk half-life is a factor of 5 shorter than the 10-minutes estimated from systematics in [Lederer, 1978] using a beta-decay Q-value of 2.21 MeV [Möller, 1988]. This implies that the beta decay to ^{252}Cf proceeds via an allowed transition. The estimated ^{252}Bk excitation energy at an ^{18}O energy of 95 MeV is -5.2 MeV. For an ^{18}O energy of 107 MeV, the excitation of ^{252}Bk would be -2 MeV, if the additional 12 MeV is apportioned according to the fraction of projectile mass transferred. However, there is some experimental evidence that 60% of the energy is transferred to the heavy product [Lee, 1983]. This is the first report of a half-life and production cross section for ^{252}Bk.

4.2.2.1.2 ^{253}Bk

After 21-days of counting, no evidence for the 6.61 MeV ^{253}Es, grand-daughter of ^{253}Bk, was observed. The grand-daughter of ^{253}Bk was chosen because its alpha energy is well above the Cf daughters of the lighter Bk isotopes and the ^{253}Cf, beta-decay daughter of ^{253}Bk, is known to have a small alpha branch (<0.3%). A limit was set for the ^{253}Bk half-life and production cross section in the same manner as described for ^{241}Bk. It was assumed that 4 counts/day of the ^{253}Es are required to yield a statistically significant indication of the ^{253}Bk growth with irradiation time. The estimated ^{253}Bk beta-decay Q-value is 1.39 MeV [Möller, 1988]. Using a log(ft) of 6, the ^{253}Bk half-life is estimated as 1 hour from the systematics in [Lederer, 1978]. From Figure 4-19, if the estimated half-life of the ^{253}Bk is about 1 hour, the production cross section is less than about 400 nb.

The estimated ^{253}Bk production cross section with an ^{18}O energy of 104 MeV is 10 μb (estimated from the systematics in [Lee, 1983]). After calculation of the transfer product excitation energy by the method given in [Hoffman, 1990A], it was determined that the ^{18}O bombarding energy was too low for

optimum production of ^{253}Bk. The estimated excitation energy of the ^{253}Bk produced in the ^{5}H transfer reaction using ^{18}O at 95 MeV is -10 MeV. For an ^{18}O energy of 107 MeV, the excitation energy of ^{253}Bk would be about -7 MeV, if the additional 12 MeV is apportioned according to the fraction of projectile mass transferred [Leyba, 1990] [Hoffman, 1990A]. The production cross section for ^{253}Bk at an ^{18}O energy of 107 MeV may be significantly smaller than the estimated 10 μb. If the ^{253}Bk half-life is less than about 30 minutes, the sensitivity of this experiment did not allow for detection of ^{253}Bk.

4.2.2.2 Beta–L x-ray Correlation, Search for ^{252}Bk

The ^{252}Bk was produced and transported to the beta–L x-ray coincidence apparatus described in Section 3.3. As discussed in that section, the ^{248}Cm target was coated with a layer of ^{nat}Gd to produce isotopes for use in another experiment. The ^{18}O bombardments produced large amounts of Hf isotopes which are high energy beta emitters. These products had to be removed before the sample could be placed in the beta–L x-ray apparatus because the high energy beta particles would swamp the ^{252}Bk beta activity. The Bk was isolated using the HDEHP extraction described in Section 3.3. The sample was placed in the beta–L x-ray apparatus; however, by this time, approximately 3-minutes had elapsed. The isotope is now known to posses a 20 second half-life (see previous section). The isotope was not produced in sufficient quantity to allow for detection with this method because of the 3 minutes required for separation and placement into the beta–L x-ray apparatus.

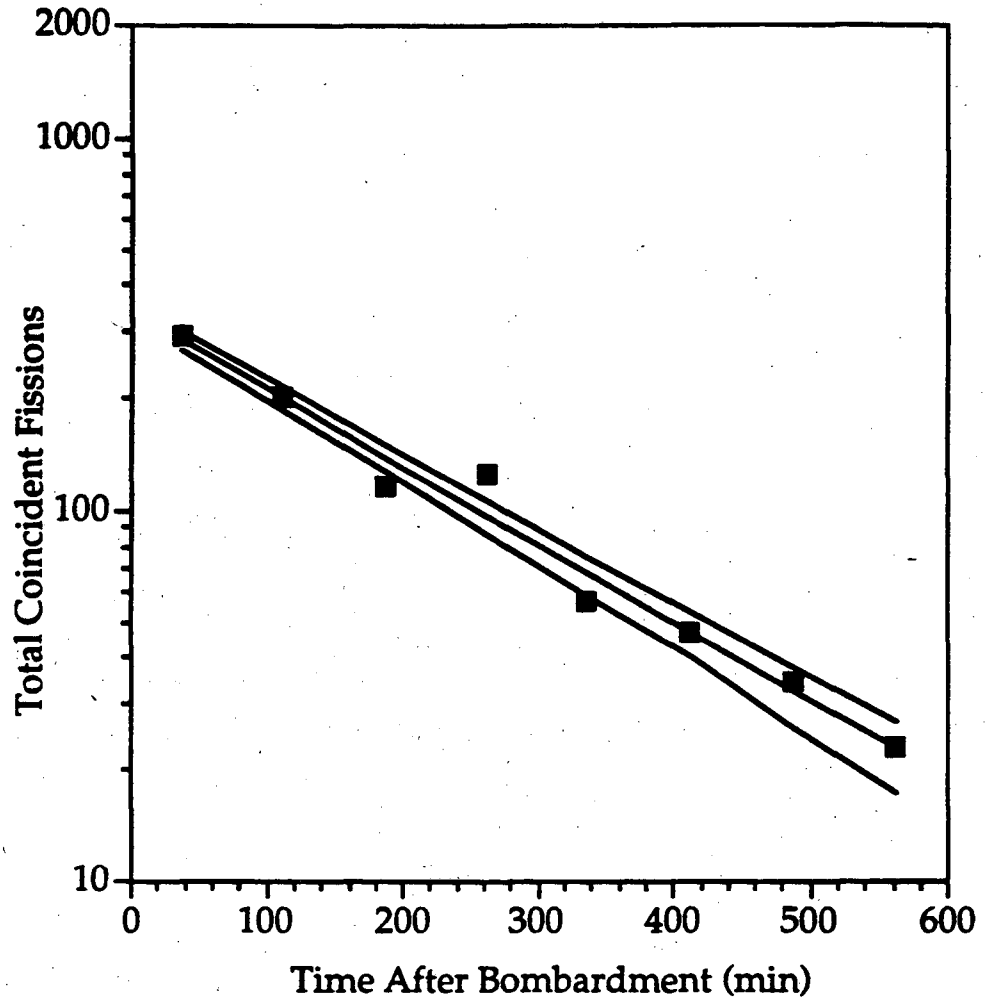

Figure 4-1. Maximum likelihood fit to coincident fissions from ECDF of ^{238}Bk as measured on MG-RAGS. In this figure, the average count rates during the time intervals are indicated by the symbols. For each fit, the center curve is the most probable fit to the data. The upper and lower curves are the limits which encompass 68% of the probability in a Poisson distribution centered on the number of counts expected during the interval from the most probable fit. Data correspond to 388 individual experiments (collections). The half-life was determined to be 144 ± 5seconds.

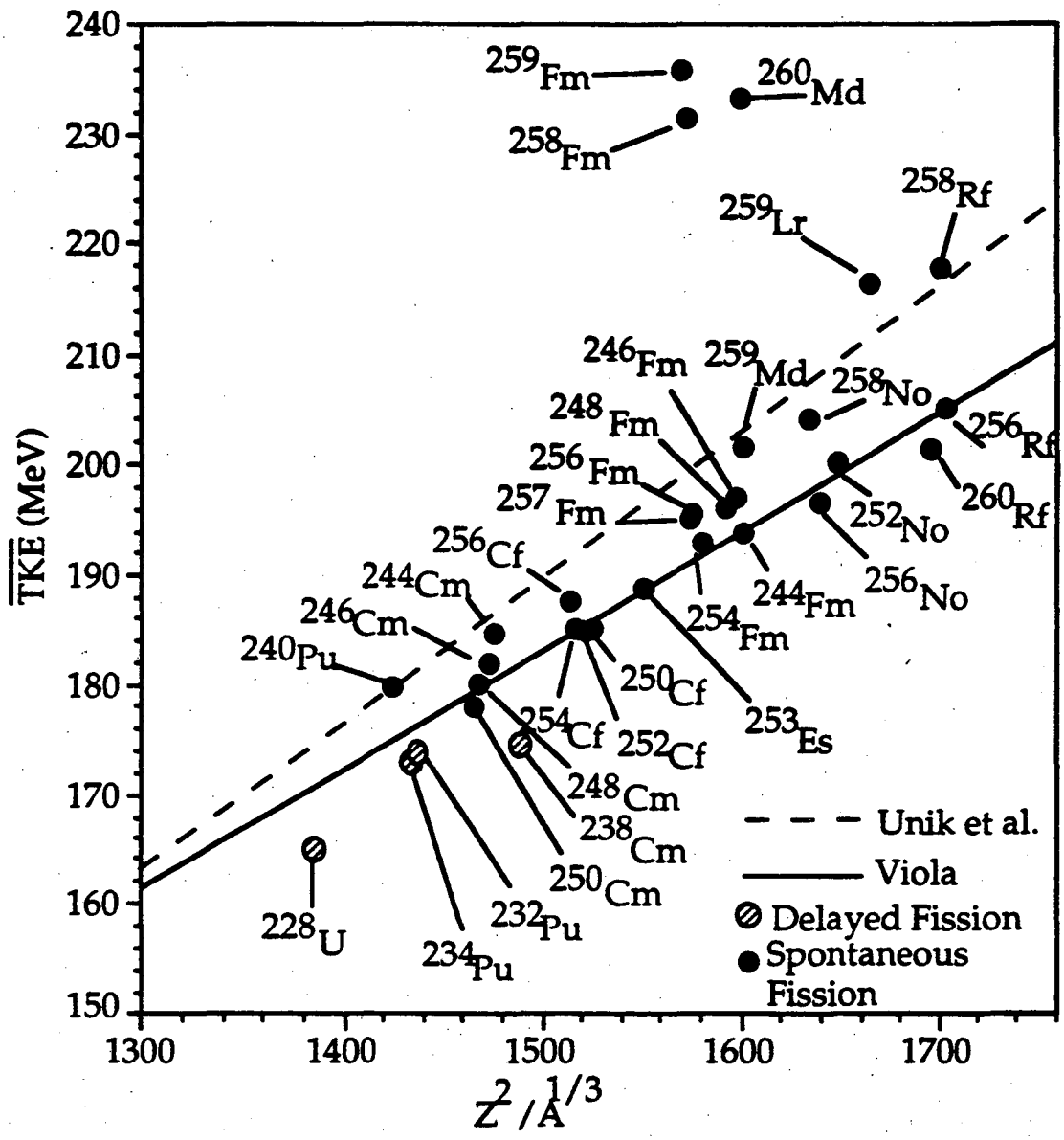

Figure 4-2. Average or most probable TKE versus $Z^2/A^{1/3}$. The solid line is the linear fit of Viola [Viola, 1966]. The dashed line is from Unik et al. [Unik, 1973]. All of the $\overline{TKE}$ values have been corrected to be consistent with the calibration parameters of Weissenberger et al. [Weissenberger, 1986]. The open circles depict values measured from delayed fission. The closed circles depict values measured from spontaneous fission.

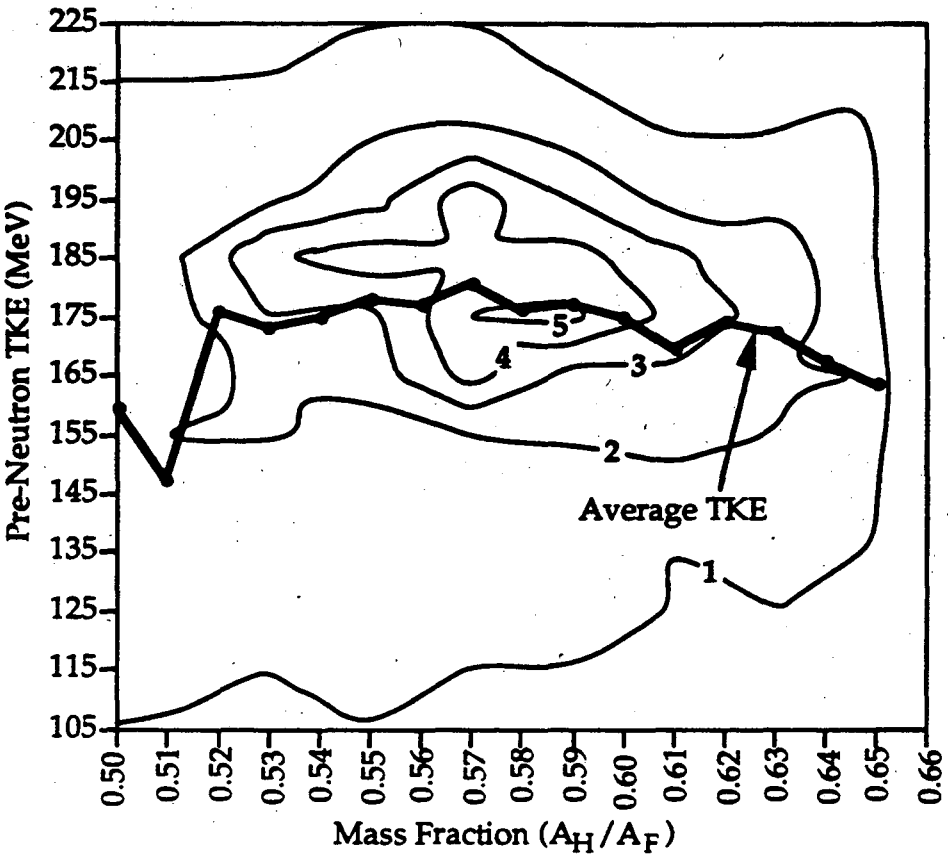

Figure 4-3. Contour diagram for ECDF of ^{238}Bk fissions as a function of pre-neutron-emission TKE and MF. The contours indicate equal numbers of events based on data groupings of 10 MeV x 0.02 units of mass fraction. Contours 1-5 indicate 5, 10, 15, 20, and 25 events, respectively. The average TKE at each mass fraction is indicated. A total of 382 events are included.

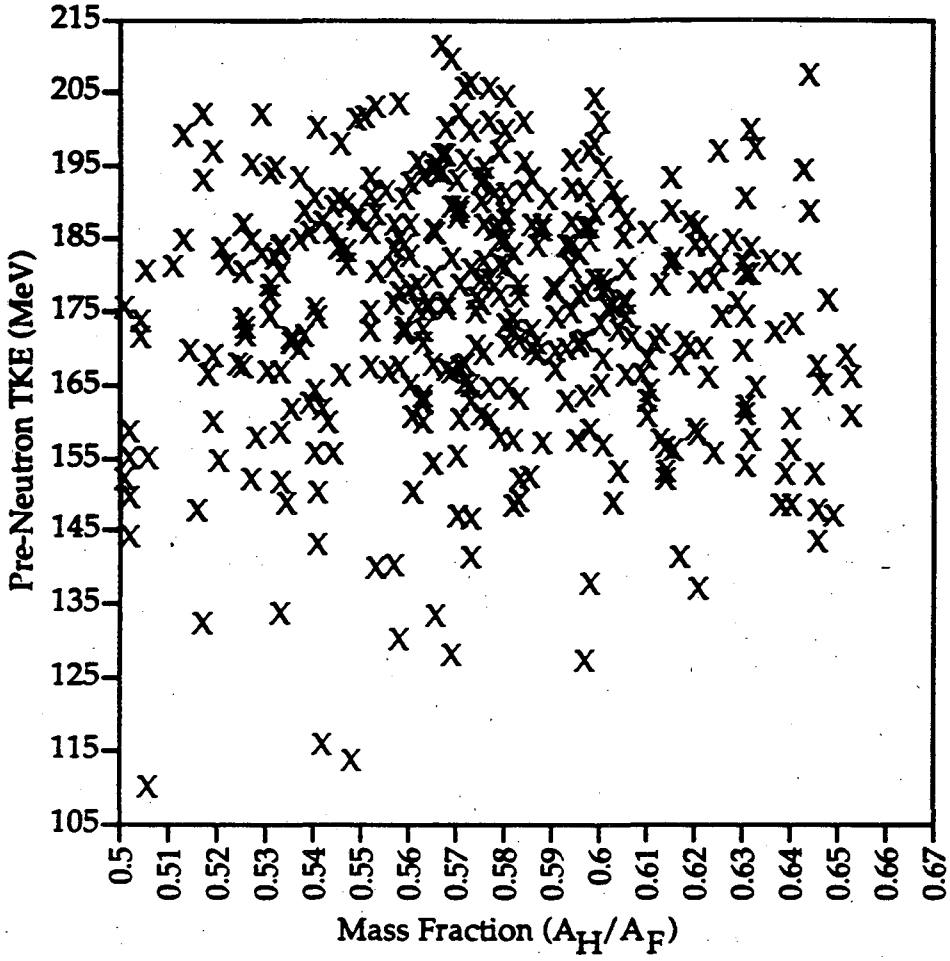

Figure 4-4. Individual events from ECDF of ^{238}Bk plotted as a function of TKE and MF. A total of 382 events is illustrated.

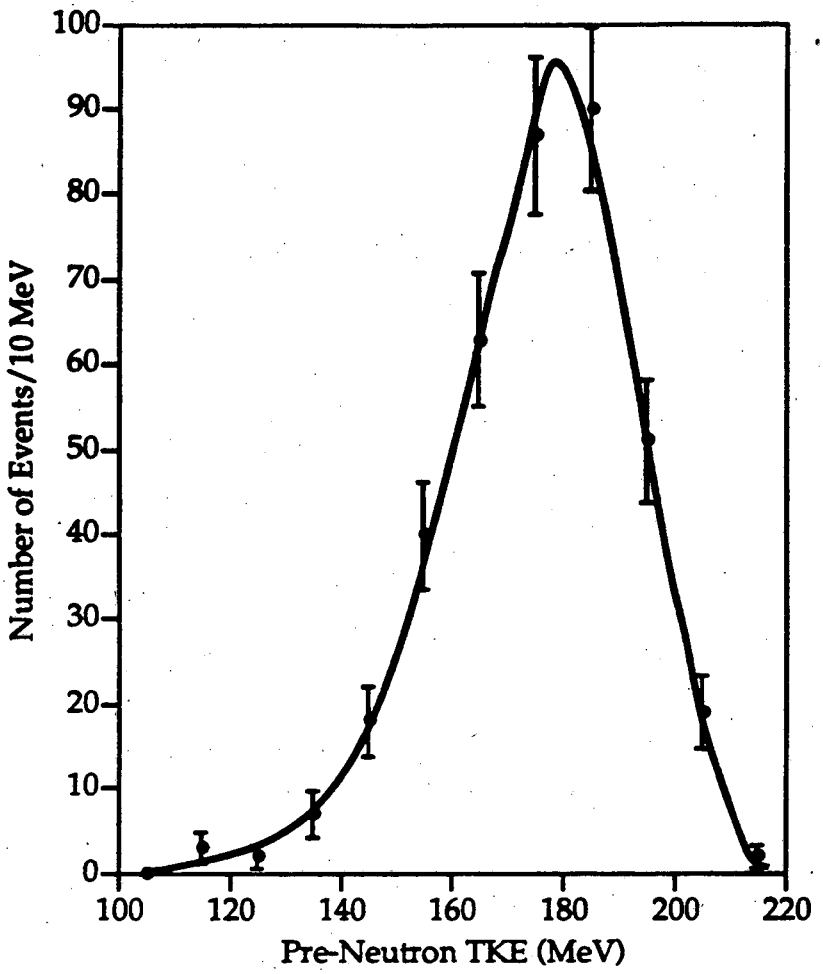

Figure 4-5. Pre-neutron emission TKE distribution from ECDF of ^{238}Bk. The data are in groupings of 10 MeV.

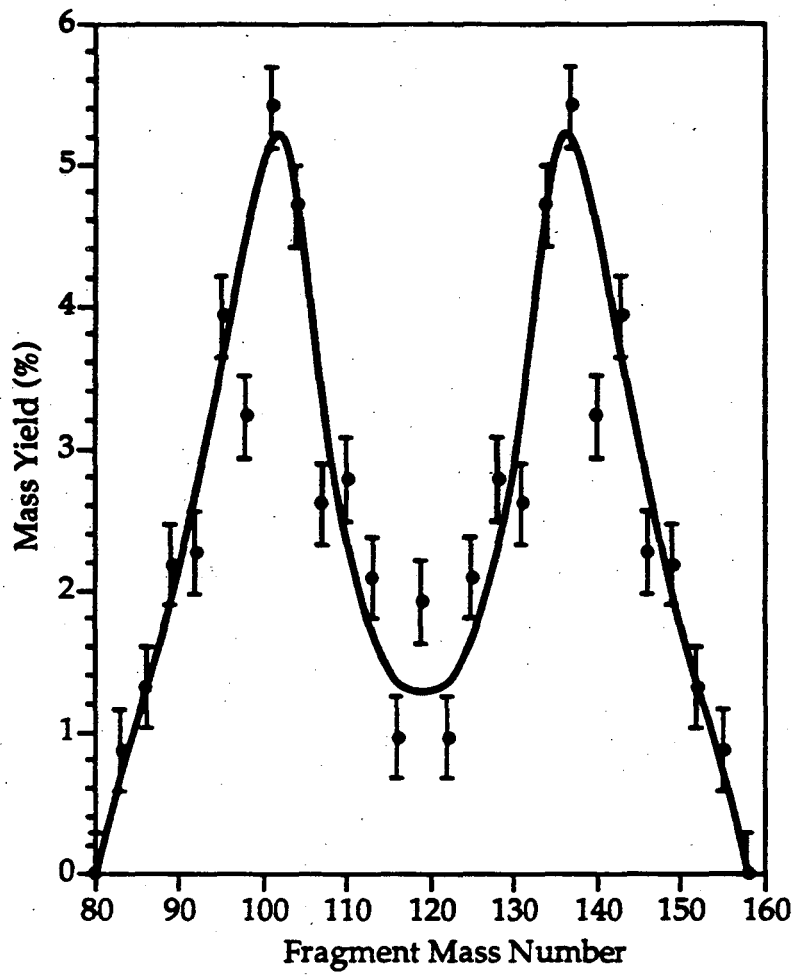

Figure 4-6. Pre-neutron emission mass-yield distribution for the ECDF of ^{238}Bk. The data were averaged over 3 mass numbers.

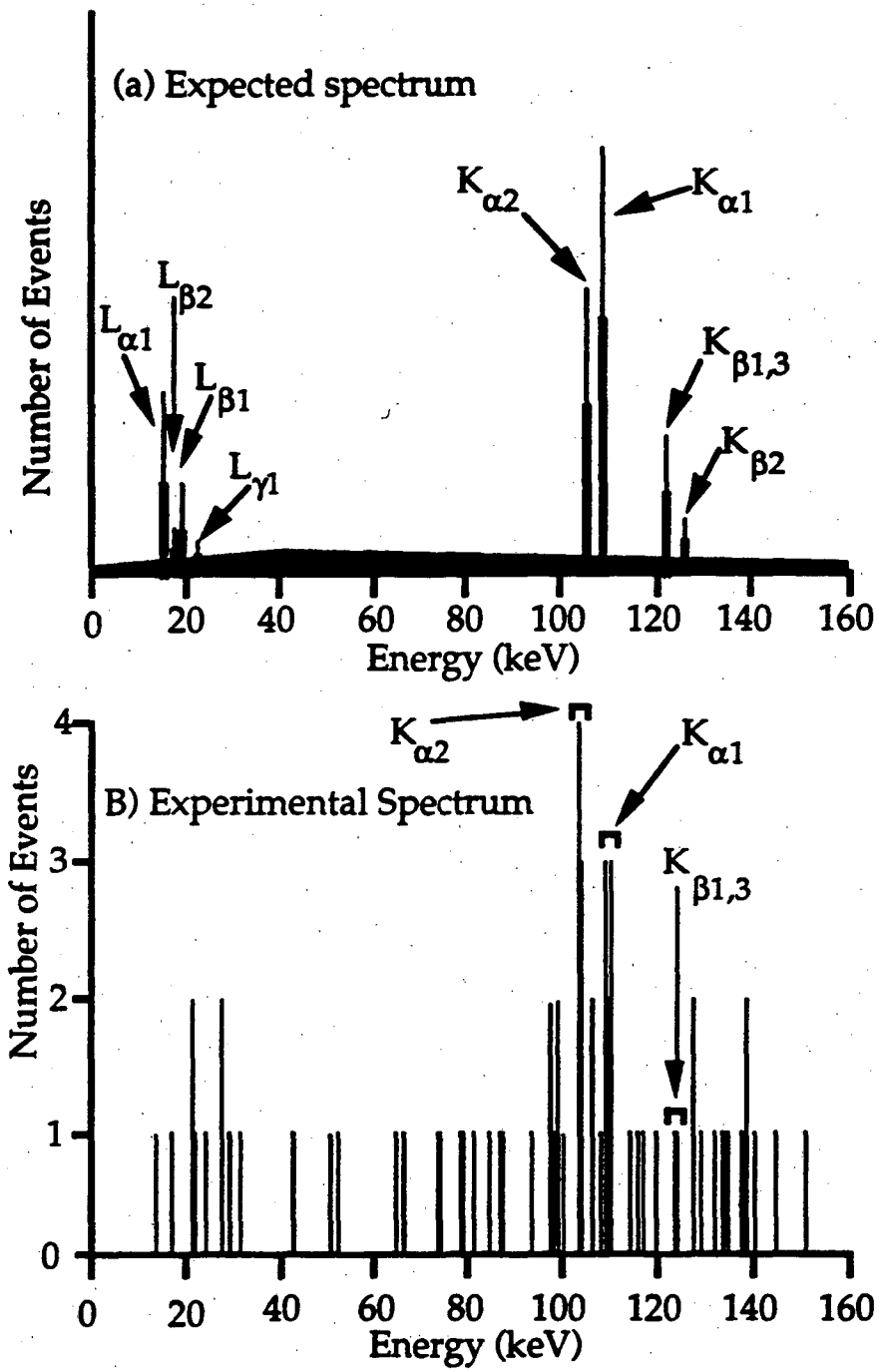

Figure 4-7. X-ray–fission coincidence data for the ECDF decay of ^{238}Bk. Seventeen events are indicated in the Cm K x-ray region.

Bk-238 Decay Scheme

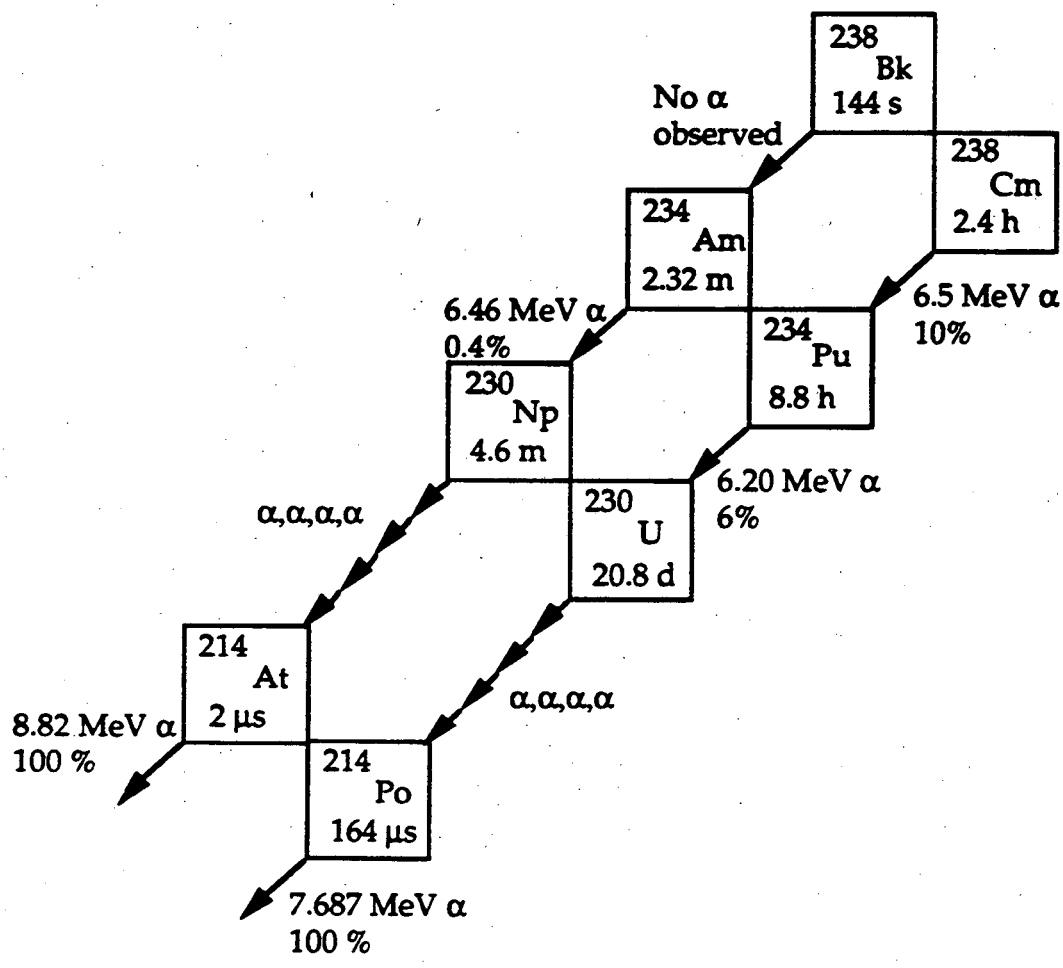

Figure 4-8. Decay Scheme for ^{238}Bk.

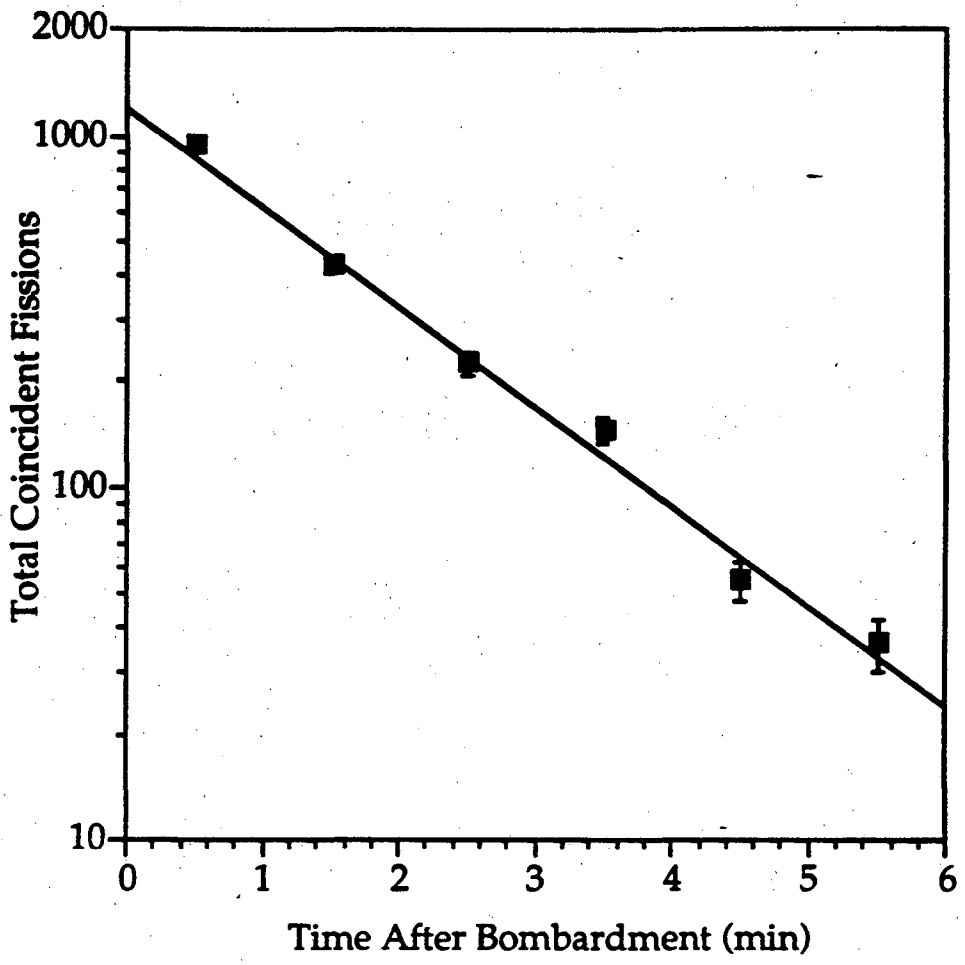

Figure 4-9. Least squares fit to coincident fissions from ECDF of ^{228}Np as measured on MG-RAGS.

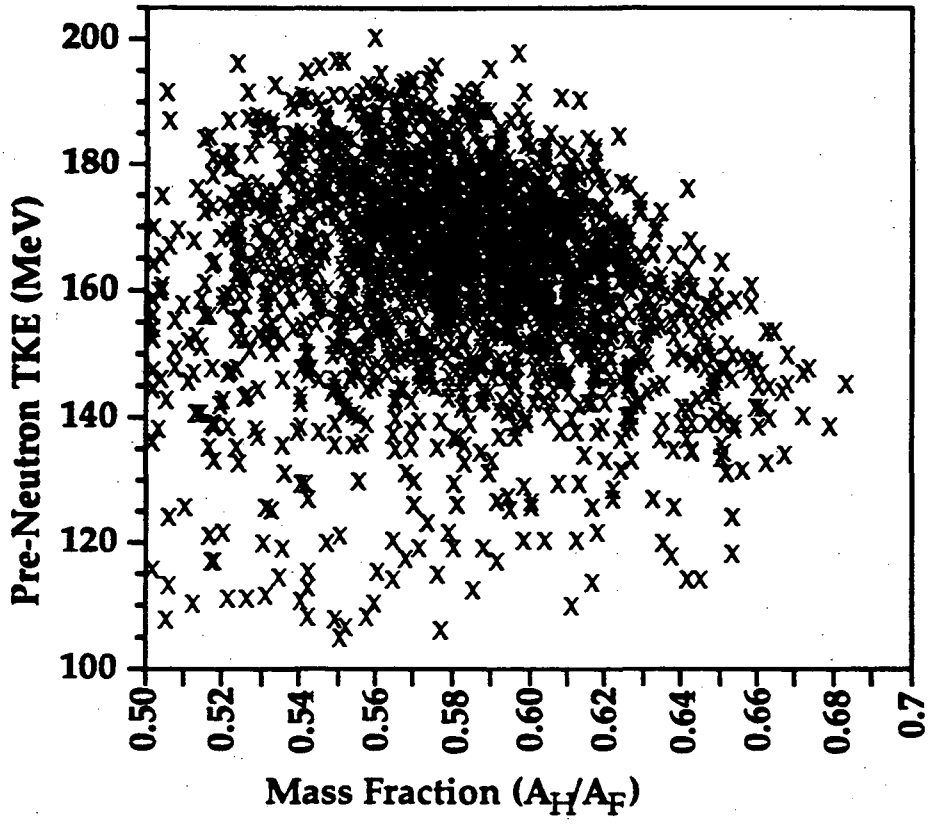

Figure 4-10. Individual events from ECDF of ^{228}Np as a function of TKE and MF.

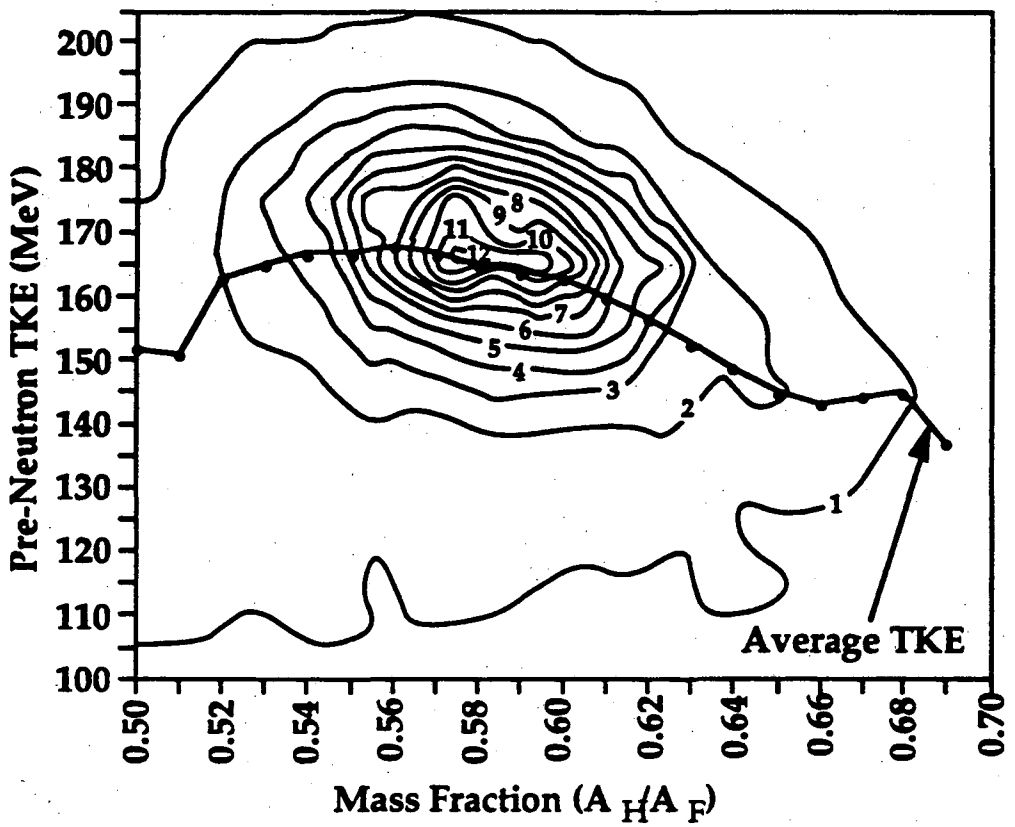

Figure 4-11. Contour diagram for ^{228}Np ECDF as a function of TKE and MF. The contours indicate equal numbers of events based on data groupings of 10 MeV x 0.01 units of mass fraction. Contours 1-12 indicate 10, 20, 30, 40, 50, 60, 70, 80, 90, 100, 110, and 120 events, respectively, based on measurement of 2373 fission events. The average TKE at each MF is indicated.

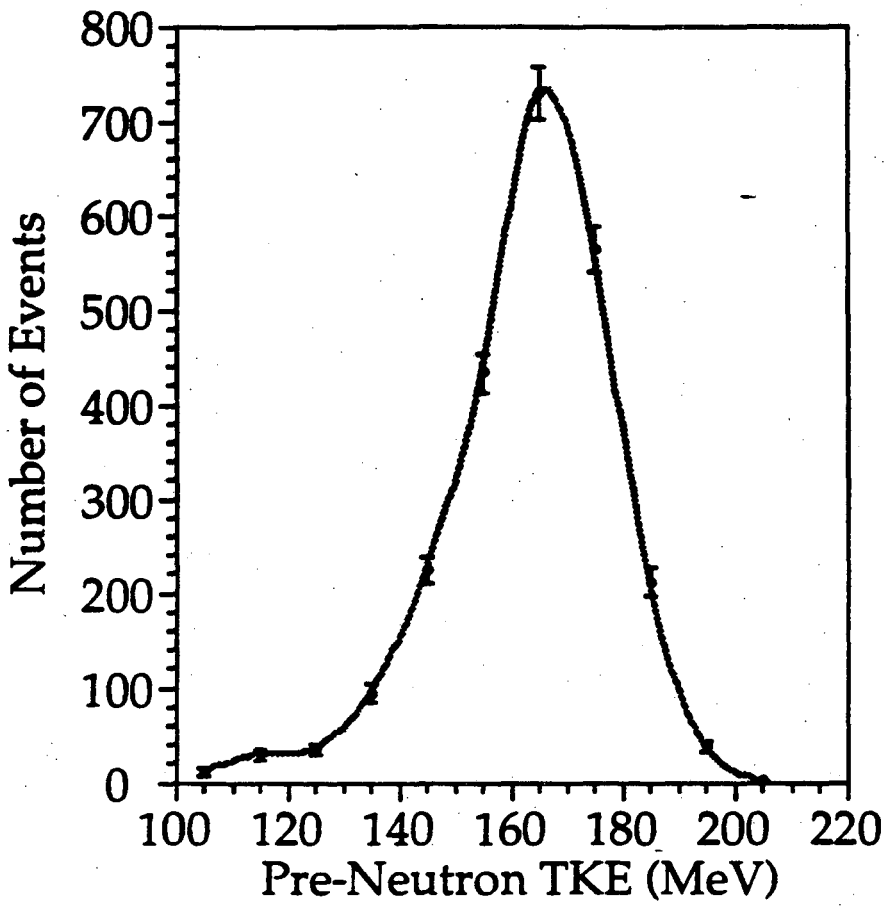

Figure 4-12. Pre-neutron-emission TKE distribution from ECDF of ^{228}Np. The data are in groupings of 10 MeV. The lower TKE associated with the symmetric mass split is associated with the small tail in the spectrum.

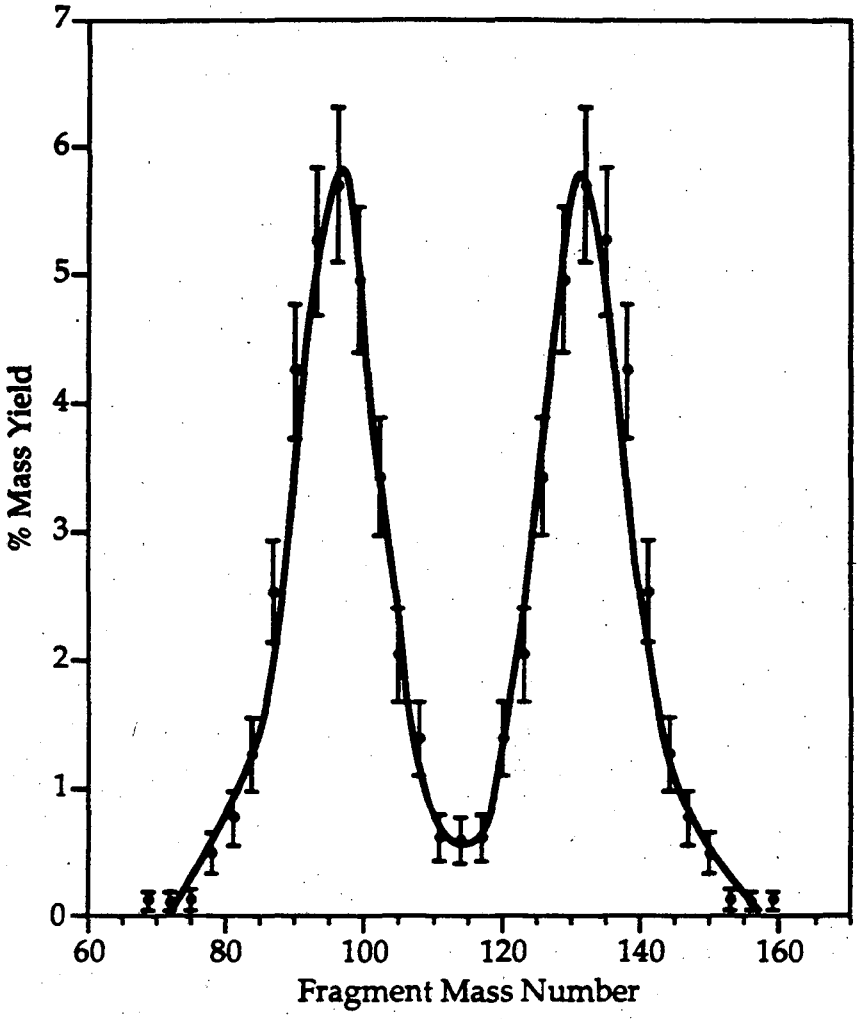

Figure 4-13a. Pre-neutron emission mass-yield distribution for ECDF of ^{228}Np. The data were averaged over 3 mass units.

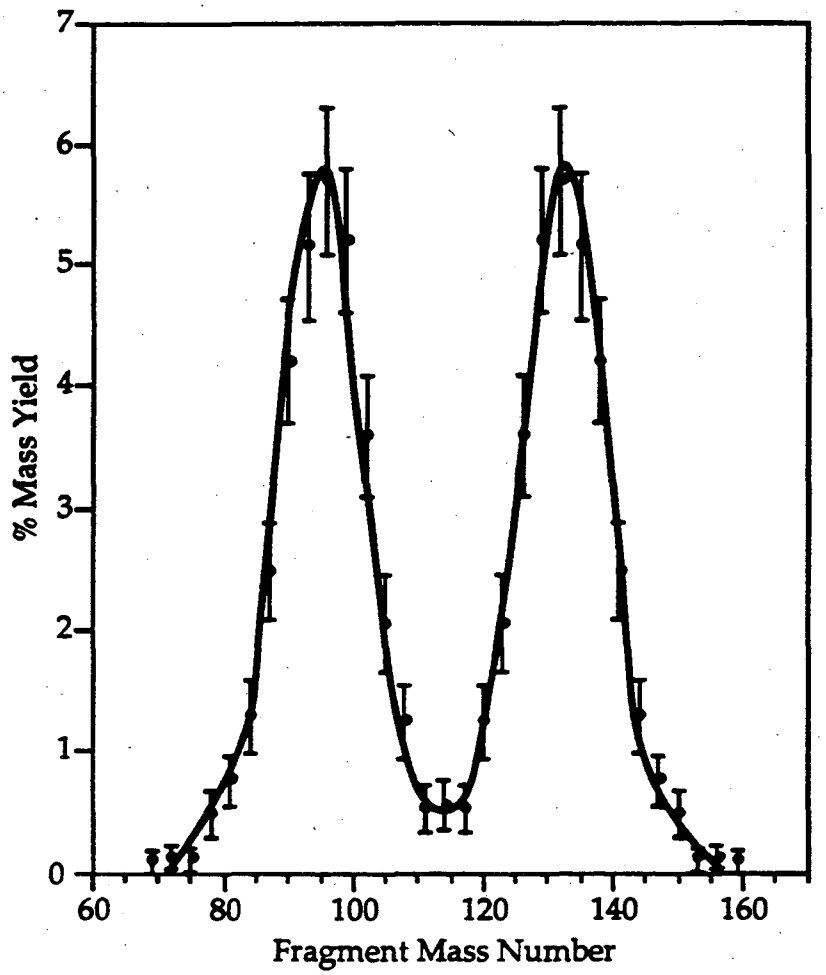

Figure 4-13b. Mass-yield distribution for ECDF of ^{228}Np without correction for neutron emission. The data were averaged over 3 mass units.

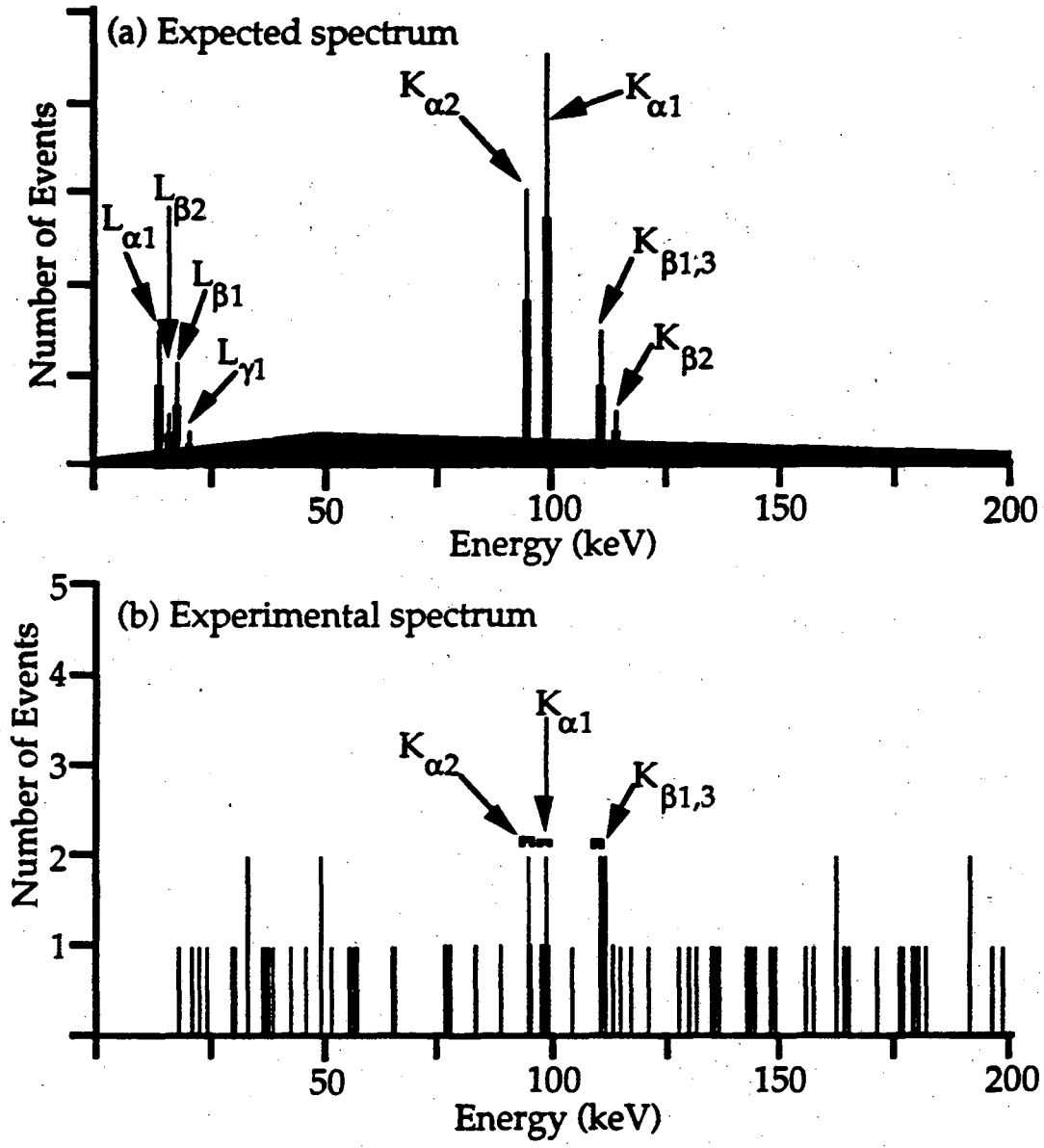

Figure 4-14. X-ray–Fission correlation data for ^{228}Np. Part (a) shows the expected x-ray spectrum with $K_{\alpha 1}$ and $K_{\alpha 2}$ peaks at 94.7 and 98.4 keV, and $K_{\beta 1+3}$ and $K_{\beta 2}$ peaks at 111 and 114.4 keV, respectively, [Lederer, 1978] together with an approximate expected energy distribution for the prompt γ-ray coincidences from the deexcitation of fission fragments. Possible contributions from L x-rays are also shown. Part (b) gives the experimental spectrum showing the 10 detected events in the U K x-ray region.

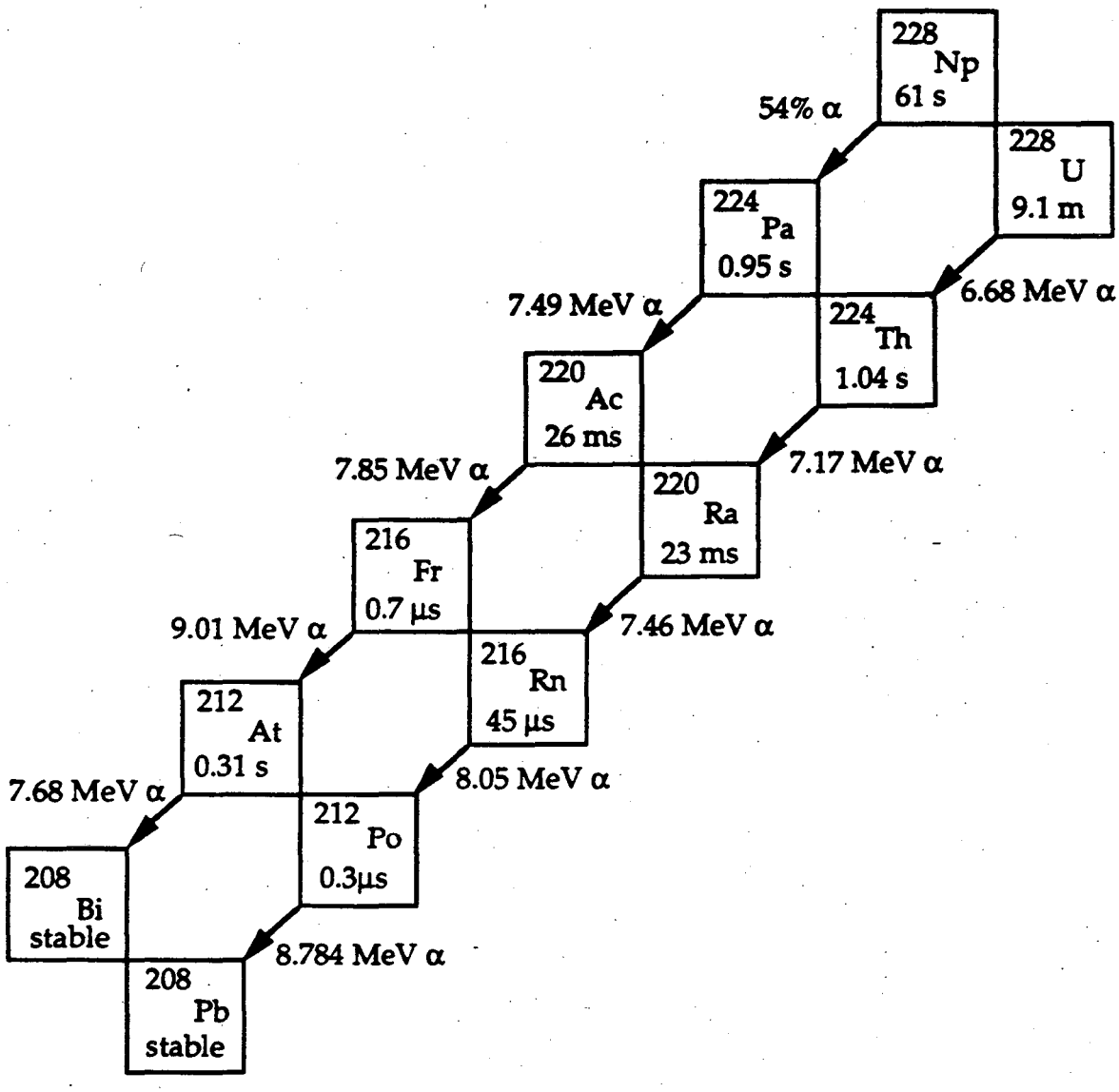

Figure 4-15. Alpha-decay chains for ^{228}Np and ^{228}U. The alpha and electron-capture branches for ^{228}Np were determined by measuring the ^{216}Fr and ^{212}Po, respectively and correcting for summing effects.

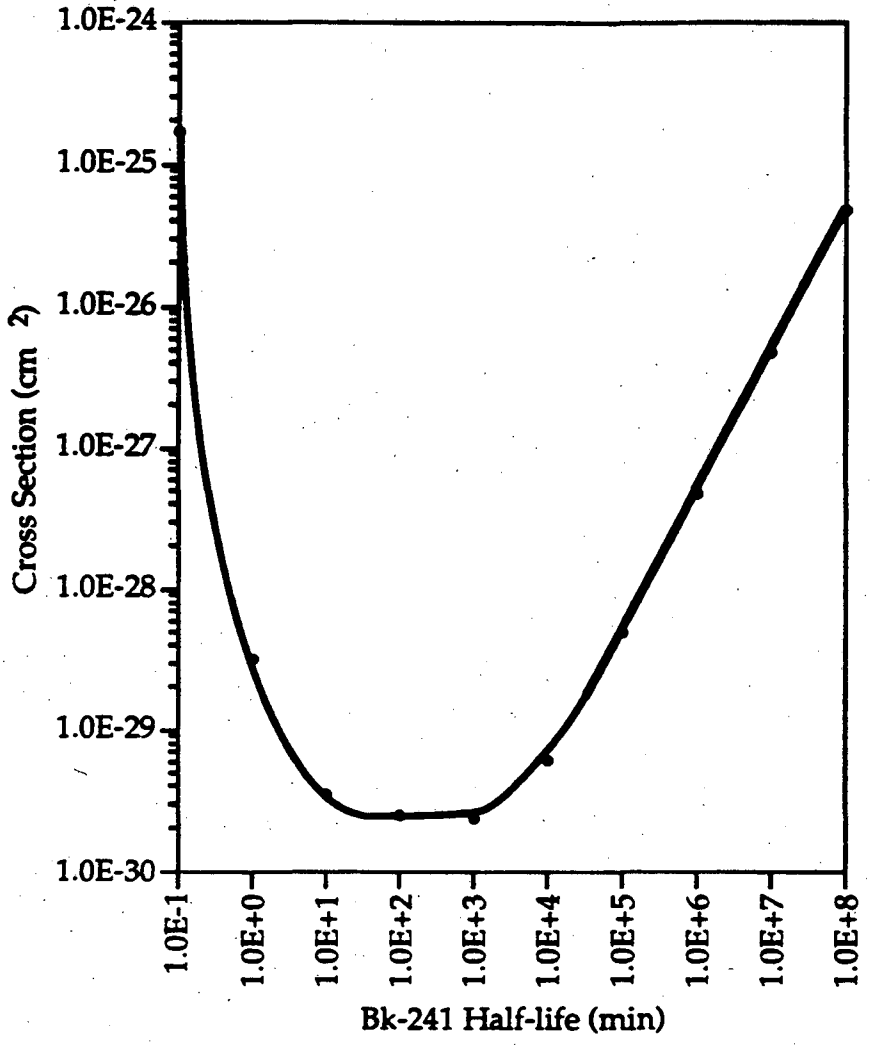

Figure 4-16. Plot of production cross section vs. half-life for ^{241}Bk. It is assumed that 4 counts/day of the ^{241}Cm 5.94 MeV alpha are required for positive identification of ^{241}Bk.

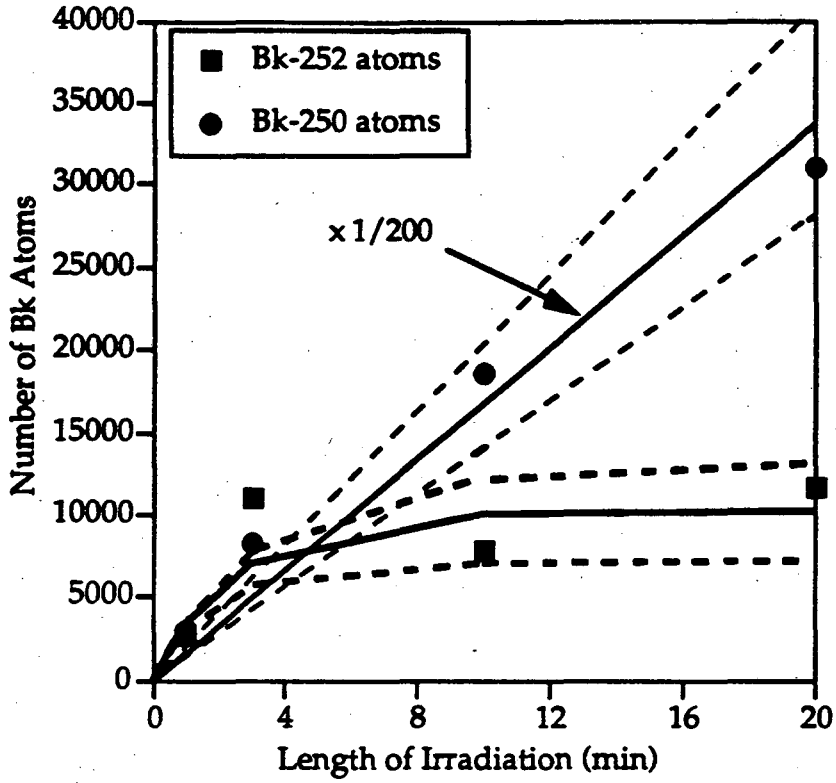

Figure 4-17. Plot of the total number of ^{250}Bk and ^{252}Bk atoms as a function of the length of irradiation. The number of atoms at each irradiation interval is indicated by the symbols. For each least-squares fit, the center curve is the fit to the data. The upper and lower dashed curves are the 1 σ limits.

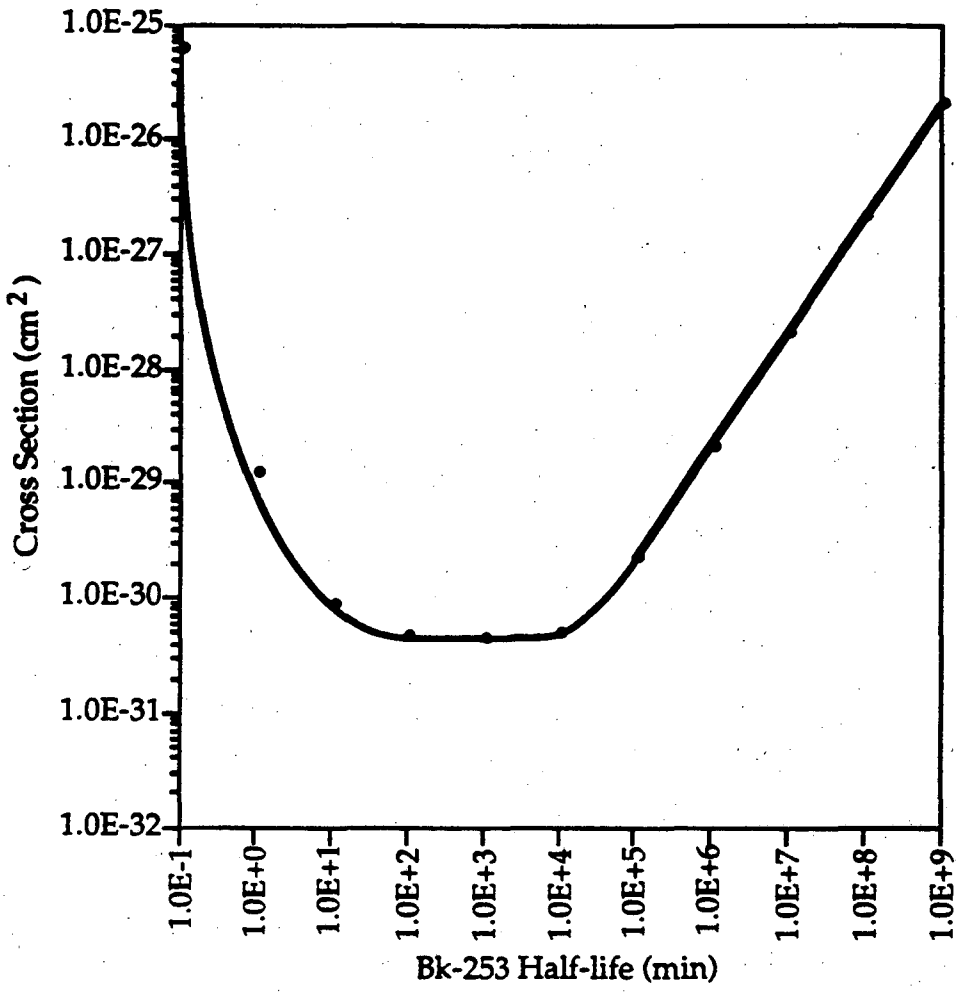

Figure 4-18. Plot of production cross section vs. half-life for ^{253}Bk. It is assumed that 4 counts/day of the ^{253}Es 6.61 MeV alpha are required for positive identification of ^{253}Bk.

5 Conclusions

5.1 ^{228}Np

ECDF was studied in ^{228}Np produced via the ^{233}U(p, 6n)^{228}Np reaction. The fission properties and half-life were measured with a rotating-wheel system. The half-life of this isotope was determined to be 61.4 ± 1.4 seconds from measurements of the fission activity. A predominantly asymmetric mass-yield distribution was observed, but a small symmetric component is indicated by the TKE/mass fraction contour plot. The most probable pre-neutron total kinetic energy of fission for the asymmetric component was determined to be 165 ± 5 MeV. The symmetric fission component had a TKE of 150 ± 5 MeV and constituted about 2% of the total number of fissions.

The observed fissions were assigned to ECDF of Np based on observation of fissions in coincidence with the x-rays of U resulting from K capture in Np. The mass and Z were assigned to ^{228}Np by observation of the ^{228}Np and ^{228}U alpha chains in chemically separated samples as well as from alpha-alpha correlations between the known daughters.

Assuming no other significant mode of decay, the ratio of EC to alpha decay is 1.5 ± 0.4. The production cross section for ^{228}Np from the ^{233}U(p, 6n)^{228}Np reaction was determined to be 35 ± 3 μb. The delayed fission probability is (2.0 ± 0.9) x 10^{-4}.

The observation of only 25% of the expected K x-ray–fission correlations may indicate that the fission occurs with a half-life which is short compared to the time required for emission of the K x-rays, and that a fission isomer in ^{228}U is not populated by the EC decay. This is consistent with the

expected disappearance of fission isomers in the neutron deficient U/Th region. We have shown that delayed fission and the K-vacancy lifetime can be used as a means of estimating the fission lifetime. Figure 5-1 gives a comparison between the measured delayed fission probabilities for ^{228}Np, ^{238}Bk, ^{232}Am [Hall, 1990B] and ^{234}Am [Hall, 1990A] and the estimated electron-capture Q-values taken from [Möller, 1988].

5.2 ^{238}Bk

ECDF was studied in ^{238}Bk produced via the ^{241}Am(α, 7n)^{238}Bk reaction. The fission properties and half-life were measured with a rotating-wheel system. The half-life of this isotope was determined to be 144 ± 5 seconds from measurements of the fission activity. A predominantly asymmetric mass-yield distribution was observed for the fissioning species. The presence of a small symmetric component cannot be ruled out because of the poor statistics and possible degradation of the fragment kinetic energies due to sample thickness. The most probable pre-neutron total kinetic energy of fission was determined to be 174 ± 5 MeV. Evidence for a small symmetric component was observed with a significant drop in the average TKE at symmetric mass splits, but statistics preclude positive assignment.

The observed fissions were assigned to ECDF in Bk by observation of fissions in coincidence with the x-rays of Cm resulting from K capture in Bk. The observation of 15 ± 4 K x-rays compared to the expected 18 ± 4 indicates that the K-vacancies filled before fission of ^{238}Cm occurred. This may indicate that ECDF in ^{238}Bk proceeds via a fission shape isomer in the EC daughter and that the shape change associated with tunnelling through the first barrier is faster than 10^{-17} to 10^{-15} seconds (see Figure 1-2). If the shape change to the second potential well were slower than 10^{-15} seconds, gamma decay would

dominate and the P_{DF} would be zero. The fission lifetime is between 10^{-15} and 10^{-9} seconds. If the fission occurred faster than 10^{-15} seconds, fewer than expected K x-ray–fission coincidences would have been detected. If the fission occurred slower than 10^{-9} seconds, a delay would have been observed in the TAC spectrum.

The mass and Z were assigned to ^{238}Bk by observation of the ^{238}Cm alpha chain and fissions in chemically separated Bk samples. The electron-capture branch in ^{238}Bk is assumed to be 100% because no evidence for an alpha branch was observed.

The production cross section for ^{238}Bk from the ^{241}Am(α, 7n)^{238}Bk reaction was determined to be 150 ± 10 nb. The delayed fission probability is $(4.8 \pm 2) \times 10^{-4}$. Figure 5-1 gives a comparison between the log of the delayed fission probabilities for ^{228}Np, ^{238}Bk, ^{232}Am [Hall, 1990B] and ^{234}Am [Hall, 1990A] and the estimated electron-capture Q-values taken from [Möller, 1988]. An exponential relationship is evident. This may indicate that the height of the fission barrier in the region between ^{228}Np and ^{238}Bk remains fairly constant. The exponential relationship (see semi-logarithmic plot of P_{DF} vs. Q_{EC} in Figure 5-1) indicates that the major parameter influencing the P_{DF} is the electron-capture Q-value (see Equation 1-6). The P_{DF} increases by about 4 times for an increase of 0.25 MeV in Q_{EC}.

5.3 ^{241}Bk

No evidence was obtained for the existence of ^{241}Bk produced in the reaction ^{241}Am(α, 4n)^{241}Bk. The absence of any ^{241}Cm in the chemically separated Bk samples may indicate that ^{241}Bk has a half-life significantly shorter than the estimated 40 minutes taken from the electron-capture systematics given in [Lederer, 1978]. This estimate was made using a Q_{EC} of

2.19 MeV [Möller, 1988]. This is surprising because actinides typically have first-forbidden transitions. The limit on the half-life of ^{241}Bk is 10 to 1000 minutes at a sensitivity of 3 μb. The limits on the production cross section and half-life are shown in Figure 4-16. As can be seen in Figure 4-16, this experiment was less sensitive to half-lives outside the 10 to 1000 minute range because the minimum detectable cross section increases significantly.

The calculations of SPIT [Haynes, 1988] estimate the production cross section of ^{241}Bk to be 1 mb. Because no evidence for the existence of ^{241}Bk was obtained in this experiment to the level of about 3 μb, either the ^{241}Bk half-life is significantly shorter than the estimated 40 minutes or SPIT is overestimating the cross section by several orders of magnitude. Because SPIT has been shown to be accurate within one order of magnitude [Haynes, 1988], it is likely that the ^{241}Bk half-life is significantly shorter than 40 minutes. If the ^{241}Bk half-life is about 1 minute, the production cross section limit would be within one order of magnitude of that calculated by SPIT (see Figure 4-16). However, the estimated log(ft) for a 1 minute half-life, with a 2.19 MeV Q_{EC} [Möller, 1988] is 4.5. This is somewhat smaller than the known log(ft) values in this region and implies a nearly superallowed transition.

In the case of ^{238}Bk described earlier, the log(ft) value was about 5.2. For ^{242}Bk, the half-life is known to be 7 minutes [Lederer, 1978] and the estimated Q_{EC} is 3 MeV [Möller, 1988]. The log(ft) for ^{242}Bk is 5.3. The log(ft) value for ^{241}Bk is expected to be somewhat larger than either ^{242}Bk or ^{238}Bk because of the significantly lower Q_{EC} and because the EC of ^{241}Bk involves conversion of an odd-proton, even-neutron isotope to an even-proton, odd-neutron isotope. Given the range of log(ft) values for ^{238}Bk and ^{242}Bk, it is marginally possible that ^{241}Bk has a log(ft) of 4.5. If several transitions with

log(ft) values of 5 are possible, the overall log(ft) would appear to be consistent with a value of 4.5. The log(ft) values excluded in this experiment are 5.4-7.3 for transitions to the ground state in the ^{241}Cm daughter. This log(ft) range was estimated using the systematics in [Lederer, 1978].

5.4 ^{252}Bk and ^{253}Bk

The ^{252}Bk was produced in the reactions of 107 MeV ^{18}O with a 0.65 mg/cm^2 ^{248}Cm target via a ^{4}H transfer reaction. The recoiling products were collected with a He/KCl jet system for time intervals of 1, 3, 10 and 20 minutes at a beam intensity of 0.5 pμA. The Bk was separated in each of the collections using an HDEHP separation and stored according to the irradiation time. From tracer studies, the separation factor between the Bk^{4+} and the trivalent actinides was determined to be better than 8×10^5. The ^{252}Cf growth curve was consistent with a ^{252}Bk half-life of 1.8 ± 0.5 minutes and a production cross section of 47 ± 10 μb. The amount of ^{252}Cf in the samples does not increase beyond irradiation times of 3 minutes (see Figure 4-17). This observation, together with the tracer results, indicates that the ^{252}Cf resulted from the beta decay of ^{252}Bk. The ^{252}Bk half-life is a factor of 5 shorter than the 10-minutes estimated from systematics in [Lederer, 1978] using a beta-decay Q-value of 2.21 MeV [Möller, 1988]. This implies that the beta decay to ^{252}Cf proceeds via an allowed transition. The estimated ^{252}Bk excitation energy at an ^{18}O energy of 95 MeV is -5.2 MeV. For an ^{18}O energy of 107 MeV, the excitation of ^{252}Bk would be -2 MeV, if the additional 12 MeV is apportioned according to the fraction of projectile mass transferred. However, there is some experimental evidence that 60% of the energy is transferred to the heavy product [Lee, 1983]. This is the first report of a half-life and production cross section for ^{252}Bk.

After 21-days of counting, no evidence for the 6.61 MeV ^{253}Es, grand-daughter of ^{253}Bk, was observed. The grand-daughter of ^{253}Bk was chosen because its alpha energy is well above the Cf daughters of the lighter Bk isotopes and the ^{253}Cf, beta-decay daughter of ^{253}Bk, is known to have a small alpha branch (<0.3%). A limit was set for the ^{253}Bk half-life and production cross section in the same manner as described for ^{241}Bk. It was assumed that 4 counts/day of the ^{253}Es are required to yield a statistically significant indication of the ^{253}Bk growth with irradiation time. The estimated ^{253}Bk beta-decay Q-value is 1.39 MeV [Möller, 1988]. Using a log(ft) of 6, the ^{253}Bk half-life is estimated as 1 hour from the systematics in [Lederer, 1978]. From Figure 4-19, if the estimated half-life of the ^{253}Bk is about 1 hour, the production cross section is less than about 400 nb.

The estimated ^{253}Bk production cross section with an ^{18}O energy of 104 MeV is 10 μb (estimated from the systematics in [Lee, 1983]). After calculation of the transfer product excitation energy by the method given in [Hoffman, 1990A], it was determined that the ^{18}O bombarding energy was too low for optimum production of ^{253}Bk. The estimated excitation energy of the ^{253}Bk produced in the ^{5}H transfer reaction using ^{18}O at 95 MeV is -10 MeV. For an ^{18}O energy of 107 MeV, the excitation energy of ^{253}Bk would be about -7 MeV, if the additional 12 MeV is apportioned according to the fraction of projectile mass transferred [Leyba, 1990] [Hoffman, 1990A]. The production cross section for ^{253}Bk at an ^{18}O energy of 107 MeV may be significantly smaller than the estimated 10 μb. If the ^{253}Bk half-life is less than about 30 minutes, the sensitivity of this experiment did not allow for detection of ^{253}Bk.

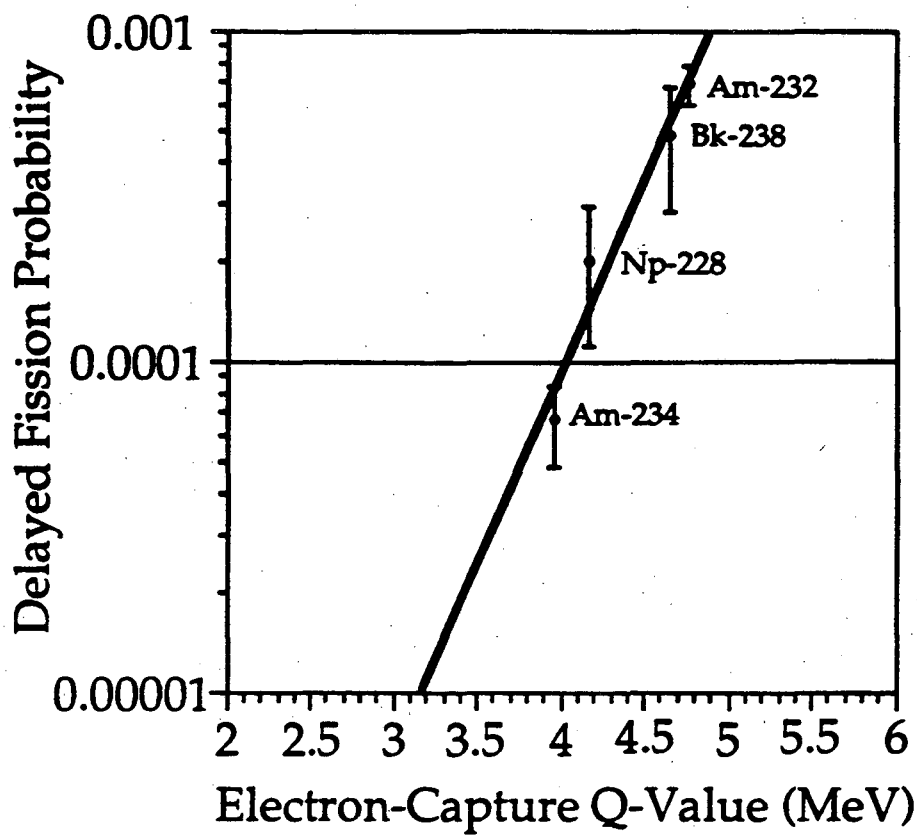

Figure 5-1. Relationship between the delayed fission probability and the estimated electron-capture Q-value (Q_{EC}). The Q_{EC} values are from [Möller, 1988]. The delayed fission probabilities for ^{234}Am and ^{232}Am are from [Hall, 1990A], and [Hall, 1990B].

6 Future

Delayed fission has allowed the determination of fission properties of nuclei which could not ordinarily be studied. The delayed fission study of ^{228}Np has illustrated that the K-vacancy lifetime and ECDF can be used to deduce the time scale of fission [Kreek, 1992B]. ECDF can also be used to study the details of the fission barrier in unprecedented detail [Gregorich, 1991]. The current availability of large Ge γ-ray detector arrays, such as the soon to be operational GAMMA-SPHERE [Delaplanque, 1988], will make studies of fission isomers feasible. If a level scheme can be determined for the fission isomer, details of the fission barrier can be extracted. Information about the level structure, lifetimes and energies can be used to determine the absolute heights and widths of both the inner and outer fission barriers. These data will aid in the development of a comprehensive model of fission.

Continued study of ECDF in isotopes with 136 neutrons, such as ^{230}Am, may yield more information about the triple-humped mass-yield distributions seen in the Ra region and to a much smaller extent in ECDF of ^{228}Np.

Further studies of ^{238}Bk should be completed to establish whether or not an enhanced symmetric mass-yield results from ECDF. Sufficient statistics should confirm the low energy component in the average TKE at symmetric mass splits.

The milking technique presented in this dissertation and [Kadkhodayan, 1991] can be used to determine the half-lives of nuclei which are currently 'undiscovered'. This is useful in refining the half-life and decay

systematics currently available. Additional nuclei such as ^{236}Am, ^{235}Am could be studied by measuring the 2.85-year ^{236}Pu and 25.3-minute ^{235}Pu daughters, respectively, in this manner. The availability of extremely rare isotopes for use as targets, such as ^{249}Bk and ^{251}Cf, should make production of additional isotopes further on the neutron-rich side of the valley of beta stability possible. Some of these could be studied using the daughter milking technique. An additional attempt should be made to discover ^{253}Bk. However, the ^{18}O projectile energy should be appropriately increased.

7 References

[Aumann, 1974] D.C. Aumann, G. Müllen, *Nucl. Instrum. Meth.* A 115, 75 (1974)

[Balagna, 1971] J.P. Balagna, G.P. Ford, D.C. Hoffman and J.D. Knight, *Phys. Rev. Lett.* 26, 145 (1971).

[Bedov, 1956] V.B. Bedov and V.N. Kosyakov, USSR*, Proceedings of the Int'l Conf. on Peaceful Uses of Atomic Energy, 7, 369-376 (1956).

[Berlovich, 1969] E.E. Berlovich and Yu.P. Novikov, Dok. Akad. Nauk SSSR 185, 1025 (1969) [Sov. Physics-Doklady 14, 349 (1969)].

[Bjørnholm, 1967] S. Bjørnholm, J. Borggreen, L. Westgaard and V.A. Karnaukhov, *Nucl. Phys. A* 95, 513 (1967).

[Browne, 1973] E. Browne and F. Asaro *Phys. Rev. C.* 7, 6(1973)

[Browne, 1986] E. Browne and R.B. Firestone, Table of Radioactive Isotopes (John Wiley & Sons, New York, 1986).

[Burbidge, 1957] E. M. Burbidge, G. R. Burbidge, W. A. Fowler and F. Hoyle, *Rev. Mod. Phys.* 29, 547 (1957).

[Casten, 1990] R.F. Casten et al., Isospin Laboratory Report #LAPL 91-51, 1991.

[Chetham-Strode, 1956] A. Chetham-Strode, Ph.D. Thesis, U.C. Berkeley and Lawrence Berkeley Laboratory, Report # UCRL-3322, 1956.

[Choppin, 1956] G.R. Choppin and R.J. Silva, *J. Inorg. Nucl. Chem.* 3. 53 (1956).

[Delaplanque, 1988] "GAMMASPHERE - A Proposal for a National Gamma-Ray Facility," M.-A.Delaplanque and R.M. Diamond, eds., Lawrence Berkeley Laboratory Publication No. PUB-5202 (1988).

[Evans, 1971] J.E. Evans et al., *Nucl. Instr. Meth.*, 102, 389, 1972.

[Fields, 1973] P.R. Fields, I. Ahmad, R.F. Barnes and R.K. Sjoblom, *Nuclear Physics* A208, 269 (1973).

[Flerov, 1968] G.N. Flerov, Yu.Ts. Oganesyan, Yu.V. Lobanov, Yu.A. Lazarev, and S.P. Tretiakova *Nucl. Phys. A* 160, 181 (1971).

[Gangrskii, 1980] Yu. P. Gangrskii, M. B. Miller, L. V. Mikhailov and I. F. Kharisov, *Sov. J. Nucl. Phys.* 31, *162* (1980).

[Gregorich, 1991A] K.E. Gregorich, *Nucl. Instr. Meth* A302, 135-142 (1991).

[Gregorich, 1991] K.E. Gregorich, private communication, 1991.

[Habs, 1978] D. Habs, H. Klewe-Nebenius, V. Metag, B. Neumann and H. J. Specht, *Z. Physik A* 285, 53 (1978).

[Hahn, 1939] O. Hahn and F. Strassmann, *Naturwissenschaften* 27(11), 1939.

[Hall, 1989A] H.L. Hall et al., *Nucl. Instr. Meth.* A 276, 649 (1989).

[Hall, 1989B] H.L. Hall et al., *Phys. Rev. Let.* 63 , 2548 (1989).

[Hall, 1989C] H.L. Hall et al., *Phys. Rev. C* 39, 1866 (1989).

[Hall, 1989D] H.L. Hall, Ph.D. Thesis, Lawrence Berkeley Laboratory Report Number LBL-27878 (1989).

[Hall, 1990A] H.L. Hall et al., *Phys. Rev C* 41, 618 (1990).

[Hall, 1990B] H.L. Hall et al., *Phys. Rev. C* 42, 1480 (1990).

[Hall, 1992] H.L. Hall and D.C. Hoffman, Ann. Rev. Nucl. and Particle Sci., 42, 147-175 (1992).

[Hatsukawa, 1989] Y. Hatsukawa, Nucl. Phys. A500, 90 (1989).

[Haynes, 1988] G.R. Haynes, J.D. Leyba and D.C. Hoffman, private communication (1988).

[Henderson, 1990] R.A. Henderson et al., Lawrence Berkeley Laboratory Report #30798, 1989-1990.

[Higgins, 1960] G. H. Higgins, The Radiochemistry of the Transcurium Elements, Subcommittee on Radiochemistry, National Academy of Sciences - National Research Council (1960).

[Hill, 1953] D.L Hill and J.A. Wheeler, *Phys. Rev.* 89, 1102, (1953).

[Hingmann, 1985] R. Hingmann et al., Gesellschaft für Schwerionenforschung, Darmstadt, Report No. GSI 85-1, 88 (1985).

[Hoff, 1986] R.W. Hoff, Weak and Electromagnetic Interactions in Nuclei, (H.V. Klapdor, ed., Springer-Verlag Publishers, Heidelburg, 1986) p.207.

[Hoff, 1988] R.W. Hoff, Inst. Phys. Conf. Ser. No. 88; J. Phys. G: Nucl. Phys. 14(Suppl.): S343-56 (1988).

[Hoffman, 1974] D. C. Hoffman and M. M. Hoffman, *Ann. Rev. Nucl. Sci.* 24, 151 (1974).

[Hoffman, 1980] D. C. Hoffman, D. Lee, A. Ghiorso, M. Nurmia, and K. Aleklett, *Phys. Rev. C* 22, 1581 (1980).

[Hoffman, 1989] D. C. Hoffman and L. P. Somerville, in Charged Particle Emission from Nuclei, edited by D. N. Poenaru and M. Ivascu (Chemical Rubber Company, Florida, 1989, Vol. III)

[Hoffman, 1990A] D.C. Hoffman and M.M. Hoffman, Lawrence Berkeley Laboratory Report #29502, 1990

[Hoffman, 1990B] D.C. Hoffman in Kleinberg, J., Ed., Los Alamos National Laboratory Report LANL-1721, p. 199, 1990.

[Hornshøj, 1975] P. Hornshøj et al., *Nucl. Phys* A239, 15 (1975).

[Hubert, 1980] F. Hubert, A. Fleury, R. Bimbot and D. Gardes, *Ann. Phys., Fr.* 5,1 (1980).

[Itkis, 1988] M.G. Itkis, V.N. Okolovich, A. Ya. Rusanov and G.N. Smirenkin, *Sov. J. Part. Nucl.* 19(4), 301 (1988).

[Itkis, 1989] M.G. Itkis, V.N. Okolovich, G.N. Smirenkin, *Nucl. Phys.* A502,

243c-260 (1989).

[Jensen, 1958] R.C. Jensen and A.W. Fairhall, *Phys. Rev.* 109, 942 (1958).

[Kadkhodayan, 1991] B. Kadkhodayan et al., *Radiochimica Acta* 56, 1-5 (1992).

[Klapdor, 1979] H.V. Klapdor, C.-O. Wene, I.N. Isosimov and Yu.W. Naumow, *Z Physik A* 292, 249 (1979).

[Klapdor, 1981] H.V. Klapdor et al., *Z. Physik A* 299, 213 (1981).

[Knauer, 1968] J. B. Knauer and B. Weaver, Oak Ridge National Laboratory Report ORNL-TM-2428 (1968).

[Kodama, 1975] T. Kodama and K. Takahashi, *Nucl. Phys.* A239, 489 (1975).

[Konecny, 1969] E. Konecny, W. Nörenberg and H.W. Schmitt, *Nucl. Phys.* A139, 513 (1969).

[Kratz,1973] K.L. Kratz and G. Hermann, *Z. Physik* 263, 435 (1973).

[Kreek, 1992A] S.A. Kreek et al., *Nucl. Instr. Meth* A317, 251-253 (1992).

[Kreek, 1992B] S.A. Kreek et al., ECDF of ^{228}Np, manuscript in progress (1992).

[Kreek, 1992C] S.A. Kreek et al., ECDF of ^{238}Bk, manuscript in progress (1992).

[Kupriyarov, 1984] V.M. Kupriyarov, Yad. Fiz. 39, 281 (1984).

[Kuznetsov, 1966] V.I. Kuznetsov, N.K. Skobelev and G.N. Flerov, *Yad Fiz.* 4, 279 (1966) [*Sov. J. Nucl. Phys.* 4, 202 (1967)].

[Kuznetsov, 1967] V.I. Kuznetsov, N.K. Skobelev and G.N. Flerov, *Yad Fiz.* 5, 271 (1967) [*Sov. J. Nucl. Phys.* 5, 191 (1967)].

[Lazarev, 1987] Yu.A. Lazarev et al., *Europhys Lett.* 4, 893 (1987).

[Lederer, 1978] C. M. Lederer and V. S. Shirley, editors, Table of Isotopes, (John Wiley & Sons, Inc., 1978, 7th edition)

[Lee, 1983] D.M. Lee, K.J. Moody, M.J. Nurmia, G.T. Seaborg, H.R. von Gunten, and D.C. Hoffman, *Phys. Rev.* C 27, 6 (1983).

[Leres, 1987] R. G. Leres, Lawrence Berkeley Laboratory Report LBL-24808, 1987 (unpublished).

[Leyba, 1990] J.D. Leyba, Ph.D. Thesis, UC Berkeley (1990) (unpublished).

[Liu, 1983] Yuan-Fang Liu, Cheng Luo, K. J. Moody, D. Lee, G. T. Seaborg, H. R. Von Gunten, *J. Rad. Chem.* 76(1), 119-124 (1983).

[Magda, 1987] M.T. Magda, J. Phys. (London) G13, L127 (1987).

[Magnusson, 1948] L.B. Magnusson and T.J. LaChapelle, *J. Am. Chem. Soc.* 70 3534 (1948).

[McMillan, 1940] E.M. McMillan and P.A. Abelson, *Phys. Rev.* 57 1185 (1940).

[Meyer, 1986] B.S. Meyer and D.N. Schramm, *Astrophys J.* 311, 406(1986).

[Meyer, 1989] B.S. Meyer et al., *Phys. Rev. C* 39, 1876 (1989).

[Möller, 1988] P. Möller, W. Meyers, W. Swiatecki and J. Treiner, *At. Data Nucl. Data Tables* 39, 225 (1988).

[Müllen, 1975] G. Müllen and D.C. Aumann, *Nucl. Instr. Meth.* 128, 425 (1975).

[Northcliffe, 1970] L.C. Northcliffe and R.F. Schilling, *Nucl. Data Tables* A7, 233 (1970).

[Peppard, 1957A] D. F. Peppard, S. W. Moline, G. W. Mason, *J. Inorg. Nucl. Chem.*, 4, 344-348 (1957).

[Peppard, 1957] D. F. Peppard, G. W. Mason, S. W. Moline, *J. Inorg. Nucl. Chem.*, 5, 141 (1957).

[Perry, 1971] D.G. Perry and A.W. Fairhall, *Phys. Rev. C* 4(3), 977 (1971).

[Poenaru, 1989] D. N. Poenaru and M. Ivascu, in Charged Particle Emission from Nuclei, vol III, (CRC Press, Boca Raton, 1989)

[Polikanov, 1962] S.M. Polikanov et al., *Sov. Phys. JETP* 15, 1016 (1962)

[Poskanzer, 1961] A.M. Poskanzer and B.M. Foreman Jr., *J. Inorg. Nucl. Chem.* 16, 323 (1961).

[Reeves, 1976] H. Reeves and O. Johns, *Astrophys. J.*, 206, 958(1976).

[Schmitt, 1965] H. W. Schmitt, W. E. Kiker and C. W. Williams, *Phys. Rev.* 137, B837 (1965).

[Scofield, 1974] J.H. Scofield, *At. Data Nucl. Data Tables* 14, 121 (1974).

[Seaborg, 1990] G.T. Seaborg and W.D. Loveland, The Elements Beyond Uranium (John Wiley and Sons, Inc., New York, 1990).

[Seaborg, 1991] G.T. Seaborg, Lawrence Berkeley Laboratory Report No. LBL-31179, 1991.

[Shalev, 1977] S. Shalev and G. Rudstam, *Nucl. Phys.* A275, 76 (1977).

[Skobelev, 1972] N.K. Skobelev, *Yad Fiz.* 15, 444 (1972) [*Sov. J. Nucl. Phys.* 15, 249 (1972)].

[Smith, 1956] H.L. Smith and D.C. Hoffman, *J. Inorg. Nucl. Chem.* 3. 243 (1956).

[Somerville, 1976] L.P. Somerville, Lawrence Berkeley Laboratory Report No. LBL-5075, (1976).

[Somerville, 1977] L.P. Sommerville et al., Lawrence Berkeley Laboratory Nuclear Science Division Annual Report, 1976-77, Report No. LBL-6575, 1977.

[Somerville, 1978] L.P. Somerville et al., *Bull. Am. Phys. Soc.* 23(1), 45, DE6(1978).

[Specht, 1972] H.J. Specht, J. Weber, E. Konecny, and D. Heunemann *Phys. Lett. B* 41, 43 (1972).

[Strutinsky, 1967] V.M. Strutinsky *Nucl. Phys. A.* 95, 420 (1967).

[Swiatecki, 1983] W.J. Swiatecki, *Aust. J. Phys.* 36, 641-648, 1983.

[Theilemann, 1983] F.-K. Theilemann, J. Metzinger and H.V. Klapdor, *Astron, Astrophys.* 123, 162(1983).

[Thompson, 1950] S.G. Thompson, A. Ghiorso and G.T. Seaborg, *Phys. Rev.* 77, 838 (1950).

[Thompson, 1950A] S.G. Thompson, A. Ghiorso and G.T. Seaborg, *Phys. Rev.* 80, 781 (1950).

[Unik, 1973] J.P. Unik et al., Proceeding of the Third International IAEA Symposium on the Physics and Chemistry of Fission, Rochester, 1973, (IAEA, Vienna, 1974), Vol. II,p.33.

[Vandenbosch, 1973] R. Vandenbosch and J.R. Huizenga, Nuclear Fission (Academic Press, New York, 1973).

[Viola, 1966] V.E. Viola, *Nucl. Data* A1, 391 (1966).

[Wapstra, 1959] A.H. Wapstra, G.J. Nijgh, C. Van Lieshout, Nuclear Spectroscopy Tables (North Holland Publishing Company, Amsterdam, 1959).

[Weber, 1976] J. Weber, H.C. Britt, A. Gavron, E. Konecny and J.B. Wilhelmy, *Phys. Rev.* C 13(6), 2413 (1976).

[Weissenberger, 1986] E. Weissenberger, P. Geltenbort, A. Oed, F. Gönnenwein and H. Faust, *Nucl. Instrum. Meth. A* 248, 506 (1986).

[Weisskopf, 1951] V.F. Weisskopf, *Phys. Rev*, 83,1073(1951).

[Wene, 1974] C.-O. Wene and S.A.E. Johansson, *Phys. Scripta* 10A, 156 (1974).

[Wene, 1975] C.-O. Wene, *Astron. & Astrophis.* 44, 233 (1975).

[Wilkins, 1976] B. Wilkins et al., *Phys. Rev* C 14(5) 1832 (1976).

[Wilkins, 1992] B. Wilkins private communication (1992).

[Yokoi, 1983] K. Yokoi, K. Takahashi and M. Arnould, *Astron. Astrophys.* 117, 65(1983).

[Zhagrov, 1973] E.A. Zhagrov, I.M. Kuks, Yu.A Nemilov, Yu.A. Selitskii, V.B. Funstein, *Nucl. Phys* A213, 436-444 (1973).

LAWRENCE BERKELEY LABORATORY
UNIVERSITY OF CALIFORNIA
TECHNICAL INFORMATION DEPARTMENT
BERKELEY, CALIFORNIA 94720